1-1-2014

Pre-clinical investigation of the effect of combining the cytotoxic agent Temozolomide with a dual mTORC2 inhibitor for the treatment of glioblastoma and establishment of an imageable surgical resection model of glioblastoma

Kieron J. Sweeney
Royal College of Surgeons in Ireland

RCSI

Title: Pre-clinical investigation of the effect of combining the cytotoxic agent Temozolomide with a dual mTORC1 and mTORC2 inhibitor for the treatment of glioblastoma and establishment of an imageable surgical resection model of glioblastoma

Author: Kieron J. Sweeney M.B., B.Ch, B.A.O., M.R.C.S.I.

Royal College of Surgeons in Ireland

Thesis submitted for examination for award of degree of Doctor of Medicine (M.D.)

Submitted: 11th February 2013

Research conducted in the Department of Physiology and Medical Physics, R.C.S.I.

Supervisors: Prof. Jochen Prehn, Dr. Annette Byrne, Mr Donncha O'Brien

This work was funded by Science Foundation Ireland under Grant No SFI 08/1N.1/B1949

Animal License from the Dept of Health and Children: B100/3654

Animal experiments conducted with Research Ethics Committee (REC) approval under the following:

REC 691, REC 703 and REC 706

I declare that this thesis, which I submit to RCSI for examination in consideration of the award of a higher degree Doctor of Medicine (M.D.), is my own personal effort. Where any of the content presented is the result of input or data from a related collaborative research programme this is duly acknowledged in the text such that it is possible to ascertain how much of the work is my own. I have not already obtained a degree in RCSI or elsewhere on the basis of this work. Furthermore, I took reasonable care to ensure that the work is original, and, to the best of my knowledge, does not breach copyright law, and has not been taken from other sources except where such work has been cited and acknowledged within the text.

Signed Kieran J. Sweeney

Student Number 11112859

Date 6/5/14

Table of Contents

Table of Figures

List of common Abbreviations

5-aminolevulinic	5-ALA
Apparent Diffusion Coefficient	ADC
Bioluminescence Imaging	BLI
Cancer Stem Cell	CSC
Chemotherapy	CTx
Computer Tomography	CT
Diffusion Tensor Imaging	DTI
Diffusion Weighted Image	DWI
Epidermal Growth Factor Receptor	EGFR
Extent of Resection	EOR
Extracellular signal-Regulated Kinases	ERK
F18-fluoroethyl-tyrosine	FET
FLuid Attenuated Inversion Recovery	FLAIR
Glioblastoma like Stem Cells	GSCs
Glioblastoma/Glioblastoma Multiforme	GBM
Gray	Gy
Magnetic Resonance Imaging	MRI
Mammalian Target Of Rapamycin	mTOR
Mammalian Target Of Rapamycin Complex	mTORC
Mitogen-Activated Protein Kinase	MAPK
O6-Methylguanine-DNA Methyltransferase	MGMT
Phosphatase and Tensin homologue	PTEN
Phosphoinositide 3-Kinase	PI3K
Protophoryhin IX	PpIX
Radiotherapy	RTx
Rat Sarcoma	RAS
Receptor Tyrosine Kinases	RTK
Temozolomide	Tmz
Vascular Endothelial Growth Factor	VEGF
World Health Organisation	WHO

Abstract

Glioblastoma is the most common primary brain tumour. It is an incurable disease and is commonly referred to as the worst of the "incurable cancers" by neurosurgeons and neuro-oncologists. It is heterogeneous on a cellular and genetic level. The genetic mutations that occur in glioblastoma lead to dysregulation of several principal pathways, the most commonly dysregulated pathways involve mTOR. mTOR is involved in the control of several cellular processes including autophagy and apoptosis. Despite maximal treatment, median survival remains abysmal ranging from 15 to 16 months. Current standard of care consists of two phases. The first phase involves maximal safe surgical resection. This intervention reduces the tumour burden and improves the efficacy of the second phase. This second phase involves chemotherapy and radiotherapy commonly referred to as the "Stupp protocol". This phase employs a common strategy of inducing apoptosis in an attempt to control the residual disease. Within this thesis we explore both phases of treatment for glioblastoma.

Firstly, we established the *in vitro* efficacy of the mTOR inhibitor, AZD 8055 using the glioblastoma cell line U87MG, and glioblastoma tissue derived from a patient in Norway referred to as patient 3. We then assessed the *in vivo* efficacy of AZD 8055 in combination with temozolomide, using the patient derived glioblastoma tumour material from patient 3, in an orthotopic bioluminescence murine model. We demonstrated that although AZD 8055 is a strong inhibitor of the mTOR pathway when used as a monotherapy or combined with temozolomide, this did not translate into either increased survival or a reduction in tumour growth *in vivo*. By interrogating the points of crosstalk between autophagy and apoptotic pathways, we hypothesized that mTOR inhibition induced a protective autophagy which antagonised the apoptosis induced by temozolomide. Secondly, we validated a novel animal model of surgical resection. We established that orthotopic implantation of glioblastoma cells can be safely resected, and that the residual tumour, which has invaded the surrounding brain parenchyma, can be reliability imaged

in vivo. We advocated the use of this model for the investigation of local delivery of novel therapies into the surgical resection cavity or in the assessment of systemic therapeutic agents targeting residual tumour that has migrated into the normal brain parenchyma.

Chapter 1: Introduction

1.1: General overview of Glioblastoma

Primary Central Nervous System (CNS) tumours can arise from any tissue within this system. The majority of cell volume within the CNS is due to neurones and their supporting glial cells. Glial cells can further be subdivided into microglia and macroglia. The embryologic origin of microglia is probably mesodermal, the function of which is to act as resident mononuclear phagocytes of the nervous system. Macroglia are of neuroectodermal origin. Macroglial cells can be further subdivided into (i) Astrocytes- which are the core component of the blood brain barrier, (ii) oligodendrocytes-which form the myelin sheaths of each neurone and (iil) ependymal cells- cuboidal cells that line the ventricular system and choroid plexus forming the blood-CSF barrier [1]. Glioma is the most common primary brain tumour. It is histologically derived from macroglial cells with several cell histological subtypes existing –oligodendroglial tumours, ependymal tumours, choroid plexus tumours and astrocytic tumours. The World Health Organisation (WHO) histological grading system for the astrocytic tumours ranges from I-IV. Astrocytic tumours designated WHO grade I are benign tumours called pilocytic astrocytomas. These tumours are surgically curable. The most malignant form of astrocytoma is Grade IV and is referred to as Glioblastoma (GBM- previously known as Glioblastoma Multiforme) [2]. Gliomas of astrocytic, oligodendroglial and ependymal origin account for more than 70% of all primary brain tumours, of which 65% of these are classified as GBM [3]. GBMs can arise as de novo lesions or can progress from lower grade gliomas; this is referred to as a secondary glioblastoma. The current standard of care involves maximal safe surgical resection followed by adjuvant chemotherapy and radiotherapy yielding a median survival of 16 months.

1.2 Epidemiology

1.2.1 Incidence

The incidence of primary central nervous system neoplasms have been reported higher in developed, industrial countries. It has also been reported that there appears to be racial differences, with a higher incidence among Caucasians when compared to African or Asian descent, although socio-economic factors cannot be excluded [3]. Ireland has a high incidence of astrocytic brain tumours (see Figure 1). The peak age is 40-65 and there is a slight male preponderance (see Figure 2).

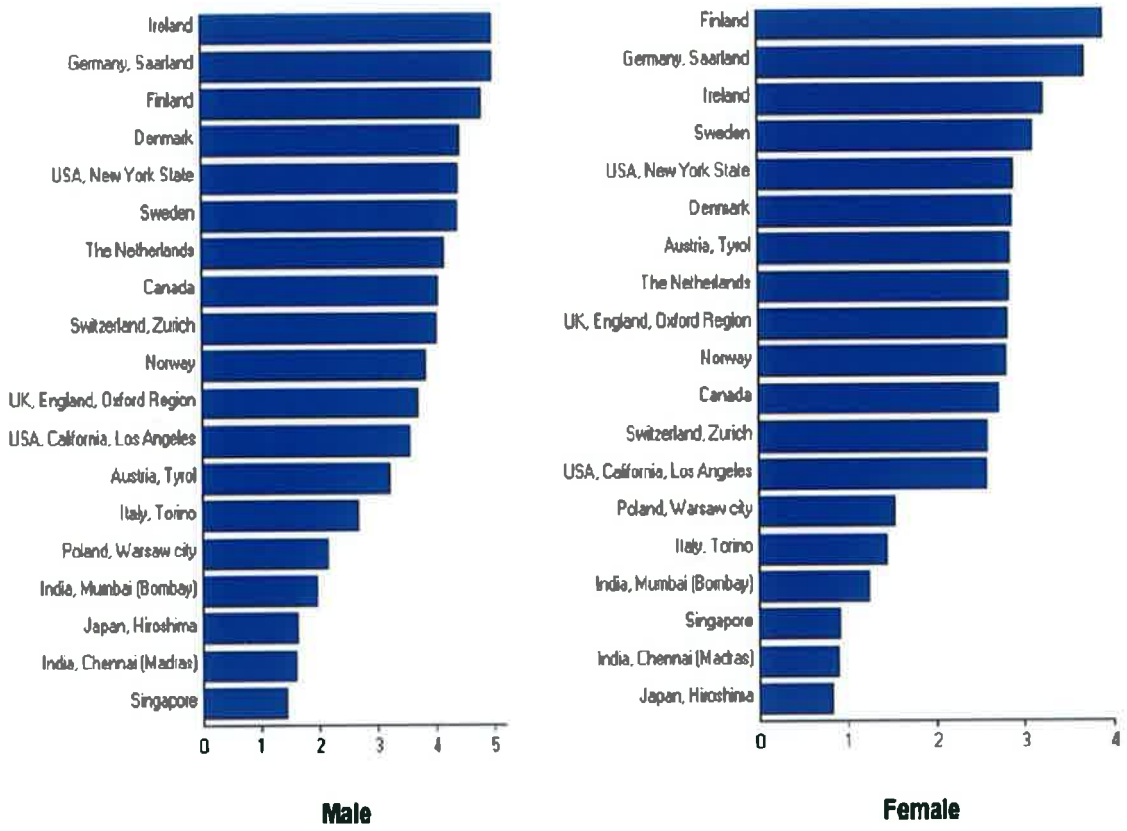

Figure 1- Incidence rates of astrocytic brain tumours in various countries worldwide adjusted to the World Standard Population (all ages; per 100,000 persons per year) demonstrating the high incidence of astrocytic tumours in the Irish population. From Ohgaki et al (2005).

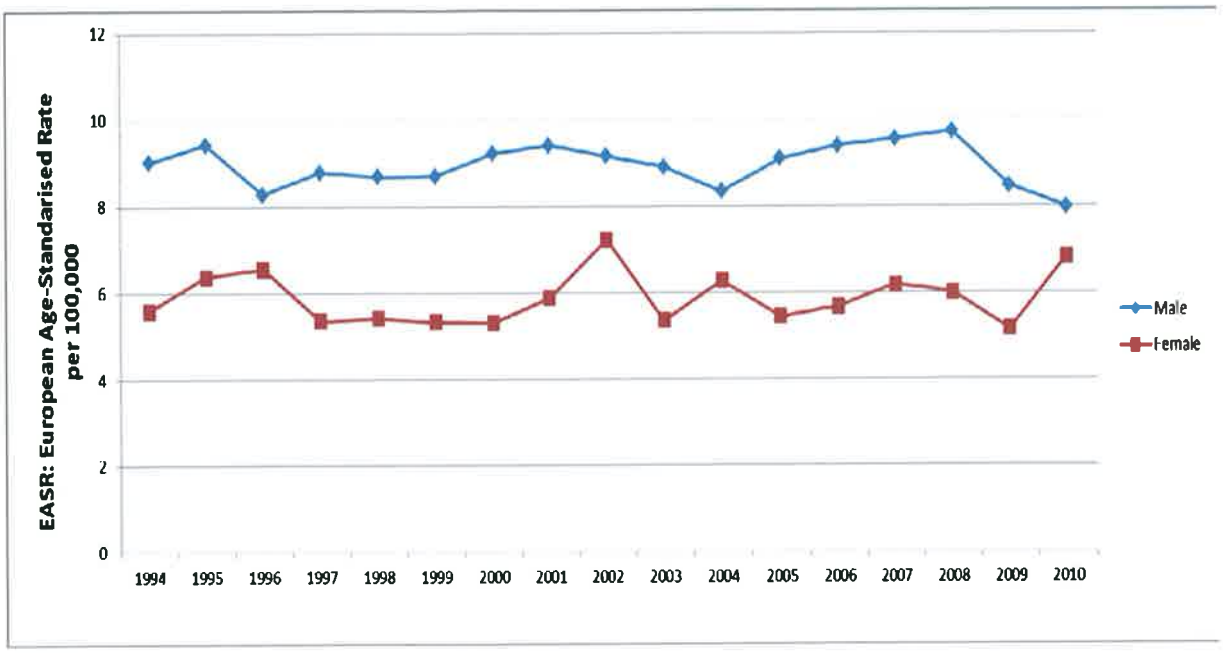

Figure 2-Incidence of High Grade Gliomas in Ireland from 1994-2010. European Age-Standardised Rate (per 100,000) for both male (blue), female (red). This graph is reproduced from statistics acquired from the Irish National Cancer Registry online search facility.

1.2.2 Risk Factors

Only 1% to 5% of gliomas are classified as hereditary [2]. The vast majority that occur are sporadic. Several large scale epidemiological studies have been undertaken to assess various environmental, occupational, dietary, infectious and iatrogenic risk factors.

There is some weak evidence that exposure to lead with a blood lead concentration of greater than 1.4µmol/L carries a twofold increase in risk [4, 5]. There has been no demonstrable link between smoking and adult onset glioma with conflicting reports on paternal smoking being associated with childhood gliomas [6, 7]. There is also some weak evidence that consumption of N-Nitroso compounds detected in preserved food, cured meats or high calorie intake can be associated with an increased risk of gliomas and that some foods such as dark yellow vegetables and beans may be protective[8]. Regarding exposure to electromagnetic fields and cellular phone usage there have being conflicting reports [9, 10]. Polyomavirus simian virus 40 (SV40), John Cunningham virus

(JCV) or human cytomegalovirus (HCMV) have all been implicated as playing a role in the pathogenesis of gliomas [11, 12].

There appears to be a protective effect with late menopause and hormone replacement therapy [13]. The only conclusive exposure risk factor is ionizing radiation. Most of this evidence comes from studies of children who were diagnosed with Acute Lymphoblastic Leukaemia (ALL) who received cranial radiotherapy [14]. Even low dose radiotherapy that was used to treat benign conditions such as tinea capitis has been shown to increase the risk of developing central nervous system tumours [15].

1.3 Diagnosis

1.3.1 Clinical Features

Patients typically present with new onset, progressive neurological symptoms or signs. These symptoms and signs at presentation are related to anatomic position of the tumour. Lesions in non-eloquent regions such as the right frontal lobe can grow to be quite large and can present with symptoms of raised intracranial pressure and mass effect such as headaches, nausea and vomiting and altered mental status. Lesions arising within or adjacent to eloquent areas typically present with seizures and focal neurological defects such as dysphasia and hemiparesis.

1.3.2 Investigations

Usually a Computer Tomography (CT) scan of the head is organised in the acute setting. The non-contrast CT is a useful, quick and inexpensive imaging modality which will identify mass lesions. CT is based on the absorption of X-rays. Different tissues absorb x-rays in different amounts giving rise to absorption coefficients. Using computer algorithms, these absorption coefficients can be reconstructed to provide limited anatomical information. If a mass lesion is identified, a post-contrast CT can be

performed. The key radiological hallmarks of GBM on a non-contrast CT are an irregular isodense or hypodense mass predominately affecting the white matter tracts. There is a central hypodensity representing necrosis. On the post-contrast scan there will be a strong ring enhancement around the periphery of the central necrosis. Magnetic Resonance Imaging (MRI) is the modality of choice for investigation and characterisation of intracranial space occupying lesions. Strong magnetic fields are applied to align the magnetic moment of protons in the tissues. A radiofrequency electromagnetic current is then applied flipping the spin of the protons. Once this is discontinued the protons return to their original position as aligned by the magnetic coil, referred to as relaxation time. As different tissues have different proton density, different tissues have different signals which can be detected in 3-dimensions. The typical MRI sequence involved in the investigation of a space occupying lesion is T1, pre- and post-contrast, T2, FLuid Attenuated Inversion Recovery (FLAIR), and the diffusion sequences, Diffusion Weighted Image (DWI) and Apparent Diffusion Coefficient (ADC). The radiological features of GBM on standard MRI sequence are as follows: T1- an irregular isointense to hypointense white matter based lesion. Following gadolinium administration there will be a thick irregular ring of enhancement. On T2 weighted and FLAIR images there will be a hyperintense white matter signals surrounding the central area of necrosis. Both DWI and ADC will show no diffusion restriction [16].

1.5 Management

1.5.1 Surgery

1.5.1.1 Extent of resection

While it was always known that resection of GBM tumour alleviated presenting symptoms and provided histological diagnoses, it was not until 2001 that a significant survival benefit was shown to correlate to the Extent of Resection (EOR) [17]. The finding established an "all-or-none" treatment paradigm where it was believed that anything less than a 98 %

reduction in tumour volume at the time of surgery did not confer any survival benefit. This paradigm persisted until 2011 were Sanai et al. demonstrated a stepwise increase in survival advantage beginning with subtotal resections of 78 % which yielded a median survival of 12.5 months. Those patients that underwent a total resection or EOR=100% had a median survival of 16 months. [18].

Resection is usually limited by the location of the lesion and the boundaries of tumour resection are usually limited by anatomical and functional considerations. GBM lesions often compromise eloquent brain areas such as language, motor and sensory regions or may be situated in areas that are surgically difficult to access such as the insula. Various imaging options, both singularly and in combination, exist for the surgeon to maximize surgical resection while causing minimal morbidity such as functional MRI (fMRI) to identify eloquent areas and Diffusion Tensor Imaging (DTI) to identify important white matter tracts.

1.5.1.2 Aids to improve resection

1.5.1.2.1 Fluorescent guided resection

As previously mentioned, the extent of surgical resection has prognostic impact for the patient with resections greater than 78% of tumour volume being significant when combined with multi-modality treatment [19, 20].

Intra-operatively it can be difficult to distinguish normal brain from infiltrated brain especially after the necrotic centre has been removed. 5-aminolevulinic (5-ALA) is a non-fluorescent naturally occurring precursor of haemoglobin. It can be administered orally. It is metabolised by tumour cells of epithelial and mesenchymal origin leading to intracellular accumulation of the fluorescent protophoryhin IX (PpIX). Once exposed to violet blue light the cells with high concentrations of protophoryhin IX fluoresce red [21].

Valdes et al. have demonstrated that here is a strong correlation between the intracellular concentration of protophoryhin IX , visible detection of fluorescence and histopathological score (WHO scores) and Ki-67 immunohistochemistry to assess tissue proliferation [22]. Valdes et al previously established that approximately 95% of normal tissue contains concentrations of PpIX less than 0.1µg/mL [23]. Using *ex vivo* PpIX fluorimetry the authors noted approximately 40 % of tumour positive biopsy samples were not detected visibly but did have greater than 0.1 µg/mL of PpIX concluding that there is need for improvement in technology to allow for a greater sensitivity in the visual detection of the fluorescence.

Radiologically, Roberts et al established the relationship between pre-operative gadolinium enhancement on MRI, observable intraoperative fluorescence and histopathological score [24]. Stockhammet et al demonstrated the association between F18-fluoroethyl-tyrosine (FET)-positron emission tomography (PET) and intra-operative fluorescence [25].

Fluorescent guided resection provides the operating neurosurgeon with real time visual recognition of tumour material. The associations between intra-cellular concentrations of PpIX, histopathological and immunohistochemical scores along with correlations between intra-operative fluorescence and pre-operative imaging have translated as expected in the clinical setting [26]. A large multicentre randomised control phase III trial was performed by the ALA-Glioma study group in 2006. It compared the extent of resection guided by 5-ALA fluorescence to that achieved by resection under normal white light. Interim analysis of the results lead to the trial ending prematurely as it became clear of the benefit of fluorescent guided resection. The patients assigned to the 5-ALA group had higher rates of complete resection and 6 month progression free survival [26]. In 2009 a multicentre prospective, single-arm, uncontrolled phase II study was undertaken to assess the benefit of 5-ALA guided resection in the setting of recurrent GBM. The results were consistent with that of the trials in resection of primary tumours and showed

that prior treatment with radiotherapy or chemotherapy did not lessen the high predictive value of 5-ALA [21].

1.5.2 Chemotherapy and Radiotherapy

Following surgical resection, and ideally within six weeks, the next stage of treatment commences and consists of concomitant chemotherapy and radiotherapy followed by adjuvant chemotherapy [27-29] The most widely used regimen, known as "Stupp protocol", is based on the European Organization for Research and Treatment of Cancer (EORTC) and National Cancer Institute of Canada (NCIC) trial [28, 29] Radiotherapy consists of delivering 60 Gray (Gy) over 30 fractions which can take up to six weeks to complete. During this time the patient receives concomitant temozolomide (TMZ) administered at a dose of 75 mg/m^2 daily from the first to the last day of radiotherapy. The adjuvant/maintenance phase consists of 200 mg/m^2 daily for 5 days repeated for a minimum of 6 cycles. TMZ is an oral alkylating agent. It targets DNA by alkylating the N7 or O6 positions of guanine residues and induces G2/M cell cycle arrest, senescence and tumour cell death by p53-dependent and p53-independent apoptosis [30-33]. In addition to activating cell death, pre-clinical evidence suggests that sub-lethal concentrations of TMZ may reduce the irradiation-induced invasion of GBM cells [34] and inhibit angiogenesis when used at low, non-toxic doses [35, 36].

Of note, patient responses to TMZ vary significantly and are negatively regulated by the presence of O6-Methylguanine-DNA Methyltransferase (MGMT). Although methylation of the MGMT promoter region can be modified after adjuvant treatment [37], numerous studies have established the prognostic significance of MGMT promoter methylation in adjuvant treatment with radiotherapy alone or when combined with TMZ [38] and can improve the median survival to 21.7 months compared to a median of 15.3 months in unmethylated GBMs [39].

Other alkylating treatments that are licensed in recurrent GBM include irinotecan, cyclophosphamide and nitrosoureas, such as Procarbazine, Lomustine, and Vincristine (PCV) chemotherapy [40]. Bevacizumab, a humanized monoclonal antibody against Vascular Endothelial Growth Factor (VEGF), is licensed in the US for the treatment of recurrent GBM. Recently, carmustine wafers have been licensed in Europe and US for the treatment of GBM as a surgical adjuvant and in recurrent/salvage treatment [41]. These consist of a biodegradable polymer matrix that is impregnated with 1,3-Bis(2-Chloroethyl)-1-Nitrosurea (BCNU, Carmustine, marketed as Gliadel®). At the end of surgical resection, the operating surgeon can place these wafers along the wall of the surgical cavity. Carmustine is released from wafers over 21 days, the majority of which is released over the first 5-7 days, and which can diffuse to a depth of 12 mm [42]. There is some evidence of a 2-3 month median survival gain when Gliadel and the "Stupp protocol" are used together. However, this needs to be weighed against the reported increased risk of side-effects such as seizures, cerebral oedema, wound problems and intracranial infection and the expense of the treatment.

1.5.3 Histopathology

GBM is infamous for its cellular heterogeneity. The cell of origin in the tumourigenesis of GBM has been under debate in the literature recently [43, 44]. There are two main theories to explain the cellular heterogeneity of GBM, the clonal evolution theory and the Cancer Stem Cell (CSC) theory. However, it may be a combination of the two [45, 46]. Clonal evolution describes how a GBM tumour can be heterogeneous. After monoclonal initiation, each clonal expansion becomes heterogeneous due to the acquisition of genetic mutations. The CSC theory describes a subpopulation of cells within the GBM tumour capable of self-renewal and differentiation. CSCs have the intrinsic ability to replenish the CSC pool, while the differentiated cells proceed to make up the tumour bulk. Interclonal cooperatively describes how these two theories are not mutually exclusive.

Each colony can have a profound effect on the other mediated by the microenvironment, through the release of paracrine mediators or by cell-cell interaction, acting as a syncytium.

There are a number of cellular niches within the GBM bulk [44, 47], which form a structural as well as functional syncytium leading to recruitment and transformation of normal surrounding cells [48]. Macroscopically, GBMs are described as poorly delineated white matter based lesions demonstrating infiltration, angiogenesis and a central area of necrosis. The classic histological description of GBM is a poorly differentiated glial tumour with cellular features of anaplasia with marked nuclear pleomorphism, atypia and hyperchromtin, with a glassy cytoplasm and a high level of mitosis [49].

1.6 Prognosis

Glioblastoma is an incurable disease and commonly referred to as the worst of the "incurable cancers" by neurosurgeons and neuro-oncologists [50]. Prior to the publication of the landmark paper in 2005 by Stupp et al which highlighted the survival benefit of surgery followed by concomitant chemotherapy and radiotherapy with adjuvant chemotherapy, median patient survival remained abysmal at 13.5 months in 20-44 year old patients, 9.5 months in 45- 64 year olds and 5.5 months in the 65-79 year olds. This improved to 18.5, 12.5 and 6.5 months for the respective age groups[51].

Other prognostic factors identified in large clinical studies include the extent of surgical resection [18] (see section 1.5.1.1), MGMT methylation status [38] (see section below), patient age and Karnofsky performance score [52]. Karnofsky Performance Score (KPS) is a holistic clinical scoring system ranging from 100% to 0%, where 100% represents a patient with no signs or symptoms of disease to 0% representing death. It is commonly used in large clinical studies as a way of eliminating treatment bias.

1.7 Genetic/epigenetic alterations

The Cancer Genome Atlas Research Network published a landmark paper in the Lancet in 2008. In this manuscript the group clarified the genomic landscape of GBM. Of the 601 genes analysed, the most frequent of mutations occurred in TP53 (42%), PTEN (33%), neurofibromatosis-1 (NF1) (21%), EGFR (18%), CDK (14%), RB1 (11%), Murine Double Minute 2 (MDM2) (11%) PIK3R1 (10%), and PIK3CA (7%). [53]. These mutations lead to dysregulation of five principal intracellular pathways: p53 signalling, pRB (Retinoblastoma) signalling, PI3K-PTEN-Akt-mTOR signalling, RAS/MAPK signalling and STAT3 and ZIP4 signalling [54].

The earliest identifiable mutation to occur in the mutagenesis of glioma is the Isocitrate Dehydrogenase (IDH) 1/2 mutation. This mutation occurs almost exclusively in Low Grade Gliomas (LGGs) and secondary GBMs. This missense mutation occurs in the gene coding for isocitrate dehydrogenase, the enzyme that catalyses the oxidative carboxylation of isocitrate to α-Ketoglutarate in the citric acid cycle. This results in the reduction of NADP to NADPH [55]. This mutation rarely occurs in primary GBMs with some authors suggesting those that have been reported are actually undiagnosed secondary GBMs [56]. The presence of the IDH 1/2 mutation significantly prolongs survival in LGGs.

Based on genomic analysis primary GBMs can be divided into four principle subtypes [49, 57, 58].

I. Classical/Proliferative GBMs: Histologically resemble astroglia; chromosomal abnormalities include chromosome 10 deletions and amplifications in chromosome 7. The signature genetic mutation is amplification in EGFR.

II. Mesenchymal GBM: Histologically have high levels of angiogenesis, necrosis, infiltration and a marked inflammatory response; signature genetic mutations

include NF1 with high expression of mesenchymal markers, such as CHI3L1 (also known as YKL40) and MET.

III. Neural GBM: Histologically may resemble features of normal brain parenchyma with expression of neuron markers, such as NEFL, GABRA1, SYT1, and SLC12A5

IV. Proneural GBM: Signature genetic mutations include PDGFA, IDH1, and TP53

Malignant transformation results not only from structural changes to key genes but also from regulation of gene transcription and translation [59]. A rudimentary explanation of gene transcription and translation begins with unwrapping of packaged chromatin from core histones and the binding of the transcription machinery to the gene promoter region. The transcribed messenger RNA (mRNA) is then further modified by microRNA (miRNA). There are three principal forms of epigenetic modification that interplay with the genetic and chromosomal abnormalities that ultimately result in malignant transformation. These are histone modifications, DNA methylation and microRNA regulation [60, 61].

Histone Modifications: In chromatin, the DNA is tightly packaged around an octamer histone complex to form a nucleosome. Each octamer is composed of two copies of four core histones: H2a, H2B, H3 and H4, each of which possesses an amino-terminal tail that is subject to post-translational modification. Acetylation of this tail weakens the bond between the histone complex and the DNA helix thereby facilitating gene transcription. Acetylation is via histone acetyl transferase (HATs) and deacetylation is mediated by histone deacetylases (HDACs). Histone methylation may facilitate or suppress transcription depending on the site of methylation [62]. The Cancer Genome Atlas Research Network identified aberrations in GBM involving HDACs (HDAC2 and HDAC9), histone demethylases (JMJD1A and JMJD1B), histone methyltransferases (SET7, SETD7, MLL, MLL3 and MLL4) [53].

DNA methylation: The upstream/ 5 prime end of the gene promoter region on the anti-sense DNA strand contains islands of cytosine-guanine repeats (CpG islands). RNA polymerase must attach to the promoter region for transcription to occur. Hypermethylation is a form of promoter site deactivation and involves the addition of a methyl group to the 5'-position of cytosine nucleotides within the CpG islands, whereas hypomethylation promotes transcription. Therefore, the methylation status of gene promoters involved with tumour suppression (GATA4, NDRG2), DNA repair (MGMT), cell cycle regulation (p14ARF) and Programmed Cell Death pathways (TMS1/ASC, WWOX) have all been implicated in gliomagenesis [63]. Interestingly, the O6-methylguanine-DNA methyltransferase (MGMT) gene codes for a DNA repair enzyme that when expressed protects the normal cell from malignant transformation and protects GBM cells from chemotherapeutic agents such as temozolomide. However, promoter methylation of the MGMT gene has been shown to correlate with patient survival and response to chemo- and radiotherapy [64, 65]

microRNA regulation: miRNAs are small non-coding double stranded RNA molecules that modify gene expression by either suppressing translation or influencing mRNA degradation. miRNAs are involved in cell proliferation (miRNA 7 via EGFR and Akt pathways-see section below), G1/S cell cycle progression (miRNA-221/222), cell survival miRNA 181a/181b/181c), cell migration and cell invasion [66] and as such can act as either a tumour suppressor or in oncogenic fashion [67, 68]. In GBMs up to 17 unregulated and 33 downregulated miRNAs have been so far identified.

1.8 Pathway dysregulation

1.8.1 p53 signalling

p53 protein is a tumour suppressing protein encoded by the TP53 gene which is located on the short arm of chromosome 17. The p53 protein has a dual role acting as a

transcription factor and intermediary in apoptosis, cell-cycle progression and senescence. p53 levels increase in response to numerous cellular stress including DNA damage, oxidative stress and microtubule disruption [69]. Regulating p53 activation are two principal proteins MDM2 and MDM4. CDKN2A regulates MDM2. Therefore, mutations can occur in one or all four genes leading to oncogenic dysregulation of this pathway resulting in proliferation despite genomic instability. Individually, the frequency of CDKN2A, TP53 mutations, MDM2 and MDM4 amplifications in GBM is approximately 49%, 37.5%, 14% and 4% respectively. This equates to approximately 87% of GBMs with dysregulation of this signalling pathway as some GBMs may have several key mutations [53].

1.8.2 pRB Signalling

The Retinoblastoma protein is another tumour suppressor protein involved in inhibition of cell-cycle progression. Its gene is located on the long-arm of chromosome 13. It functions by binding to a family of transcription factors known as E2F thereby inhibiting transcription. The RB gene is regulated by a family of Cyclin Dependent Kinases (CDKs) and therefore either mutation in the RB gene or amplification of the CDK genes leads to oncogenic dysregulation of the cell-cycle. The frequency of mutation in the six principal CDKs (CDKN2A/(P16/INK4A), CDKN2B, CDKN2C, CDK4, CCND2 and CDK6) are 52%,47%,2%,14%,2% and 1% respectively. The pRB gene mutation frequency equates to 11%. This pathway is dysregulated in 78% of GBMs as some GBMs may have several key mutations.

1.8.3 JAK/STAT3 and ZIP4 signalling

Signal Transducers and Activators of Transcription (STAT) are a family of cytoplasmic proteins involved in transcription. These proteins are activated by the binding of cytokines especially interlukin-6 (IL6). Dysregulation of this pathway results in increased cell

survival and angiogenesis. There is direct input from EGFR into this pathway [70, 71] and notable crosstalk between this pathway and downstream signalling in the PI3K/mTOR and MEK/ERK mediated by IL-6 [72]. IL-6 amplification occurs in up to 50% of GBMs as some GBMs may have several key mutations [73].

1.8.4 RAS/MAPK signalling

Rat Sarcoma (RAS) are oncogenes belonging to the G-protein family, the activities of which are regulated by Receptor Tyrosine Kinases (RTKs) especially Epidermal Growth Factor Receptor (EGFR) (discussed below) and Platelet-Derived Growth Factor (PDGFR). Activated RAS regulates Mitogen-Activated Protein Kinases (MAPK) such as RAF and ERK that control mitogenic signals involved in cellular growth as well as the PI3K/mTOR pathway. A mutation in the RAS gene leads to a constitutively activated Ras protein. NF1 regulates Ras. This coupled with amplification of RTKs lead to up regulation of this pathway. When one considers the mutational frequency of RTKs such as EGFR (45%), PDGFR (13%) along with the mutational frequency of NF1(18%) and RAS (2%), the RAS/MAPK pathway is dysregulated in 88% of GBMs as some GBMs may have several key mutations.

1.8.5 PI3K-PTEN-Akt-mTOR signalling

This pathway is involved in numerous cellular pathways from transmitting extracellular growth signals to regulation of growth, proliferation, and nutrient and energy status. This pathway also modulates Programmed Cell Death (PCD) pathways via mammalian Target of Rapamycin (mTOR). Growth signals bind to a family of cell surface receptors known as RTKs. Within this family are a number of important subtypes in GBM, most notably EGFR, PDGFR and Vascular Endothelial Growth Factor Receptor (VEGFR). Therefore amplification in any of the genes for these RTKs may result in oncogenic growth signals.

EGFR mutation or amplification is one of the most common genetic alterations in GBM and has been associated with resistance to conventional treatment [74, 75]. The EGFR family comprises an important group of receptor tyrosine kinase (RTK) molecules. These molecules include the closely related trans-membrane proteins: ErbB-1 (EGFR, HER1), ErbB-2 (neu, HER2), ErbB-3 (HER3) and ErbB-4 (HER4). Major downstream signalling pathways activated by EGFR include Ras/Rapidly Accelerated Fibrosarcoma (Raf)/MAPK Kinase (MEK)/Extracellular signal Related Kinase (ERK) 1/2/MAPK and PI3K/AKT/mTOR [76].

Downstream of these RTKs lies mTOR. mTOR is an evolutionarily conserved serine/threonine kinase. With a molecular weight of approximately 300kDa, mTOR belongs to the phosphatidylinositol kinase kinase (PIKK) family [77]. It lies at a nexus of several critical intracellular pathways co-ordinating various extra-cellular signals and intracellular processes involved in nutrition, growth, proliferation, cytoskeletal organisation, apoptosis, autophagy and protein biosynthesis. It assembles into two discrete complexes. mTORC1 complex consists of the Regulatory-Associated Protein of mTOR/ Rapamycin-sensitive Adapter Protein of mTOR (RAPTOR), 40 kDa Proline-Rich AKT Substrate (PRAS40), DEP domain containing mTOR-interacting protein (DEPTOR), and mammalian lethal with SEC13 protein 8 (mLST8). mTORC2 complex consists of mammalian stress-activated map kinase-interacting protein 1 (mSIN1), protein observed with RICTOR (PROTOR), Rapamycin-Insensitive Companion of mTOR (RICTOR), DEPTOR and mLST8 [78].

These complexes differ in their subunit composition, substrate specificity and regulation. mTORC 1 is the key nutritional state sensor, promoting anabolic processes while inhibiting catabolic processes [79]. mTORC1 phosphorylates P70 S6k, which is a serine/threonine kinase that regulates translation through the phosphorylation of the S6 ribosomal unit [80]. Phosphorylation of p70 S6K leads to nuclear localisation to promote cell proliferation by facilitating cell cycle G1 – S phase transition and cell survival [81].

mTORC 2 controls cytoskeleton organization and cell migration, cell survival, and cell cycle progression. Both complexes regulate autophagy however only mTORC1 does so directly [79, 82-84].

PTEN (Phosphatase and tensin homologue) tumour suppressor gene, is located on the long arm of chromosome 10, and encodes for a phosphatase that catalyses the dephosphorylation of phosphatidylinositol 3,4,5 triphosphate (PIP3), negatively regulating the activity of mTORC1 and mTORC2 [85-87].

The mutational frequency in GBM of EGFR (45%), PDGFR (13%), PI3K (15%), PTEN (36%) and AKT (2%) leads to this pathway being upregulated in 88% of primary GBMs as some GBMs may have several key mutations and therefore makes this the most frequently upregulated pathway.

1.9 Programmed Cell Death

Programmed cell death (PCD) plays a vital role in all aspects of cell states and is defined as cell death mediated by an internal programme. There are at least three separate but interlinked forms of programmed cell death, apoptosis, autophagy and programmed necrosis. In the normal cell undergoing development and maturation, apoptosis is involved in various processes such as organogenesis. Again, in the normal cell but under physiological stress, autophagy can be employed to recycle spent organelles. Therefore PCD provides a controlled balance to cell proliferation and differentiation. However, in the pathological cell such as the transformed cancer cell, PCD pathways can be deregulated allowing the cancer cell to evade endogenous and exogenous death signals [88, 89]. As described in section 1.5.2, the current standard treatment for GBM is TMZ with radiotherapy. Both TMZ and radiotherapy are DNA damaging agents and cause their cytotoxic effects by inducing apoptosis and to a lesser degree, autophagy.

1.9.1 Apoptosis

Apoptosis is the major pathway of programmed cell death when irreparable cellular stress occurs. The cellular features of apoptotic cell death are cell shrinkage, nuclear condensation (pyknosis) and fragmentation (karyorrhexis), dynamic membrane blebbing and loss of adhesion to neighbours or to extracellular matrix [90]. There are several distinct pathways that culminate in apoptotic cell death. The first three pathways converge on a final common "executor" pathway. These are referred to as the intrinsic, extrinsic and perforin/granzyme pathway. The other pathway, referred to as the caspase-independent pathway involves Apoptosis-inducible Factor (AIF) [91, 92].

The Extrinsic Pathway

The extrinsic pathway involves the binding of death ligands, such as TNF-related apoptosis-inducing ligand (TRAIL) and Fas Ligand, to death receptors such as Death Receptor 4 (DR4) and Fas Receptor at the cell surface. The binding of ligand to receptor results in the formation of a binding site on the intracellular domain of the receptor-ligand complex. This new binding site allows recruitment and binding of adaptor proteins such as TNF receptor-associated death (TRADD) domain and Fas- associated death domain (FADD). The resulting ligand-receptor-adaptor complex dimerises with pro-caspase 8. This complex is known as Death-Inducing Signalling Complex (DISC) and results in the auto-catalytic conversion of pro-caspase 8 to caspase 8. Caspase 8 initiates apoptosis by converging on the final common "executor" pathway beginning with caspase 3 [93].

The Intrinsic Pathway

The intrinsic pathway is initiated by various internal non-receptor signals and stimuli and is mediated by the mitochondria. These signals induce a change in the inner mitochondrial membrane by opening of a Mitochondrial Permeability Transition (MPT) pore leading to increased mitochondrial permeability, loss of mitochondrial membrane

potential and the release of pro-apoptotic molecules such as cytochrome-c, Smac/DIABLO, and the serine protease HtrA2/Omi into the cytoplasm. Cytochrome-c binds with pro-caspase 9 leading to its activation. Controlling these mitochondrial apoptotic events are a family of proteins with pro-apoptotic and anti-apoptotic properties called the Bcl-2 family, such as Mcl-1. This pathway also converges on the final common "executor" pathway beginning with caspase 3 [90, 93]. DNA damage such as that caused by TMZ or radiotherapy can activate both intrinsic and extrinsic pathway [94].

Perforin/Granzyme Pathway

CD8+ cells can kill antigen-bearing cells by not only the extrinsic pathways but also by an alternative pathway. Perforin, a protein stored in granules of the CD8+ cells are released and insert into the plasma membrane of the target cell. These transmembrane proteins form a pore which triggers the release of two serine protease, granzyme A and granzyme B from CD8+ granules into the target cell. These serine proteases can induce apoptosis either by acting on the mitochondria, directly activating caspase 3 or inducing DNA damage [90, 95].

Caspase-independent/Apoptosis-inducible Factor (AIF)

AIF is a 67kDa flavin adenine dinucleotide-containing, NADH-dependent oxidoreductase that is N-terminally anchored to the inner mitochondrial membrane. Apoptotic stimulation results in increased permeability of the outer mitochondrial membrane and cleavage of AIF into a 57kDa soluble fragment. This fragment translocates to the nucleus to participate in large scale DNA fragmentation [91, 92].

1.9.2 Autophagy

Autophagy is an evolutionarily-conserved catabolic process that is mediated by three pathways, macroautophagy, microautophagy and chaperone-mediated autophagy [96]. Macroautophagy is characterised by the formation of the double membrane organelle, the autophagosome. The formation of this organelle requires PI3k- class III, Autophagy related gene 6 (Atg 6 aka Beclin 1), p150 and Atg 14. The formation of these complexes is regulated by several signalling networks which converge on mTOR. Autophagy is inhibited by the activation of the signalling pathways PI3K-I/Akt and MAPK/Erk 1/2. AMP-activated protein kinase (AMPK) can either inhibit or induce autophagy depending on the AMP/ATP ratio. P53 can facilitate or suppress autophagy depending on whether the p53 protein is located in the nucleus or cytoplasm, nuclear p53 facilitates autophagy, whereas cytoplasmic p53 suppresses autophagy. Autophagy occupies a unique position; it can either have a pro-survival or pro-death effect on the cell. It appears that autophagy has a pro-survival role in the normal cell having a tumour suppressive effect. In the tumour cell, autophagy can be pro-death in the early stages of cancer cell transformation or pro-survival in the established cancer cell [97, 98].

1.9.3 Programmed Necrosis

Programmed necrosis, also known as Necroptosis, is morphologically defined as cellular and organelle swelling leading to rupture into the intracellular space. This is a relatively recently discovered pathway in programmed cell death pathways and as such some components of this pathway remain unclear. What is clear is that necroptosis is mediated after TNF ligand binding to TNFR, sharing a common initial pathway with apoptosis. The binding of ligand to receptor activates Receptor-Interacting Protein 1 (RIP 1). Subsequent formation of the RIP1-RIP 3 complex, referred to as the necrosome eventually leads to necroptosis [99-101].

1.9.4 mTORs role in Programmed Cell Death Pathways

mTOR occupies a unique position by acting as a relay point through which pathways involved in growth, differentiation, apoptosis and autophagy, converge. An upregulated mTOR pathway, either through activating genetic mutations (as described above) or through Endoplasmic Reticulum (ER) stress, leads to phosphorylation of p70 S6k, 4EBP1, Akt, and PRAS40 to prevent apoptosis. An upregulated mTOR pathway can suppress autophagy through the phosphorylation of the mammalian homologue of Atg13 and ULK1/2 to promote the association between Bcl-2/Bcl-xL and Beclin 1. This is principally modulated through mTROC1 [102].

1.9.5 Other Points of Crosstalk among Programmed Cell Death Pathways

There is considerable crosstalk and interdependence between the major forms of programmed cell death. Both p53 and p62 play significant roles in the regulation of apoptosis and autophagy. P53 can accumulate in the nucleus and cytoplasmic in the setting of cellular stress signals such as DNA damage by either TMZ or radiotherapy. Cytosolic p53 can promote apoptosis via triggering mitochondrial outer membrane permeability or activating BAX [103, 104] and suppress autophagy in a transcription-independent fashion [105, 106]. Nuclear p53 promotes both autophagy and apoptosis in a transcription dependent fashion [107, 108].

P62 (or sequestosome-1) is a 62kDA multidomain nuclear membrane pore protein that also acts as a signalling hub for apoptosis, autophagy and tumourigenesis [109, 110]. P62 modulates autophagy by activating mTROC1 [111], in turn increased autophagy reduces the cytosolic concentration of p62 as it is targeted to the autophagosome [112].

P62 facilitates the aggregation of the ubiquitinated caspase 8 leading to activation of the extrinsic apoptotic pathway [113].

1.10 mTOR Inhibitors in the Treatment of GBM

Rapamycin, a macrocyclic lactone, was first isolated in the 1960s from the bacterium *Streptomyces hygroscopicus*. This bacterium was found in soil samples from Easter Island [114]. Originally noted for its antifungal activities, it was soon recognised for its immunosuppressive properties and its ability to arrest the cell cycle. Two genes which participated in the toxicity of rapamycin were discovered and named Targets of Rapamycin (TOR) one and two [115]. Three years later the mammalian TOR was identified and its central role in cellular physiology and pathology expanded [83, 116-118].

The mTOR pathway is the most frequently upregulated pathway in GBM. Subsequently, a lot of interest has arisen with attempts to inhibit this pathway. The ability of rapamycin (also known as sirolimus) to inhibit GBM growth *in vitro* and *in vivo* has been studied as far back as 2002 and as recently as 2012 [119, 120], building on this, rapamycin analogues such as temsirolimus (CCI-779, Wyeth, NJ, USA) were identified and investigated yielding positive results *in vitro* and *in vivo* [121] . Based on these findings, phase II clinical trials where commenced in patients with recurrent GBM and demonstrated disease stability in up to 50% of patients with improved time to disease progression. However, overall survival was not improved [122, 123]. Rapamycin and its analogues (sometimes referred to as rapalogs) only partially inhibit mTORC1 activity and does not directly inhibit mTORC2 activity as they bind to a site called the FRB (FKBP-rapamycin-binding) domain. As early as 1995 it was recognised that mTORC1 and mTORC2 activities were regulated by TOR kinase [124]. Second generation mTOR inhibitors were developed to specifically target this fact by competition with ATP at the ATP-binding site of mTOR kinase. These ATP-competitive mTOR kinase inhibitors can

be broadly divided into two classes, dual PI3K/mTOR inhibitors and dual mTORC1 and mTORC2 inhibitors. Both classes demonstrated preclinical efficacy in GBM and are undergoing clinical trials in various solid cancers [125-127].

1.11 Animal models

In vivo experiments are an essential phase in the pre-clinical development of novel therapeutics in oncology. In pre-clinical neuro-oncology research it is vitally important that the tumour under investigation replicates the features of human disease. The majority of animal models tend to use rodents, either mice or rats in immunocompetent or immunocomprimised animals. With immunocompetent animals, there are two options. The first option is that tumour allograft material (such as rodent GBM cell lines) can be transplanted at an orthotopic site. However, this type of tumour does not recapitulate human GBM well. The second option is Genetically Engineered Murine Models (GEMMs). GEMMs can be generated by introducing germ-line or non-germline/somatic modifications. The advantage of this model is that the tumours more closely resemble the human tumour and develops at an orthotopic site in an immunocompetent host. The disadvantage of these models is that there is a long timeline involved in the breeding of germ-line GEMMs. The genes required to cause malignant transformation in the non-germline/somatic models are large and need to be packaged into the viral vectors [128-132].

The second broad option is to use immunocompromised rodents. These animals can receive xenograft human material, either immortalised human GBM cell lines or human GBM material derived from patients and cultured to form spheroids for implantation. This material can be transplanted ectopically into the subcutaneous fat pad. The disadvantage here is the Blood-Brain-Barrier (BBB) is not considered in this model. The BBB is one of the major limitations of developing systemic chemotherapeutic agents in GBM. The other site of implantation can be orthotopic. This model has the advantage of interrogating

human GBM material in its native environment. However in this case immune response is not considered—this can apply to both xenograft and orthograft models.

Another major factor to consider in animal model selection is the mode of delivery of the agent. Systemic agents need to cross the BBB, a tightly regulated barrier separating the central nervous system (CNS) from the systemic circulation. The other option is local delivery into the tumour. To date, no standardised surgical resection model exists for local drug delivery. In chapter 4 we describe in detail the establishment of such a model and its applications for future pre-clinical research.

1.12 Bioluminescence and Bioluminescence Tumour models

The luciferase enzyme is a naturally occurring protein found in various insects such as the North American firefly (firefly luciferase, Fluc) and sea species such as the sea pansy (Renilla Reniformis, Rluc). The substrate for these enzymes is D-luciferin and in the presence of ATP, O_2 and Mg^{2+} luciferin is converted to oxy-luciferin and a photon of light is emitted [133].

Standard cancer cell lines that have been transfected to express the luciferase enzyme using retroviral or lentiviral transductions are available for pre-clinical oncology research. Otherwise human tumour spheroid material can be transduced to express luciferase such as the novel approach employed by Jarzabek et al [134]. These transfected tumours can then be placed into an appropriate animal model. For the study of GBM it is vitally important to use an orthotopic model. Using an orthotopic model places the tumour within the brain parenchyma and "behind" the Blood-Brain-Barrier. As the animals do not produce luciferin, this substrate is injected into the animal and the photons emitted from the tumour material are imaged and quantified. Tumour growth and tumour burden closely correlates with the total flux of photons, i.e. the number of photons emitted per second per unit area. For example the U87MG cell line emits approximately 1250

photons/sec/cell. Bioluminescence models allow the investigator to rapidly image up to 5 animals at a time allowing for high-throughput *in vivo* studies. Using an orthotopic bioluminescence model in immunocompromised animals allows us to interrogate directly retrieved human material. Therefore, using a bioluminescence orthotopic model allows rapid interrogation of actual human GBM material thus achieving statistically significant results in a cost effective manner, facilitating the transition from pre-clinical drug development to clinical trials.

1.13 Rationale of Thesis

Herein we have sought to explore two issues within the sphere of applied pre-clinical GBM translational research. Mirroring the current standard of care in clinical practice of surgical resection followed by adjuvant treatment, we assessed the pre-clinical treatment strategy of combining a novel dual mTORC1/2 inhibitor AZD 8055, with the standard chemotherapeutic agent TMZ which theoretically will promote autophagy while simultaneously augmenting apoptosis induced by TMZ. We began by assessing the *in vitro* efficacy of AZD 8055 in a standard GBM cell line, U87MG and human derived GBM tissue from patient 3. We then assessed the *in vivo* efficacy of AZD 8055 in combination TMZ using the human derived GBM material from patient 3 in an immunocompromised orthotopic murine bioluminescence (BLI) model.

Secondly, we developed a novel surgical resection BLI rat model. This model may have many future applications, from allowing accurate assessment of systemic agents in targeting residual tumour that has diffusely infiltrated the surrounding normal brain parenchyma to advancement of novel intracavity and surgically mediated drug delivery.

Chapter 2: Materials and Methods

2.1 In vitro cell line culture

2.1.1 Cell lines

The Bioware luciferase-expressing GBM cell line, U87MG-luc2, was purchased from Caliper Life Science (A PerkinElmer Company, Hopkinton, MA, USA).

2.1.2 Cell line culture conditions

U87MG-luc2 cells were cultured in Eagle's Minimum Essential Medium (EMEM) (Gibco, Invitrogen, Carlsbad, CA, USA) supplemented with 10 % heat-inactivated foetal bovine serum (FBS), 1 % L-glutamine (2 mM), 1 % penicillin/streptomycin (50 units/ml), all from Sigma-Aldrich (St. Louis, MO, USA).

2.1.3 Sub-culturing of adherent cells

Cells were sub-cultured in a T-75 flask. When the monolayer reached approximately 80 % confluency, the waste media was removed and the cells were washed with sterile Hanks Balanced Salt Solution (HBSS) (Sigma-Aldrich, St. Louis, MO, USA). Cells were then enzymatically detached from the surface of the tissue culture vessel following addition of 2 mls of a 0.25 % Trypsin-EDTA solution (Sigma-Aldrich, St. Louis, MO, USA). The flasks were returned into the incubator for 2-3 minutes and then struck once to ensure total cell detachment. The enzyme was inactivated by adding 5ml in volume of complete growth medium. The cell suspension was then transferred to a sterile centrifuge tube and spun at 1000 rpm for 3 min. The supernatant was removed and the resulting pellet was re-suspended in 10 mls of culture medium pre-warmed to 37°C and seeded at the required density in an appropriate culture vessel. Cells were returned to the incubator and maintained at 37°C in humidified air with 5 % CO2.

2.2 In vitro GBM biopsy-derived spheroid culture

2.2.1 GBM biopsy tissue collection

Human GBM tumour biopsies were obtained during GBM tumour resection surgery performed at Haukeland University Hospital, Bergen, Norway. The collection of tumour tissue was approved by the regional ethical committee at Haukeland University Hospital (Bergen, Norway) and patient (patient #3) gave written informed consent to the use of biopsy tissue for research purposes. Their samples were analysed anonymously.

2.2.2 GBM biopsy-derived spheroid culture conditions

Human GBM tumour biopsy specimens were transferred to 50 ml centrifuge tubes containing complete growth medium i.e. high-glucose (4500 mg/l) DMEM supplemented with 10 % heat-inactivated FBS, four times prescribed concentration of non-essential amino acids (NEAA), 1 % L-glutamine (2 mM), 1 % penicillin/streptomycin (50 units/ml), all from Sigma-Aldrich, (St. Louis, MO, USA) and 0.1 % of Fungizone® Antimycotic (0.25 µg/ml) (Gibco, Invitrogen, Carlsbad, CA, USA). Tumour spheroids were prepared, as previously described [135]. Briefly, tissue specimens were minced into fragments of approximately 0.5 mm in size using sterile surgical blades No. 21 (Swann-Morton, Sheffield, UK) and placed into 75 cm^2 culture vessels (Nalgene Nunc, Thermo Fisher Scientific, Penfield, NY, USA) base-coated with 0.75 % agar (Difco, Detroit, MI, USA). Spheroids were maintained in complete growth medium at 37°C in humidified air with 5 % CO2. The medium and agar-coated flasks were changed once or twice a week.

2.2.3 Preparation of agar coated 6-well plates and agar coated T-75 flasks

Agar-coated flasks were made dissolving Agar Noble (Difco 214230, Becton Dickensen) in sterile water to a concentration of 3% w/v. The solution was boiled in a microwave for 3-5 minutes or until the agar is dissolved. 50mls of agar solution was then added to 150

mls of prewarmed DMEM. 10 mls of this mixture was plated into each T-75 flask and 1ml into each well of the six-well plate.

2.3 Viable cell counting

The harvested cells were counted using a haemocytometer (Hawksley, Sussex, UK). For this method, adherent cell lines were enzymatically detached from the flask using 0.25 % of Trypsin-EDTA, whereas GBM spheroids were dissociated. The cell suspension was then pelleted by centrifugation at 1000 rpm for 3 minutes and re-suspended in 5 or 10 ml of complete growth medium depending on pellet size. 100 µl of the cell suspension was placed in an Eppendorf tube and well mixed with 100 µl of trypan blue (Sigma-Aldrich, St. Louis, MO, USA). 10 µl of the cell suspension containing trypan blue was then transferred onto the haemocytometer and the numbers of live cells (unstained by trypan blue) were counted in 4 sets of 16 corner squares under a phase contrast microscope. To obtain the number of cell per ml, the total count from 4 sets of 16 corner squares was divided by 4, multiplied by 2 to adjust for the 1:2 dilution in trypan blue and multiplied by 10^4, which accounts for the volume of the haemocytometer. Using this method, a representative value of the viable cell number per ml in the original cell suspension was obtained.

2.4 Routine PCR Mycoplasma testing

Mycoplasma is a common laboratory contaminant. It is a small (0.2 µm) intracellular parasitic bacteria with no cell wall, which can grow to high concentrations in mammalian cell cultures. There are no overt signs of mycoplasma contamination and these bacteria are undetectable by standard light microscopy. However, this contamination may induce cellular changes to the infected cells, such as changes in metabolism and growth rates and have profound health consequences if mycoplasma infected cells are implanted into animals. Cell lines and GBM biopsy-based spheroids were therefore routinely tested for mycoplasma contamination using the polymerase chain reaction (PCR) Mycoplasma Test Kit I/C for Conventional PCR (PromoKine, Heidelberg, Germany) according to the

manufacturer's protocol. Briefly, samples of 1 ml supernatant, derived from cell cultures that were 90-100 % confluent, were centrifuged for 5 minutes at 500 x g to pellet cellular debris. The supernatant was transferred to a fresh tube and centrifuged at a minimum of 14 000 x g for 15 minutes. The pellet was then re-suspended in 100 µl DNA free water. Following preparation of the polymerase/rehydration buffer mix (22 µl of rehydration buffer and 1 µl of Taq DNA Polymerase were used per reaction), 23 µl of polymerase/rehydration buffer mix was added into test reaction tubes to rehydrate the lyophilised components of tubes. Following the addition of 2 µl of sample to each test reaction tube except positive and negative control tubes (2 µl of DNA-free water was added to positive and negative control tubes) the tube content was mixed by flicking the tube and incubated for 5 minutes at room temperature. The following PCR program was entered: cycle 1: 94°C for 2 minutes, cycles 2-38: 94°C for 30 seconds, 55°C for 30 seconds, 72°C for 40 seconds, cool down to 4-8°C and tubes were placed in thermal cycler. The reaction components were thoroughly mixed by vortexing the test reaction tubes before loading to 1.2 % standard agarose gel with a 5 mm-comb wells. 8 µl of each PCR reaction was loaded per lane. Electrophoresis was run for 30 minutes at 100 V. Gel evaluation was made under UV lamp. The mycoplasma-positive control and mycoplasma-positive samples showed a band at 270 bp and the internal control band at 479 bp, whereas the mycoplasma-negative control and mycoplasma-negative samples showed only the internal control band at 479 bp. The internal control DNA band at 479 bp indicated a successfully performed PCR.

2.4.1 Results

Figure 3-Mycoplasma test results. Lane 1 is positive control. Lane 2 is negative control. DNA ladder is to the left.

2.5 In vivo studies

All animal experiments were licensed by the Department of Health and Children, Dublin, Ireland. Protocols were reviewed by the Royal College of Surgeons in Ireland (RCSI) Research Ethics Committee (REC). 5-6 week old female NOD/SCID (NOD.CB17-Prkdcscid/J) mice were purchased from Charles River Laboratories International, Inc. (Kent, England) and maintained in SPF-grade scantainers (Scanbur Technology, Karlslunde, Denmark) within the RCSI Biomedical Research Facility (BRF). In each animal facility the animals were allowed to acclimatise for at least 1 week following delivery, prior to commencement of procedures.

2.5.1 Generation of GBM xenograft models

2.5.1.1 Intracranial (i.c.) GBM xenograft models in mice

Animals were anesthetised by intraperitoneal (i.p.) administration of Ketamine (100 mg/kg) (Narketan 10 %, Vétoquinol, Lure cedex, France)/Xylazine (5 mg/kg) (Xylapan®, Vétoquinol, Lure cedex, France). The head of the recipient mouse was secured in a stereotactic frame (David Kopf, Tujunga, CA, USA). Local analgesia/anesthesia (7 mg/kg of Lidocaine or alternatively 8 mg/kg of Marcaine) was applied subcutaneously 3 minutes before a short parasagittal incision was made. A burr-hole was performed 0.5 mm

posterior to the bregma and 2.5 mm to the right of the sagittal suture using a micro-drill. 15 GBM biopsy-derived spheroids with diameters ranging between 300-400 µm were implanted deep to the cerebral cortex and into the caudate/putamen of the mice. GBM biopsy-based spheroids were slowly injected, using an 18G Hamilton syringe (Hamilton, Bonaduz, GR, Switzerland) at 1.5 mm depth below the brain surface. The syringe was left in place for 5 minutes prior to withdrawal. The skin was closed in a single layer with simple interrupted sutures with an Ethilon 3-0 suture (Ethicon Inc., Novartis Animal Health Inc., Basel, Switzerland). After surgery, the animals were placed in a recovery chamber before being returned to their cages. Close observation of the animals was maintained until recovery from anaesthesia and resumption of normal movement around the cage. Following tumour cell implantation, animals were observed daily and animal weights recorded. Any changes in general condition or behaviour were noted in score sheets.

2.5.1.2 In vivo passaging of GBM biopsy-derived spheroids

The pool of GBM biopsy-based spheroids were expanded via serial transplantation in immunocomprimised mice resulting in generation of a standardised pool of spheroids with phenotypically identical characteristics such as invasion and angiogenesis. Comparative genomic hybridisation array confirmed the same genetic alterations present in the primary biopsy and in resulting xenografts as determined previously [136].

2.5.1.3 *In vivo* passaging results

Passaging BLI signal was recorded and analysed each week, displayed an uniform growth kinetic curve with a clear growth exponential phase. At 7 weeks the animals were sacrificed and the brains minced and placed in culture (see Figure 4). These spheroids formed the pool of spheroids for the in vitro and in vivo studies in Chapter 3.

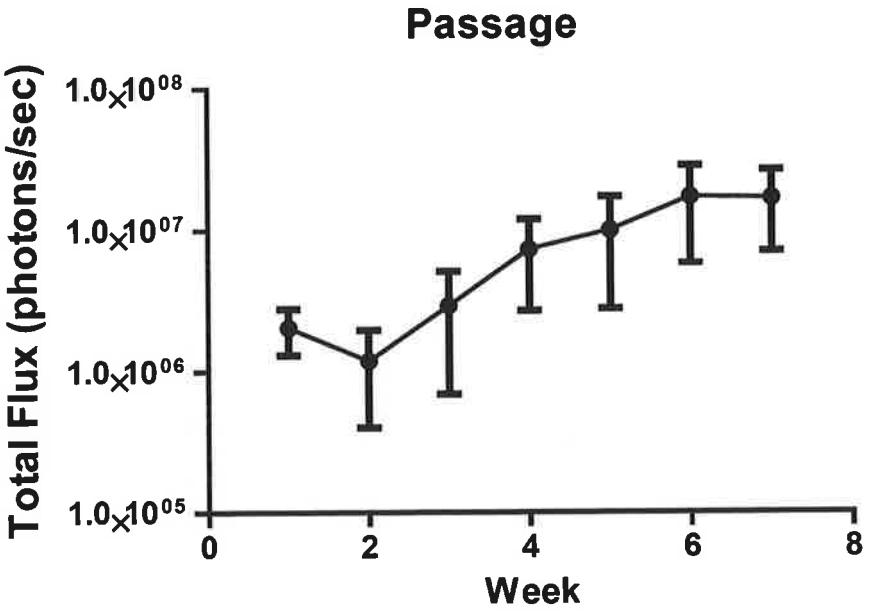

Figure 4-Plot of mean BLI signal from passaging mice (n=5). The BLI signal declined at week two until the tumours become established. From week two onwards the was an exponential growth of the tumour. Error bars represent Standard Error of Mean (SEM).

2.5.2 Implantation of U87 MG- Luc 2 cells in Rats

10 Foxn1^{rnu} T-cell-deficient, athymic nude rats (Charles River laboratories) were weighed and anaesthetized via intraperitoneal delivery of anaesthetic (ketamine (80mg/kg)/ xylazine 10mg/kg). Respiration was closely monitored along with the general condition of the animal. Skin was prepared by removing hair with a depilatory cream. The rats were then fixed in a stereotactic frame and skin disinfected with alcohol.

A small right parasagittal skin incision was made followed by a craniostomy with a high speed dental drill at the level of the bregma 3mm right of the midline. After the dura was punctured, 2µl containing 10^6 U87 MG-luc 2 cells were aspirated using a Hamilton syringe. The syringe was loaded into the stereotactic arm and cell suspension slowly injected at a depth of 2.5mm. The syringe was slowly withdrawn. Any residual cell suspension was removed from the cranium. The skin was closed in a single layer with

4/0 interrupted simple sutures. Animals were monitored post-operatively and returned to their cages when fully recovered.

2.5.2.1 Bioluminescence imaging (BLI) of Rats

D-Luciferin [d-(-)-2-(60-hydroxy-20-benzothiazolyl)-thiazone-4-carboxylic acid](Caliper Life Sciences) formulated into a 30mg/ml solution with DPBS without calcium and magnesium and filtered through a 0.22µm filter, protected from light. A kinetic study was performed at week 1 and 2 post implantation to generate a kinetic curve of luciferase activity. This allowed us to establish the optimum time to peak BLI signal. This can change over time as the vascularisation of the tumour changes. The kinetic study consisted of injecting 150mg/kg of luciferin and imaging the animal at 5 minute intervals for 40 minutes. Images were analysed with Living Image® Software using fixed regions of interest. Animals were imaged in identical fashion each week using peak signal time established by the week 2 kinetic study (see Figure 5).

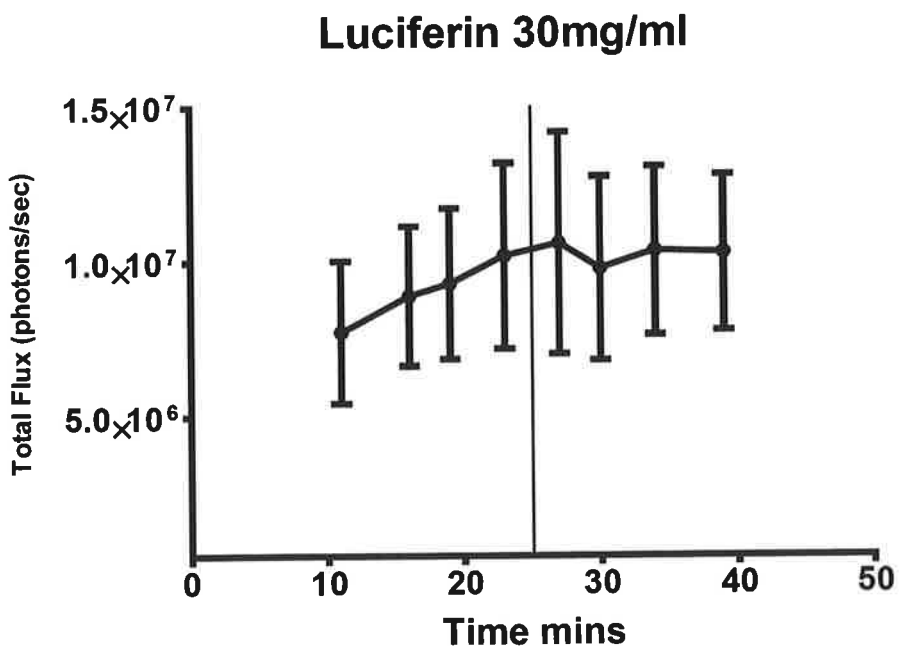

Figure 5-Kinetic study at week 2 was used to establish the optimum imaging time after the administration of luciferin. Peak BLI signal after injection was 25 minutes.

2.5.2.2 Surgical resection

When tumours were in exponential growth phase, as determined by Bioluminescence (BLI) signal, animals were randomised into 2 groups: Control/Non-surgical group and surgical group. The rats were weighed and received an intraperitoneal injection of anaesthetic (ketamine (80mg/kg)/ xylazine 10mg/kg). No antibiotics were administered for the experiment. Animal respiration and general condition were closely monitored. The skin was prepared by removing hair with a depilatory cream. The rats were then fixed in a stereotactic frame and the skin was prepared in standard surgical fashion.

Previous skin incision was extended in a curvilinear fashion and tissues reflected back. The temporalis muscle was sharply dissected from the cranium and reflected and the pericranium incised and also reflected. The previous burr hole was identified. Using an operating microscope and high speed dental drill a 4.5mm craniotomy was made centred on the previous burr hole. A durotomy was made and the tumour located. The tumour was gently dissected free using a combination of gentle suction and tumour dissection. Haemostasis was achieved with a hand-held electrocautery pen with a fine needle tip (Fiab Disposable Cautery Pen - Fine Tip Low Temperature (125mm), Promed, Ireland). The surgical cavity was irrigated and filled with sterile saline.

To repair the cranial defect and to permit post-operative bioluminescence imaging (BLI) 5mm circular glass microscope coverslips (5mm, glass, cat. no. 640700, Harvard Apparatus Ltd, U.K.) were placed and fixed with cyanoacrylate glue (Cyano Veneer Powder A2 25g, Cyano Veneer Fast 4x 5g, Promed, Ireland). The skin was closed in a single layer over the cranial window with 4/0 interrupted simple sutures and cleaned with alcohol. Animals underwent immediate post-operative Bioluminescence Imaging (BLI) and were returned to their cage when fully recovered. Animals were weighed daily post-

operatively and assessed for surgical site infection, such as erythema or wound discharge. The animals were also observed for changes in their general and neurological condition, such as lethargy or hemiparesis.

2.5.3 Preparation of AZD8055 and TMZ for in vivo administration

2.5.3.1 Vehicle preparation:

Captisol (β-cyclodextrine sulfobutyl ethers, sodium salts; Cydex, USA) was added to 60% required final volume water for injection and stirred. Once it was completely dissolved, the resulting solution was made up to final volume with water for injection. Before refrigeration the 30% capitsol solution was sterilized by filtration (0.22μM). This stock solution could be stored for up to 1 month stored at 4°C.

For treatment of mice, AZD8055 was weighed into an amber glass bottle and mixed with approximately 90% of the final required volume of 30% Captisol. The pH was adjusted to approximately 5.2 with 1M HCl and the solution was sonicated and vortexed for 2-3 minutes until complete solubilisation. The pH was then adjusted to 5.0 and the resulting solution is made up to the final volume with 30% Captisol. The solution was stored at room temperature, in the dark, for up to 7days. Temozolomide dosing solution was made up in a similar manner.

2.5.3.2 Routes of drug administration in vivo

2.5.3.2.1 Oral gavage (p.o.) administration

Mice were firmly restricted by pulling up the loose skin on the flanks to immobilize the head and straighten the mouse body. A 22 gauge x 25 mm curved oral dosing needle (VetTech Solutions Ltd., Cheshire, UK) was inserted down the oesophagus and freshly formulated AZD 8055/Temozolomide or vehicle alone was slowly injected. The needle

was carefully withdrawn and immediately following drug administration the animals were returned to their cages and monitored for any adverse effects.

2.5.3.2.2 Treatment regimen of Temozolomide and AZD8055

The mice assigned to the AZD8055 groups received AZD8055 via oral gavage at 15mg/kg once daily (o.d.). The mice assigned to the TMZ groups received TMZ via oral gavage at 25mg/kg once daily. There were four treatment groups of animals consisting of vehicle, TMZ, AZD and AZD+TMZ (see Table 1).

Table 1- Treatment regimen of the four animal groups

Group	Treatment Regimen
Vehicle	Week 4.5 - 8.5 : 30% Capistol
TMZ	Week 4.5-5.5 : 25mg/kg p.o. once daily (o.d.)
AZD8055	Week 4.5-8.5 : 15mg/kg p.o. o.d. x 4/52
TMZ+AZD8055	Week 4.5-5.5 : 25mg/kg (TMZ) p.o. o.d.& 15mg/kg p.o. o.d. (AZD) Week 5.5-8.5 : 15mg/kg p.o. o.d. (AZD)

2.5.3.2.3 Intraperitoneal (i.p.) administration of Luciferin

Mice were firmly immobilised by pulling up the loose skin on the flanks. The head and body were tilted downward. The right lower abdominal wall was disinfected with 70% isopropyl alcohol swabs (MidMeds Limited, Essex, UK). Freshly formulated luciferin solution alone was quickly injected into the peritoneal cavity using a 26 gauge 3/8" (10 mm) brown needle (BD Biosciences, Franklin Lakes, NJ, USA). Immediately following bioluminescence imaging, the animals were returned to their cages and monitored for any adverse effects.

2.6 In vivo bioluminescence imaging (BLI)

In vivo BLI was performed using the IVIS Spectrum (Caliper Life Science, PerkinElmer Company, Hopkinton, MA, USA). Before *in vivo* BLI, the heads of each mouse were shaved to decrease attenuation and scattering of transmitted light by hair. Approximately 5 minutes following an i.p. injection of 150 mg/kg of D-luciferin (Caliper Life Science, PerkinElmer Company, Hopkinton, MA, USA), animals were anaesthetised with isoflurane/O_2 mixture and BLI began 10 minutes after D-luciferin administration. Isoflurane/O_2 anaesthesia was maintained during imaging by nose cone delivery. *In vivo* BLI of luciferase expression were attained using a 1-120 seconds exposure time with medium binning, f-stop of 1 and field of view (FOV) D (22.5 cm, when 5 mice imaged at the same time), C (12.5 cm, when 3 mice imaged at the same time). Parameters were adjusted to obtain the *in vivo* bioluminescent signal above the noise level (recommended > 600 counts) and below CCD saturation (< 60 000 counts). A region of interest (ROI) was traced around the tumour area manually and corresponding total flux photons/seconds values were obtained for each image.

2.7 Ex vivo optical imaging

Immediately after necropsy, brains were washed in D-PBS and placed on sterile Petri dishes which were then placed inside the IVIS Spectrum imaging suite. To assess *ex vivo* bioluminescent signal 200 µl of D-luciferin (15 mg/ml) was added topically immediately before *ex vivo* imaging. *Ex vivo* BLI images were attained using a 1-60 seconds exposure time with medium binning, f-stop of 1 and field of view C (12.5 cm).

2.8 Histology

2.8.1 Tissue processing

The brains were carefully dissected from the cranial vault and placed in 10 ml of 10 % neutral buffered formalin (Sigma-Aldrich, St. Louis, MO, USA) for 48 hours to allow tissue fixation. Following fixation, the tissues were transferred to cassettes and using a histokinette tissue processor (Leica TP1050, Leica Microsystems, Wetzler, Germany) were dehydrated and paraffin wax embedded. Tissue samples were passed through formalin twice at room temperature for 1 hour each, dehydrated through increasing concentrations of ethanol (70 %, 95 %, 100 %, 100 % v/v) at room temperature for 1 hour each and then cleared in xylene at room temperature for three steps of 1 hour each. Samples were then passed three times through histowax at 60°C for 1 hour each. Tissues were then implanted in a new paraffin block and allowed to solidify at room temperature. Blocks of wax embedded samples were kept on ice before serial sectioning using a microtome (Leica RM2255, Leica Microsystems, Wetzler, Germany), which sliced the samples at 5 µm thick sections. These sections were mounted on adhesive superfrost plus slides (Gerhard Menzel, Thermo Fisher Scientific, Braunschweig, Germany) and examined further.

2.8.2 Haemotoxylin and eosin (H&E) staining

Routine hematoxylin and eosin (H&E) staining and analysis of U87 GBM tumour sections was performed by a veterinary pathologist Prof. Sean Callanan, School of Veterinary Medicine, Veterinary Science Centre, University College Dublin (UCD), Ireland. Briefly, formalin-fixed paraffin-embedded (FFPE) tissue sections were placed on a heating plate at 65°C for 10 minutes and the melted paraffin was wiped off. Following de-paraffination, performed in xylene (Sigma-Aldrich, St. Louis, MO, USA) or alternatively in Histo-Clear II (National Diagnostics, Atlanta, GA, USA) (2 x 5 minutes), the tissue sections were re-hydrated in descending gradient alcohols (2 x 3 minutes in 100 % ethanol and 2 x 3 minutes in 96 % ethanol/dH_2O) and dH_2O (1 x 2 minutes). The slides were then stained in acid hematoxylin solution (Sigma-Aldrich, St. Louis, MO, USA) for 5 minutes followed

by rinsing in running tap water for 20 minutes and de-colorization in 1 % acid alcohol for 1 second. Tissue sections were further rinsed in running tap water for 5 minutes and stained with alcoholic eosin Y (Sigma-Aldrich, St. Louis, MO, USA) for 30 seconds, washed with dH_2O and de-hydrated in ascending gradient alcohols (2 x 3 minutes in 96 % ethanol/dH_2O and 2 x 3 minutes in 100 % ethanol). Following, clearing with xylene or histo-clear II (2 x 5 minutes), the DPX mounting medium (Sigma-Aldrich, St. Louis, MO, USA) was used to mount cover slips on the sections.

2.9 Microscopy

2.9.1 Light microscopy

Light microscopy was used as a standard tool to count cells (via haemocytometer), to study cell morphology during cell culture and to obtain images of tissue sections following H&E. Objective lenses used were between x4 to x40 magnification with an eyepiece x10 magnification. Eclipse E600 (Nikon, Tokyo, Japan) and the Olympus CKX 41 (Olympus, PA, USA) were used.

2.10 In Vitro studies of AZD 8055 cell-signalling pathway effects in U87MG cell line and P3 patient-derived GBM spheroids

2.10.1 Spheroid dissociation

2.10.1.2 Dissociation of GBM biopsy-derived spheroids

Initially, spheroids were dissociated to single-cell suspension by two methods to assess the optimum method for protein yield for subsequent western blots. Method 1. The neuronal tissue dissociation kit (NTDK, Miltenyi Biotec, Bergisch Gladbach, Germany) was used according to the manufacturer's protocol. Briefly, the tissue was minced into small pieces, washed in 1 ml of cold HBSS free of Ca2+ and Mg2+ (HBSS (w/o), Sigma-Aldrich, St. Louis, MO, USA) and centrifuged at 300 x g for 2 minutes at room temperature. The supernatant was carefully aspirated and the tissue pellet was re-

suspended in 1950 µl of pre-warmed (37°C) enzyme mix 1 (50 µl of solution 1 and 1900 µl of solution 2). Following this, the tissue pellet was incubated with agitation in a water bath at 37°C for 15 minutes, 30 µl of enzyme mix 2 (20 µl of solution 3 and 10 µl of solution 4) was added and the sample was mixed by gentle inversion. The tissue was then mechanically dissociated 10 times by slowly pipetting up and down following incubation with agitation in a water bath at 37°C for 10 minutes. This step was repeated twice and the cell suspension was applied to a 40 µm cell strainer placed on a 50 ml tube. The cell strainer was washed with 10 ml of HBSS with Ca2+ and Mg2+ (HBSS (w), Sigma-Aldrich, St. Louis, MO, USA). Finally, the cell suspension was centrifuged at 300 x g for 10 min at room temperature, the supernatant was aspirated and cells were re-suspended in complete growth medium for further applications. Method 2. Direct mechanical lysis of the spheroids with RIPA buffer by continuous pipetting with a 1 ml pipette over ice until the spheroid was completely dissociated. RIPA buffer was made with 50mM Tris HCl pH 8, 150 mM NaCl, 1% NP-40, 0.5% sodium Deoxycholate, 0.1% SDS to which phosphate and protease inhibitors were added. 150µl of RIPA buffer and phosphate/protease inhibitor were added to the spheroid suspension. For 20 minutes the spheroids were mechanically lysed over ice and the suspension spun at 10,000g(RCF) in the cold room for 20min.

2.10.1.2.1 Results

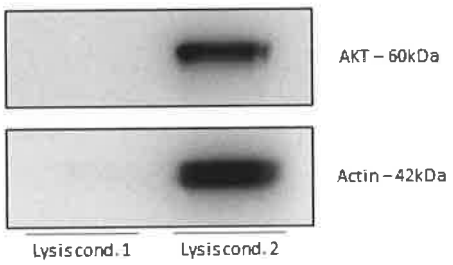

Figure 6- Lysis condition 1 with neural dissociation kit. Lysis condition 2 with direct mechanical lysis demonstrates that mechanical lysis of the treated spheroids was a more efficient method for protein

extraction. 150 µl of lysate was used. AKT was used as a test protein to establish which method yielded higher protein concentrations.

2.10.2 U-87MG Cell harvesting from 6-well plate

The cells were scraped using a standard cell scraper on ice. The resulting suspension was transferred to a 15ml tube and centrifuged at 1000rpm. The supernatant was removed and 1.5ml of PBS was added. The resulting suspension was added to an Eppendorf tube and centrifuged at 1000rpm for 3 minutes. Again the supernatant was removed and the resulting pellet lysed with 150µl of RIPA buffer with phosphatase and protease inhibitors.

2.11 BCA assays and Western Blots

Bicinchoninic Acid (BCA) assays and Western blots were performed by the post-doctorate researcher, Dr Lorna Flanagan, Ph.D at R.C.S.I. Briefly, using a Micro BCA protein determination kit (Thermo Scientific, USA) BCA reagents A, B and C where made up in the ratio of 25:25:1. 150ul of the mixture was added to 150ul of 0.9% NaCl in each well of a 96-well plate. Bovine Serum Albumin (BSA) was used as a standard. The 96 well plate was placed into an incubator at 37°C for 30 minutes and the plate was then read using the Tecan plate reader at 562nm absorbance.

The desired % of SDS-PAGE gel was made up according to the molecular weight of the proteins. The amount of protein added was calculated from the BCA assay. Once the gels were run, wet transfer was performed. Ponceau S was used to stain the ladder. 5% BSA made up in TBS-T was used as a blocking solution at 4 °C overnight. The primary antibodies where made up as per manufacturer's instructions and left overnight at 4 °C. The secondary antibody was made up in blocking buffer and placed on the TBS.T washed

blot for one hour. ECL detection reagent (Amersham Biosciences, Buckinghamshire, UK) was poured over the membrane and images taken on the image reader.

2.12 Statistical methods

Statistical methods used to analyse the difference between groups were performed using GraphPad (San Diego, CA, USA) and SPSS (IBM Corporation, Armonk, NY, USA). Data are given as means ± S.E.M (standard error of the mean). A one-way analysis of variance (ANOVA) followed by post hoc analysis were employed. Kaplan-Meier survival analysis using with Log-rank (Mantel-Cox) tests were also used. Determined p values when < 0.05 were considered to be statistically significant.

Chapter 3: Investigation of the effects of combining Temozolomide with the mTOR inhibitor AZD8055, *in vitro* and using an orthotopic animal model

3.1 Introduction

Current standard of care for GBM as established in 2005 by the landmark phase 3 clinical trial paper is maximal safe surgical resection followed by radiotherapy and concomitant temozolomide (TMZ) with adjuvant TMZ [28]. Survival before this trial was abysmal with a 2-year survival of 7% and median of 7.5 months. After widespread adoption of this regimen, recent population based studies show survival improving to 28% for 2-year survival and 16.5 months median [51]. These statistics are in sharp contrast to the potentially curable cancers such as breast or colorectal carcinomas.

Temozolomide is an orally bioavailable alkylating agent which produces DNA damage by placing a $-CH_3$ group at the O6 or N7 positions of guanine residues forming O6-methylguanine (O6-MeG) DNA adducts (see Figure 7). The methyl group is often removed by the DNA repair enzyme O6-methylguanine-DNA methyl transferase (MGMT) [33, 137].

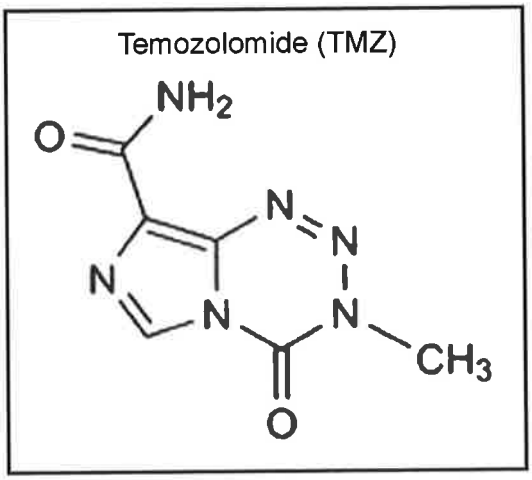

Figure 7-Chemical structure of temozolomide

Ionizin uces the formation of DNA double-strand breaks (DSBs). Like the DNA damage induced by temozolomide the mismatch repair system of enzymes are activated [138]. Depending on the p53 mutation status of the tumour, Apoptosis or Type I programmed cell death is mediated through Fas-R-Caspase-8 in wild-type and Bcl-2-caspase-9 in mutated p53 tumours [33, 94]. Therefore, the

current standard of care achieves its limited therapeutic effect via a single approach, the induction of apoptosis via DNA damage with a key prognostic factor in how the patient will respond to this strategy being the methylation status of the promoter region of the MGMT gene (see section 1.7).

Genetic mutations in GBM give rise to dysregulation of five principal intracellular pathways PI3K-PTEN-Akt-mTOR, RAS/MAPK/ERK , JAK/STAT3 , pRB signalling , p53 signalling [53]. These pathways have become attractive targets for the preclinical investigator. As the current standard of care for GBM confers only a 28% chance of two year survival by inducing apoptosis and considering the fact that the most frequently upregulated pathway involves mTOR, which also modulates apoptosis and autophagy, we sought to augment and build upon the modest success of the "Stupp Protocol" by using a dual mTORC1/2 inhibitor, AZD 8055.

AZD8055 is a an orally bioavailable ATP-Competitive mTOR kinase Inhibitor [126]. This small molecule, based on a pyridopyrimidine scaffold inhibits both mTORC1 and mTORC2 activity and is a strong inducer of autophagy *in vitro* and *in vivo* [126] (see Figure 8). Recently, AZD8055 has shown to be efficacious as a monotherapy, *in vitro* and *in vivo*, against pheochromocytoma [139], B-cell follicular lymphomas [140] and acute myeloid leukaemia [141]. To date only one published article describes AZD8055 efficacy in GBM. In this report, Chresta et al demonstrated a dose-dependent reduction in GBM tumour volume. Utilising a subcutaneous mouse model, the authors injected 10^6 U87MG cells into the flanks of female nude mice. Tumour volume was calculated using caliper measurements and the following equation: (length × width) × $\sqrt{}$(length × width) × (π/6). They recorded a stepwise reduction in tumour volume, compared to control, of 33%, 48%, and 77% with a dosing regimen of 2.5, 5, and 10 mg/kg/d twice daily, respectively. To our knowledge this is the only report of using AZD8055 in the pre-clinical investigation of GBM in combination with TMZ [126].

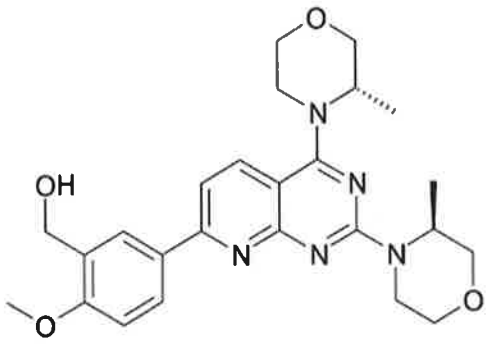

Figure 8- Chemical structure of AZD 8055 from Chresta et al (2010)

As it is the combination of TMZ and RTx, after maximal surgical resection that has had the greatest impact on patient survival, a large proportion of preclinical investigations involve combining standard treatment with novel drugs that act on one or more of the aforementioned dysregulated pathways.

In this chapter we examined the *in vitro* efficacy of AZD 8055 in the standard GBM cell line U87 and in patient derived GBM tissue. We then proceeded to assess the *in vivo* efficacy of AZD 8055 in combination with TMZ using the same patient derived GBM material in an orthotopic BLI murine model. To help explain our *in vivo* results we interrogated pathways related to Programmed Cell Death and growth/proliferation and the points of cross-talk.

3.3 Results

3.3.1 *In Vitro* investigation of the Efficacy of AZD 8055 in the Standard GBM cell Line U87MG and human GBM material From Patient 3

We demonstrated *in vitro* the ability of AZD8055 to inhibit both mTORC1 and mTORC2 in a dose dependent manner in both human GBM spheroids from patient 3 and the standard GBM cell line U87MG. There was a dose dependent reduction in

phosphorylated mTOR compared with total mTOR, phosphorylated AKT compared with total AKT and phosphorylated p70 compared with total p70 (see Figure 9).

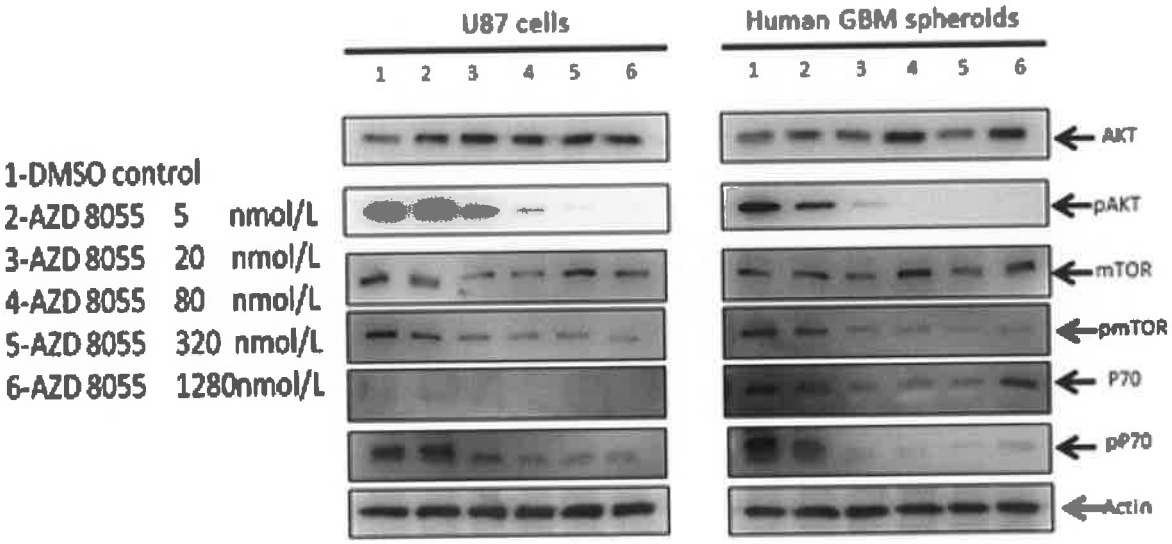

Figure 9- *In Vitro* efficacy of AZD 8055 in the standard GBM cell line U87MG, western blot on the left and human GBM material from Patient 3, western blot on the right. The concentration of AZD 8055 for each lane is displayed to the left of the western blots. There is a dose dependent inhibition of downstream phosphorylation products of mTROC1 and mTORC2.

3.3.2 *In Vitro* investigation of the Efficacy of AZD 8055 in combination with TMZ in human GBM material From Patient 3.

As we only use GBM spheroids from patient 3 in the *in vivo* efficacy studies we interrogated points of cross talk between PCDs and parallel metabolic pathways using human GBM spheroids from patient 3. When these spheroids were treated with a constant concentration of TMZ and a variable dose of AZD, we noted a dose dependent reduction in p62, MCL-1 and procaspase-3 (see Figure 10). The concentration of TMZ at 150μm has previously been demonstrated to correspond with the levels achieved in the serum of patients during treatment [142].

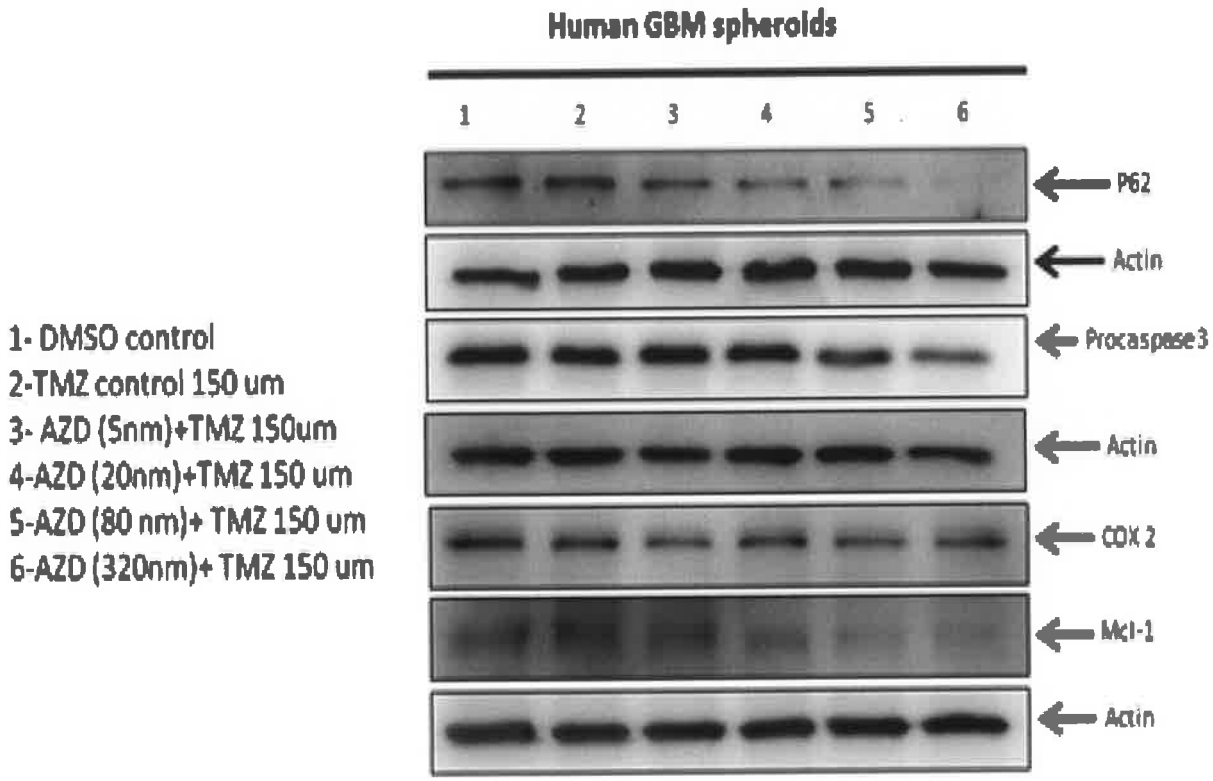

Figure 10- In Vitro demonstration of the combined effect of a constant concentration of TMZ and a variable dose of AZD 8055 on human GBM spheroids. There is a dose dependent reduction in p62, Procaspase 3 and Mcl-1.

3.3.3 In vivo Efficacy of AZD8055 combined with TMZ in an Orthotopic BLI Murine Model using human derived GBM tissue

3.3.3.1 Pre-treatment BLI growth curve

The pre-treatment BLI signal was recorded and analysed each week after implantation and displayed a uniform exponential growth curve. At 4.5 weeks, when the GBM tumour was in a linear growth phase, the animals were randomised into 4 groups for treatment as per regimen in Table 1 (see Figure 11).

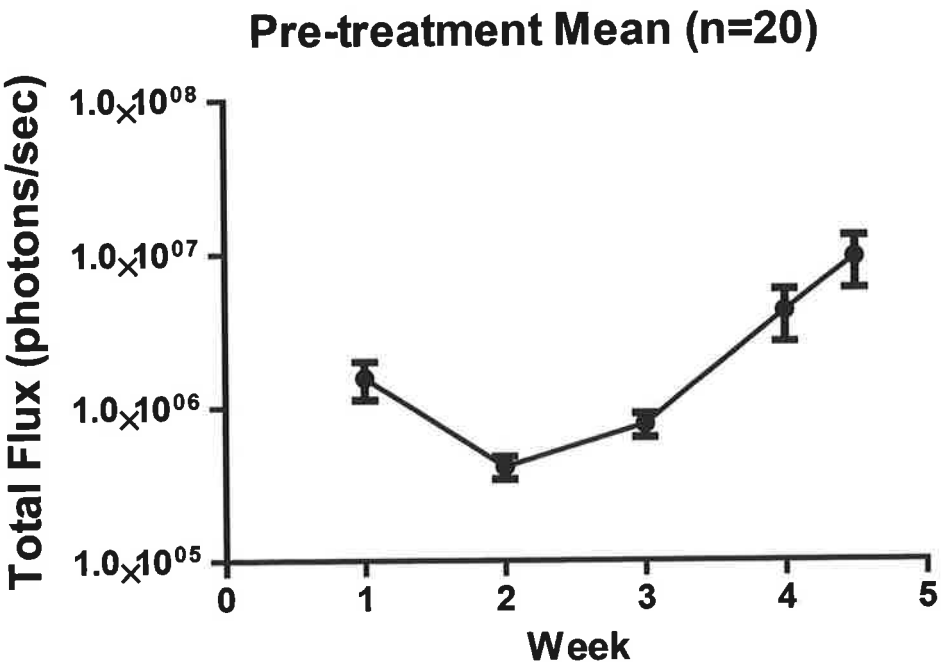

Figure 11- Plot of mean Pre-treatment BLI/tumour growth curve. As expected there is a drop in BLI signal in the first week after implantation. From week 2 onwards as the tumour becomes established there is an exponential growth phase. Error Bars represent SEM.

3.3.3.2 Survival Analysis

Kaplan-Meier survival analysis with Log-rank (Mantel-Cox) test was performed with statistical significance set at $p<0.05$ (see Figure 12). The group that was treated with TMZ alone was the only group to show a significant survival advantage $p=0.0218$, Hazard Ratio =7.561 (median survival of 30.5 days). There was no significant survival advantage in either the AZD monotherapy group $p=0.4995$ (median survival of 11 days) and AZD+TMZ combined group $p=0.2314$ (median survival of 22 days) when compared to the vehicle (median survival of 14 days).

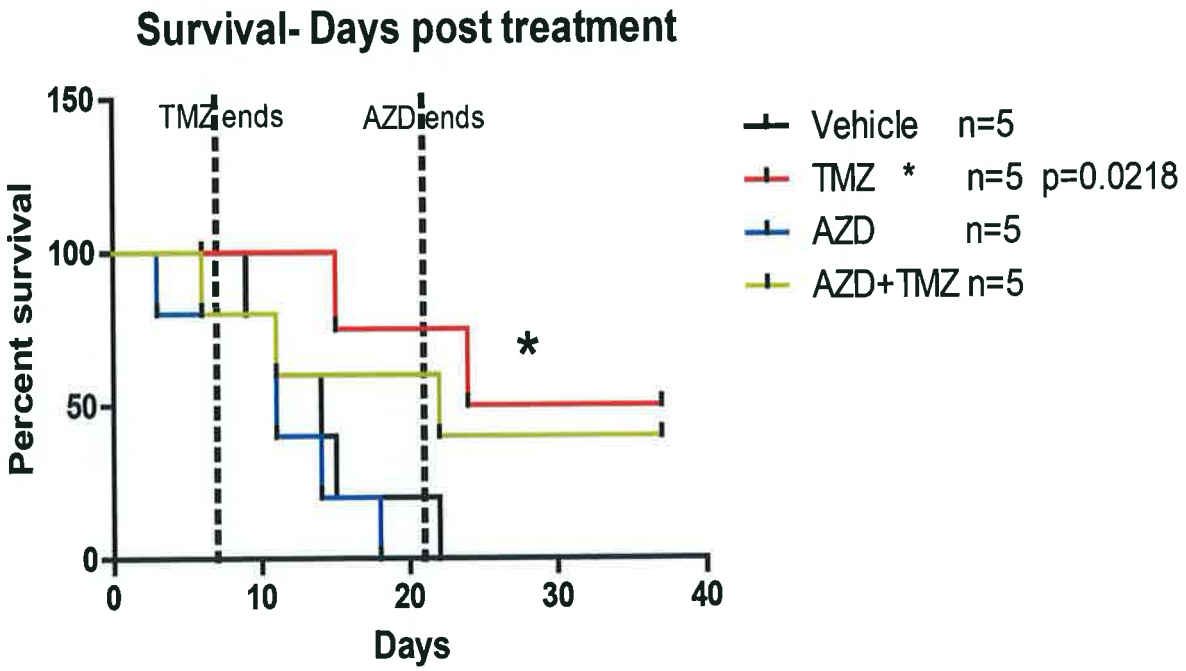

Figure 12- Kaplan Meier Survival analysis with Log-rank (Mantel-Cox) test. There is a statistically significant survival benefit to the group receiving TMZ (red). The group receiving AZD 8055 as monotherapy (blue) had no survival advantage. Although the combined group (yellow) displayed a survival curve similar to the AZD 8055 monotherapy group, this trend did not reach statistical significance.

3.3.3.3 Bioluminescence Signal from GBM tumours as a response to Treatment

Bioluminescence signals were analysed and plotted each week (see Figure 13). Treatment of the groups began at 4.5 weeks. The vehicle group displayed a uniform and typical growth kinetic shape. The temozolomide group growth curve closely follows the vehicle group from 4.5 weeks to the end of treatment at 5.5 weeks. After TMZ treatment ceases there was a notable decrease in the BLI signal of the TMZ group which indicated the treatment effect. The TMZ treatment effect becomes maximal at 6.5 weeks as evident by the reduction in BLI signal, which corresponds to reduced tumour burden. After the first week of TMZ treatment, there was no statistically significant difference between the

means in each group using two-way ANOVA with Bonferroni post-test analysis ($p<0.05$). However, by the second week there was a statistically significant difference between the vehicle group and the TMZ group, $p=0.0205$ (see Figure 14).

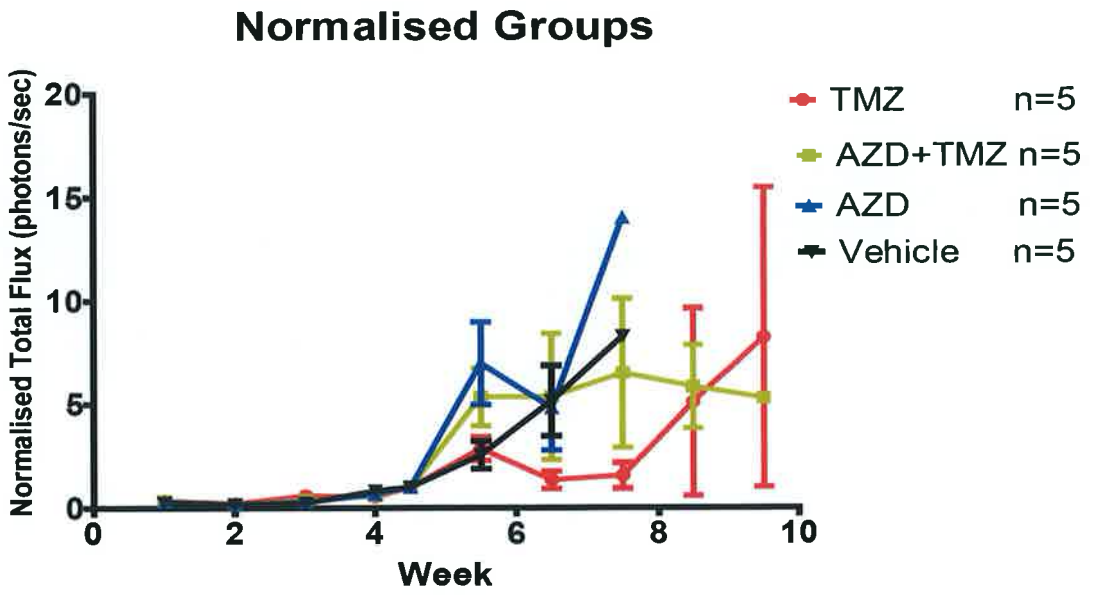

Figure 13- Plot of normalised total flux of photons the four treatment groups. Treatment commenced at week 4.5. Groups receiving AZD8055 did so for 4 weeks. Groups receiving TMZ did so for one week, from week 4.5-5.5. Error bars represent SEM. The study endpoints were signs of morbidity.

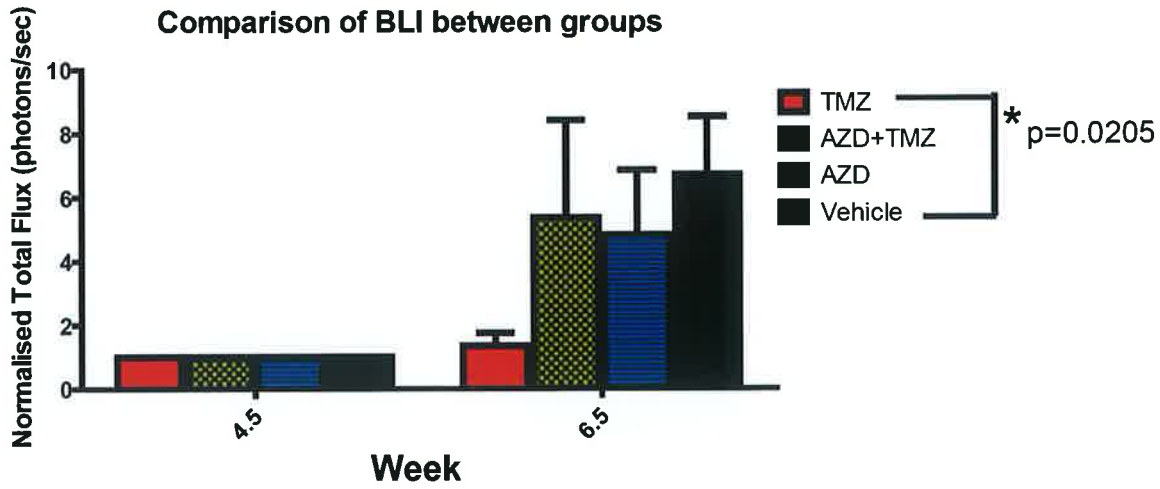

Figure 14- Bar chart displaying the statistically significant treatment effect of TMZ as monotherapy in vivo at 2 weeks compared to the vehicle group using one-way ANOVA with post-hoc analysis. Error bars represent SEM

3.4 Discussion

The single greatest improvement in GBM patient survival in the last 50 years has been attributed to the widespread adoption of the "Stupp Protocol". This protocol was established in the landmark phase 3 clinical trial, which consists of maximal safe surgical resection followed by radiotherapy and concomitant TMZ with adjuvant TMZ [28, 51]. Since that trial, a greater understanding has been acquired of the genetic mutations involved in the pathogenesis of primary GBM. Up to 88% of primary GBMs display genetic alterations in the RTK/PI3K/mTOR pathways [53]. mTOR is a serine/threonine kinase belonging to the phosphatidylinositol kinase kinase (PIKK) family of proteins. It assembles into two discrete complexes mTORC1 and mTORC2.

These two complexes lie at the centre of a sophisticated intracellular relay point that co-ordinates intracellular and extracellular signals through positive and negative feed-back and feed-forward loops with cross-talk between other pathways such as MEK-ERK [143-146]. By competitive inhibition with ATP at the ATP-binding cleft of mTOR kinase, AZD8055 inhibits both mTORC1 and mTORC2.

The human GBM material used in this paper was obtained from Patient 3 at Haukeland University Hospital (Bergen, Norway) where written informed consent for the use of the tissue for research purposes was obtained. Genetic profiling has revealed a hemizygous deletion of the PTEN gene and EGFR amplification. The U87MG cell line is an immortalized GBM cell line whose complete genome has been deciphered [136, 147].

Table 2- Highlighting the essential mutations involved in the mTOR pathway

GBM Material	PTEN deletion	EGFR amplification
U87MG	Homozygous	Yes
Patient 3 GBM spheroids	Hemizygous	Yes

Both GBM cell lines and Patient 3 GBM spheroids used have mutations that can up regulate the RTK/PI3K/mTOR pathways due to the EGFR amplification and PTEN deletions underscoring the rationale for inhibiting this pathway. We were able to demonstrate the ability of AZD8055 to inhibit both mTORC1 and mTORC2 *in vitro* by virtue of the decreased upstream and downstream phosphorylation products of these two complexes namely p70, pAKT and pmTOR . However, we failed to demonstrate *in vivo* efficacy of AZD 8055 when used as monotherapy or combined with the standard chemotherapeutic agent, TMZ. The model that we employed was significantly different to the model utilised by Chresta et al. Firstly, we used a different strain of mouse (NOD SCID/J strain). Secondly, we used a 20mg/kg once daily oral dosing regimen, compared to Chresta et als 10mg/kg twice daily oral regimen. Thirdly, we utilised patient derived human GBM material *in vivo* instead of a standardised GBM cell, however both U87MG and the human P3 spheroid material both have genetic alterations in PTEN and EGFR. Lastly, and perhaps most importantly, we used an orthotopic model. In our model the tumour was implanted into the right hemisphere of the recipient mouse. This placed the tumour behind the Blood-Brain-Barrier. This tightly regulated pharmacological barrier is one of the greatest impediments to CNS drug development. AZD and the combined AZD+TMZ group did not show either a survival benefit or tumour response that was statistically significant. This was in contrast to TMZ when used as monotherapy where, as expected, we demonstrated a statistically significant difference in BLI signal at two weeks following commencement of treatment, which correlated with a statistically significant survival advantage for this group.

Recent insights into the complex feed-back loops and cross-talk with other pathways may help to explain our observed findings of *in vitro* blockade of the mTOR pathways but poorly translated *in vivo* efficacy of dual blockade of mTORC1 and mTORC2.

AKT is a serine/threonine protein kinase that has two phosphorylation sites, serine 473 (S473) and threonine (T308). Phosphorylation at the T308 site is required for AKT kinase activity and phosphorylation at the S473 site is required to stabilise T308. mTORC2 phosphorylates AKT at S473. mTORC1 and mTORC2 function as both upstream and downstream effectors of AKT. mTOR kinase inhibition appears to cause a feedback-dependent biphasic regulation of AKT signalling [148]. In their *in vitro* study, Rodrik-Outmezguine et al demonstrated that there is rephosphorylation of T308 and that of other AKT substrates after 4 hours despite persistent dephosphorylation at S473. They further demonstrated that the rephosphorylation of T308 is caused by PI3K-dependent localization of PDK1, the T308 kinase, to the cell membrane. Furthermore attempting further upstream blockade using PI3K inhibitors or AKT inhibitors can lead to upregulation of RTK signalling [149].

The RAS/MAPK/MEK/ERK is another pathway frequently dysregulated in GBM. This pathway which is involved in the control of growth and differentiation is also regulated by growth factor receptors such as EGFR [150]. Recent evidence suggests that there is substantial cross-talk between both the PI3K/AKT/mTOR pathway and the MEK/ERK pathway not only at the RTK level but also downstream at the level of Tuber Sclerosis Complex 2 (TSC2), E-twenty-six (ETS)-like transcription factor 1 (Elk-1) [151] and p70S6K [152]. In the normal development of the oligodendrocyte from early progenitor to a mature glial cell there is sequential regulation of both pathways [153]. However in the setting of GBM both of these pathways can be up regulated and blockage of either one can lead to further up regulation of the other. This appears to be due to a p70S6K mediated feedback loop [145]. We were able to demonstrate using AZD8055 in both *in vitro* cell culture models that there was a dose dependent reduction in phospho-P70S6K.

The reduction in phospho-P70S6K has been shown to cause increased phospho-ERK and subsequent upregulation of the MEK/ERK pathway [145]. Conversely, blockade of the MEK/ERK pathway leads to upregulation of the PI3K/AKT pathways by a dominant feedback loop involving receptor tyrosine kinases [154]. Recently, Li et al have shown possible crosstalk exists between three of the major upregulated pathways JAK/STAT, PI3K/Akt and MEK/ER [155]. Thus, an alternative therapeutic strategy might be to target both pathways via simultaneous blockade at points of convergence, for example using receptor tyrosine kinases inhibitors that specifically block RTKs involved in PI3K/mTOR, STAT3 and MEK/ERK pathways or dual PI3K/ERK inhibitors such as AEZS-136. The former is more technically challenging considering the number and types of mutation that can occur in RTKs.

Finally, autophagy is an umbrella term for the evolutionarily conserved processes including macroautophagy, microautophagy and chaperone-mediated autophagy [96]. Recently in the literature, autophagy has been shown to have several opposing roles- it can either be pro-cell survival (during periods of nutrient, hypoxic or metabolic stress) or pro-cell death. Autophagy can also be involved in tumourigenesis by having a tumour suppressor role [156, 157]. It appears that both autophagy and apoptosis are initiated in glioblastoma cells when treated with TMZ [158, 159] and therefore augmenting induced autophagy while the GBM cell was undergoing cytotoxic/apoptotic cell death underscored our rationale for using AZD 8055 with TMZ. P62 or sequestosome-1 is a multidomain protein that acts as a signalling hub for apoptosis, autophagy and tumourigenesis [160, 161]. Huang et al have recently demonstrated that cytotoxic cell death induced by DNA damage can be attenuated by the simultaneous induction of autophagy through the inhibition or the mTOR pathway. This is due to downregulation of p62 [162]. We too noticed a dose response effect on p62 clearance in the human spheroids treated with concurrent TMZ and AZD8055. Thus, it would appear in the current study (and consistent with other published findings) that inhibiting a single upregulated pathway, such as the

PI3K/mTOR is not a feasible treatment strategy, as autophagy is induced and that the body of evidence implicates autophagy as a cytoprotective response in this scenario of DNA damage induced apoptosis. It appears that autophagy is induced by inhibition at all key points along the EGFR-PI3K-mTOR pathway e.g. EGFR tyrosine Kinase inhibitors (TKIs) [163], dual PI3K/mTOR inhibitors [127] and dual mTORC1/mTORC2 inhibitors [126]. Our observations suggest a rationale for using autophagy inhibitors such as chloroquine in GBMs having intact autophagy machinery.

In short, we hypothesise that although there is substantial crosstalk among these pathways and reciprocal regulation where if one pathway is blocked the other is upregulated this cannot fully explain our results when compared to other authors who have demonstrated both *in vitro* and *in vivo* efficacy in a wide range of tumours including GBM.

3.5 Conclusion

GBM is a formidable cancer with an array of genetic and epigenetic modifications leading to dysregulation of several parallel and interconnecting pathways. It would provisionally appear that the simultaneous induction of autophagy and apoptosis is not a feasible treatment strategy for glioblastoma due to substantial cross talk between the two pathways and the protective effect of autophagy in established GBM tumours. Thus, we propose a rationale for simultaneous blockade of pathways at points of convergence, points of crosstalk and autophagy. We also recognise the potential future therapeutic rational of combining cytotoxic treatments with autophagy inhibitors.

Chapter 4: Validation of a clinically relevant imageable surgical resection rat model of glioblastoma

4.1 Introduction

GBM is heterogeneous on a genetic, cellular and macroscopic level. Intratumoural hypoxic gradients can drive stem cell distribution leading to the more immature GBM stem cells residing in the inner core surrounded by a peripheral area of more differentiated cells. Hypoxic gradients can also effect epigenetic modifications such as MGMT expression [164]. Current standard of care for GBM involves surgical resection followed by adjuvant chemo-radiotherapy. The extent of surgical resection can have the single greatest survival benefit for patients with subtotal resections up to 78% providing a significant survival advantage [18]. Some authors suggest surgery can improve the efficacy of adjuvant therapy [19]. Due to the heterogeneous nature of GBMs coupled with the blood-brain-barrier, treatment of GBM is complicated by tumour recurrence and resistance to both chemotherapy and radiotherapy. The source of this resistance appears to be due to the immature GBM stem cells. The increase in median survival due to surgery mostly likely comes from the concept of cytoreduction-by removing the bulk of the tumour and thus the majority of GBM stem cells, improving the efficacy of adjuvant treatments [19, 165-167]. Surgery also reduces the compressive biomechanical forces of the tumour which can influence invasion and proliferation of GBM cells and pharmacodynamics of the drugs used [168-173].

The majority of studies which employ GBM preclinical rodent models involve a non-surgical therapeutic regimen, and do not consider the therapeutic advantage of surgery which significantly reduces the translational context. Here, we described the development of a novel cost effective imageable and high throughput rat intracranial GBM surgical resection model. We described a detailed protocol based on a modified cranial window technique to simultaneously repair the craniectomy and permit serial BLI imaging over a prolonged follow-up period. Our model has applications in the study of adjuvant systemic molecular targeted therapies and novel chemotherapeutic combinations towards the

ablation of residual GBM tumour that has infiltrated normal brain. Our model may also be used in the development of novel therapeutics delivered locally into the surgical resection cavity at time of surgery e.g. agents formulated in controlled release systems-nanoparticles/ biodegradable polymer matrices or cell/ viral mediated delivery. Moreover, application of a xenograft rat model in pre-clinical GBM therapeutic efficacy studies may better facilitate: (1) the study of combinatorial and sub-chronic/chronic dosing regimens due to practical benefits associated with larger rodents (eg ability to perform multiple oral/ intravenous dosing) (2) may facilitate improved application of state of the art translational molecular imaging strategies with specific application in the study of GBM (e.g. CT and functional MRI etc.) [174] and (3) may also better integrate with rodent toxicology (rat) studies generally required for regulatory approval of novel targeted therapies/ combinatorial treatment strategies.

4.2 Materials and Methods

4.2.4 Surgical resection

When tumours were in exponential growth phase (as determined by BLI) animals were randomised into 2 groups: Control/Non-surgical group and surgical group. The rats were weighed and received an intraperitoneal injection of anaesthetic (ketamine (80mg/kg)/ xylazine 10mg/kg). No antibiotics were administered for the experiment. The animal respiration and general condition were closely monitored. The skin was prepared by removing hair with a depilatory cream. The rats were then fixed in a stereotactic frame and the skin was prepared in standard surgical fashion.

The previous skin incision was extended in a curvilinear fashion and tissues reflected back. The temporalis muscle was sharply dissected from the cranium and reflected and the pericranium incised and also reflected. The previous burr hole was identified. Using an operating microscope and high speed dental drill a 4.5mm craniotomy was made

centred on the previous burr hole. A durotomy was made and the tumour located. The tumour was gently dissected free. Haemostasis was achieved with a hand-held electrocautery pen with a fine needle tip. The surgical cavity was irrigated and filled with sterile saline.

To repair the cranial defect and to permit post-operative BLI 5mm sterile circular glass microscope coverslips were placed and fixed with cyanoacrylate glue (see Figure 16). The skin was closed in a single layer over the cranial window with 4/0 interrupted simple sutures and cleaned with alcohol (see Figure 15).

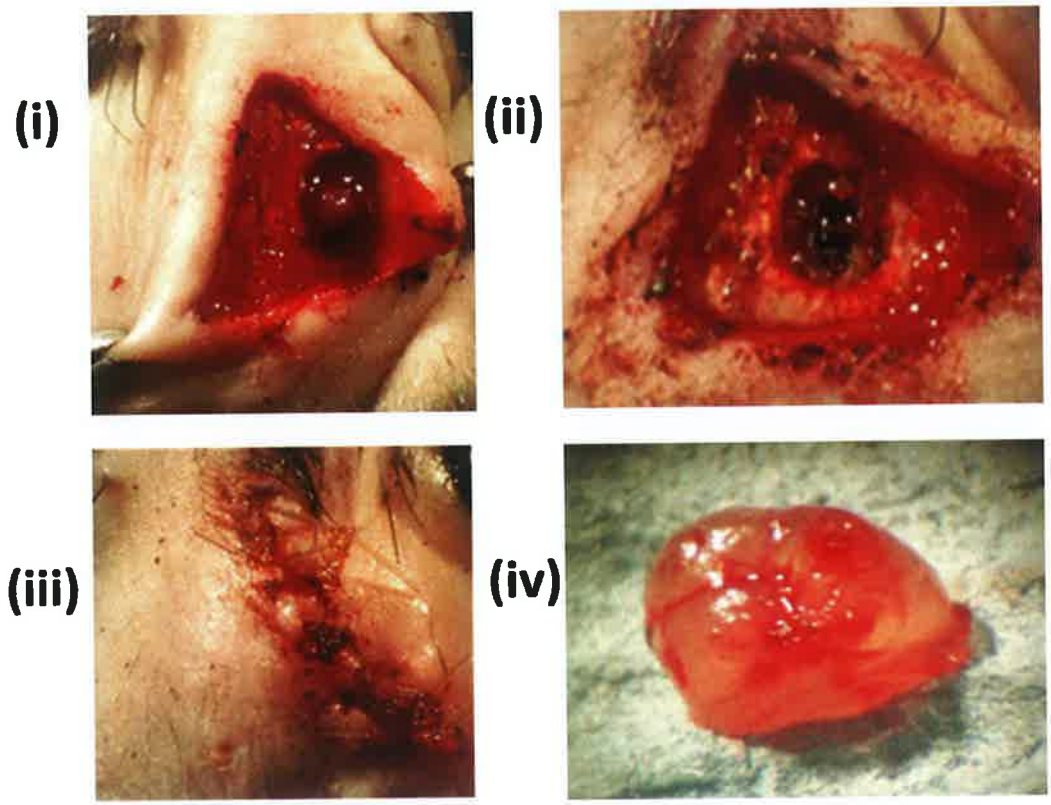

Figure 15-Detailed description of surgical resection procedure. (i) A craniectomy is fashioned using a high speed drill. (ii) After resection of the tumour there is an accessible surgical resection cavity. (iii) Closure of the skin with simple interrupted sutures. (iv) Tumour resection specimen. Magnification 1x

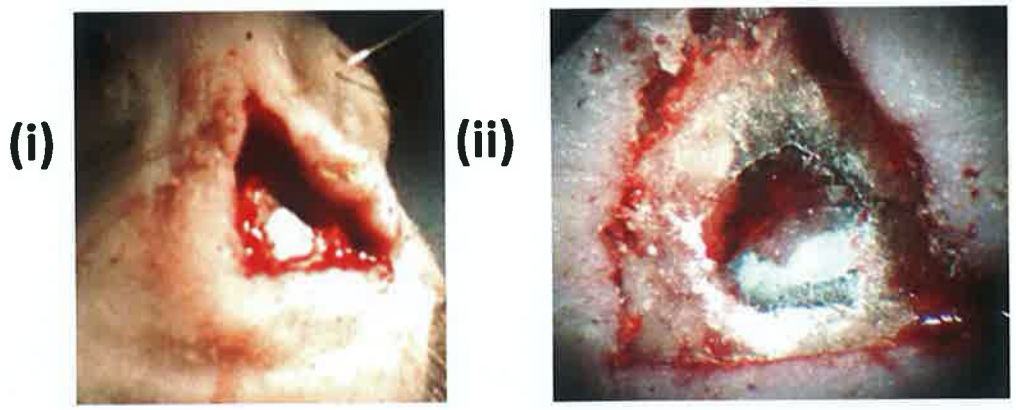

Figure 16- Demonstration of the modified cranial window technique.(i) Photograph demonstrated the low profile cranial window before closing of the skin over it. Magnification (i) 1x (ii) Close up view of the cranial window demonstrating the acrylic glue holding the microscope coverslip in place. Note a contained air-fluid level within the surgical cavity demonstrating the ability of the method to contain liquid within the surgical resection cavity. Magnification 3x.

Animals underwent immediate post-operative BLI and were returned to their cage (see Figure 17) when fully recovered. Animals were weighed daily post-operatively; the surgical wound was assessed for signs of infection, such erythema and wound discharge. The animals were observed for signs of general and neurological deterioration, such as lethargy/abnormal behaviour or hemiparesis.

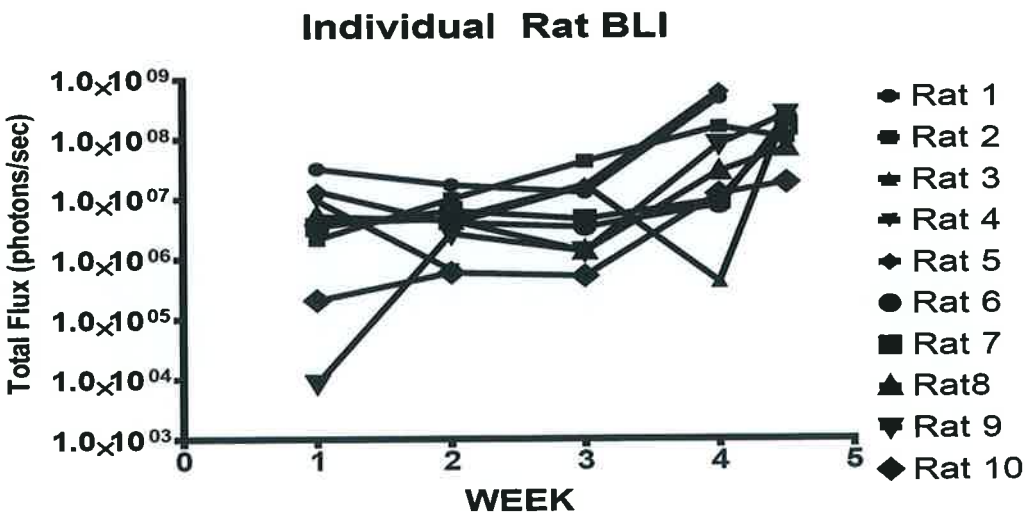

Figure 17- Graph of the individual BLI/tumour growth curve for each rat before randomisation. All rats at 4.5 weeks had similar total flux.

4.3 Results

4.3.1 Survival and pre-surgical BLI signal

At week 2 post-implantation Rat 4 lost bioluminescence signal. At 4.5 weeks post implantation both rat 1 and 5 died. These animals displayed the highest BLI signal. At this point remaining seven rats were randomised into non-surgical/control and surgical groups (see Figure 17 and Figure 18).

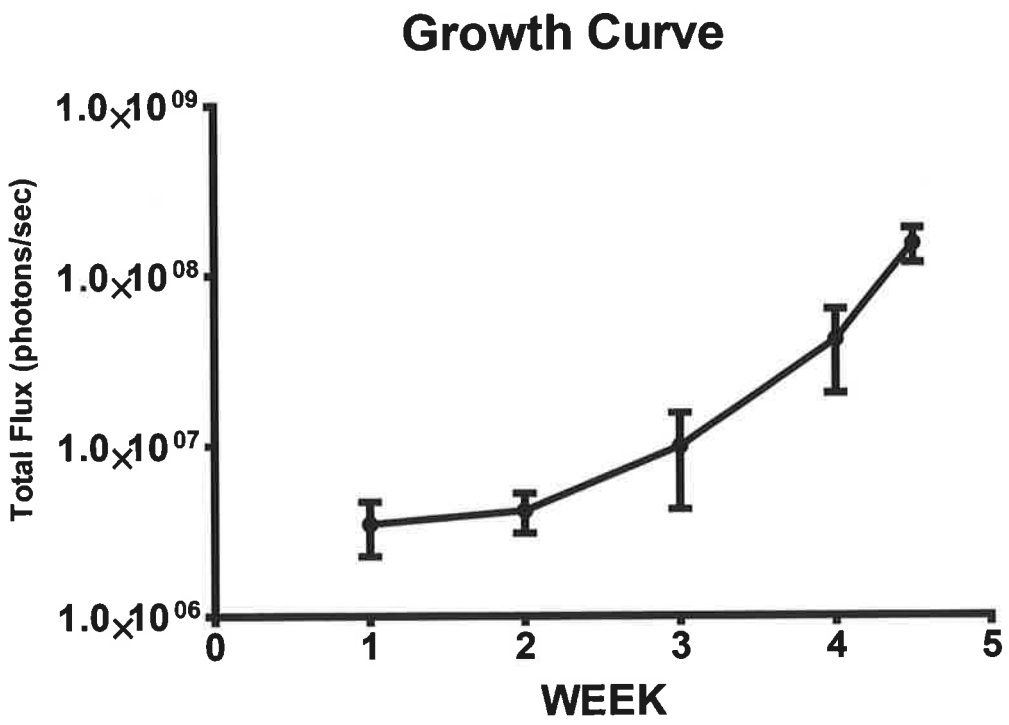

Figure 18- Mean BLI/tumour growth curve of all demonstrating a typical exponential growth to the tumours before randomisation into surgical and non-surgical/control groups. Whiskers represent SEM.

4.3.2 Surgical procedure and immediate post-operative BLI signal

All operations proceeded routinely. A gross total resection rate was achieved in 3 out 4 rats macroscopically. In one rat only a subtotal resection was achieved due to blood loss.

Post-operative bioluminescence signal confirmed the gross total resection rate, however the residual tumour noted in the post-operative imaging in RAT 2 was below threshold/background levels (see Figure 19).

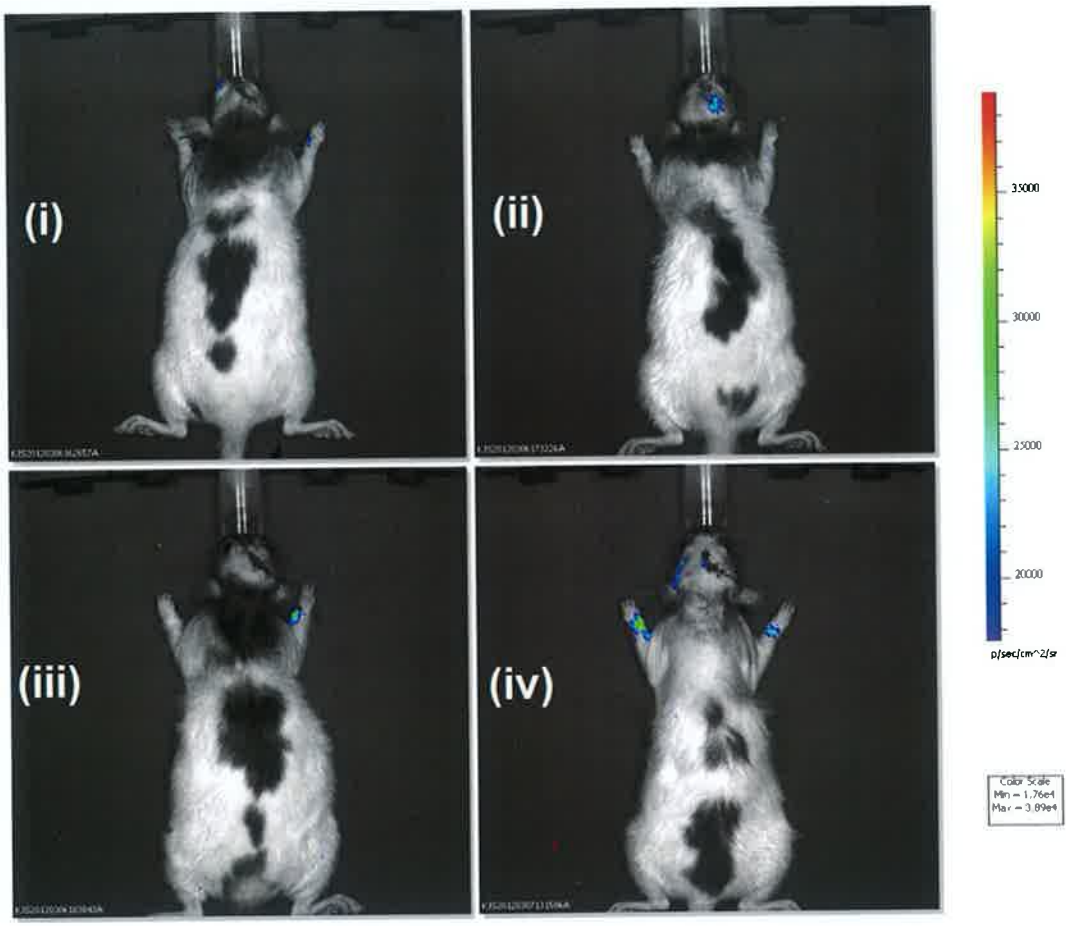

Figure 19- Immediate BLI imaging of the 4 animals that underwent surgical resection demonstrating the actual reduction in tumour volume as evident by the *in vivo* BLI signal. (i)- Rat S1, (ii) Rat-S2, (iii) Rat-S3, (iv) Rat-S4.

4.3.3 Survival and post-surgical BLI signal

All 4 surgical rats survived to the end of the study period. Censor point was at 4 weeks to facilitate further histological analyses. In the surgical group, weights and general condition were consistent throughout the study period. This compared to the non-

surgical/control group (see Figure 21 and Figure 20). In the control group one rat died in the first post-operative week, and a second died in the second as the BLI signal/tumour volume increased significantly (see Figure 22). BLI signal in the surgical groups had a large post-operative decline down to background levels. Importantly, post resection there was tumour recurrence as evidenced by increasing BLI signal and *ex-vivo* imaging (see Figure 23, Figure 24, Figure 25 and Figure 26). Kaplan-Meier Survival analysis revealed surgery conferred a statistically significant survival advantage (Log-Rank p=0.0101 and Hazard Ratio= 25.79) (see Figure 27).

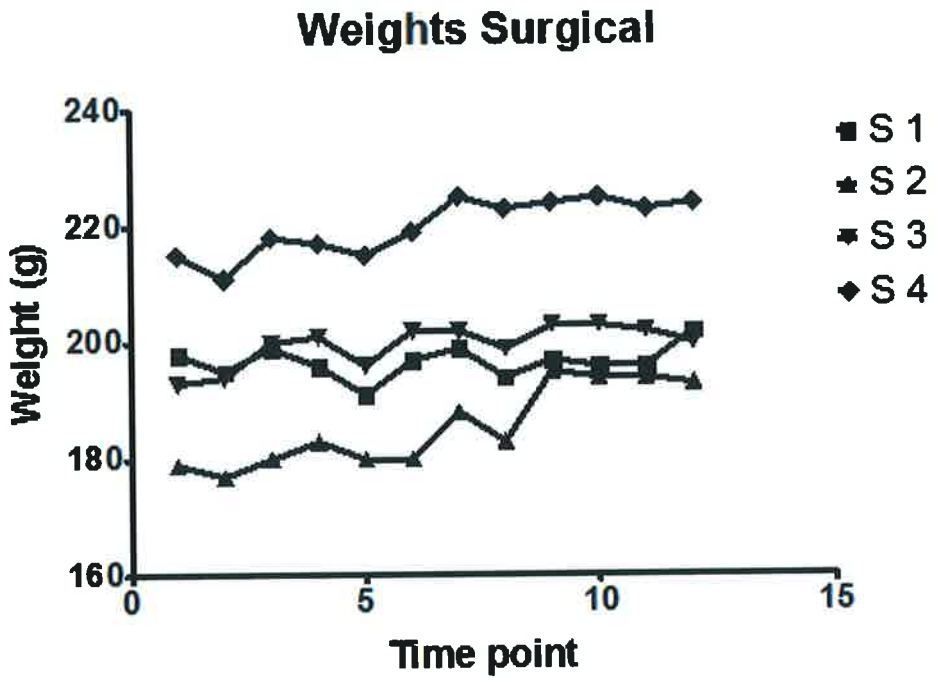

Figure 20-Graph demonstrating the consistent weights of the rats in the surgical group. S1-S4 refers to the individual animals

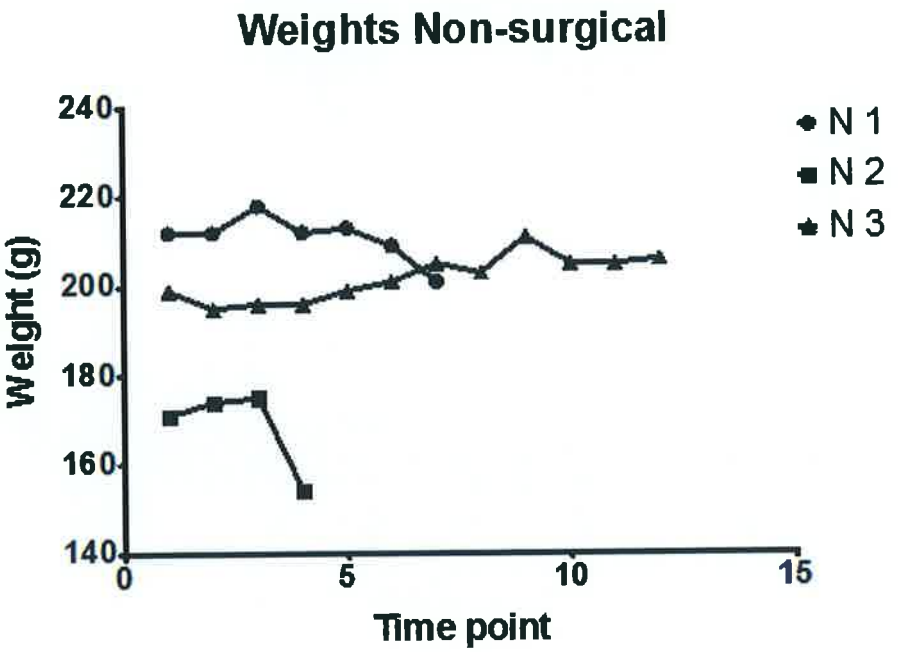

Figure 21- Graph demonstrating the follow-up weights of the non-surgical group. N1-N3 refers to the individual animals. The animal's weights declined as the tumour burden increased.

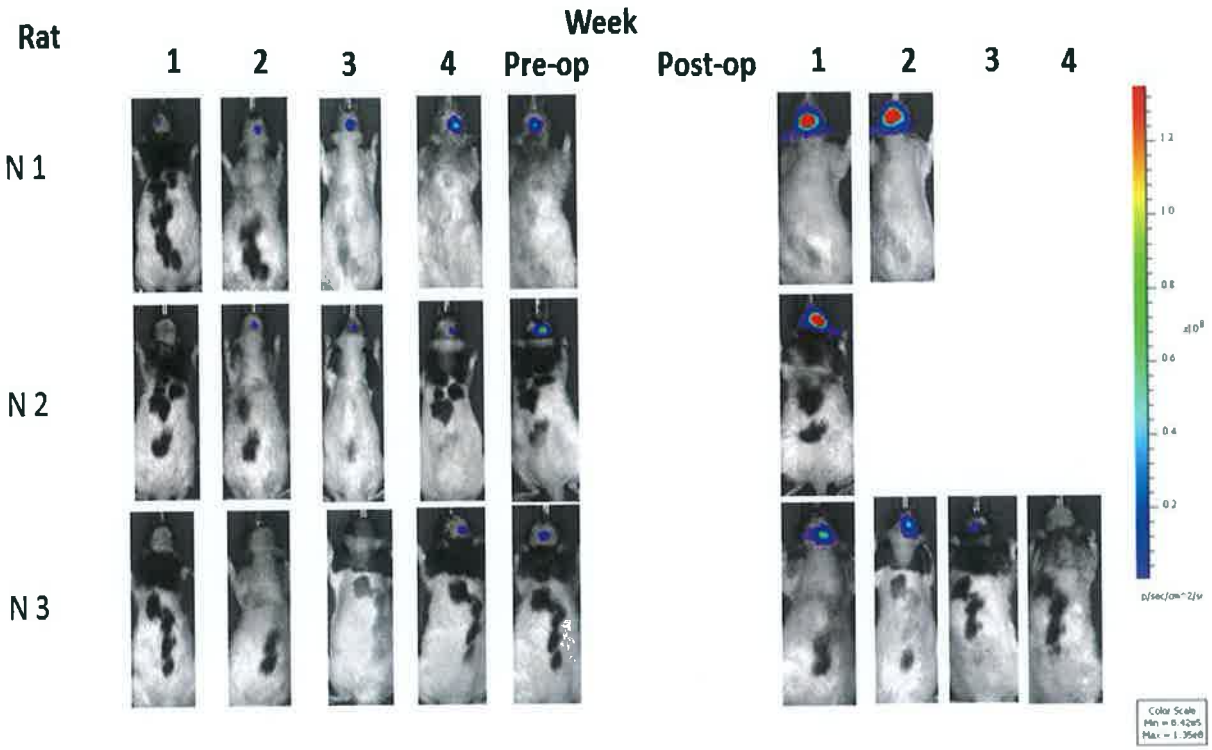

Figure 22- Standardised BLI signal from the non-surgical group. N1-N3 refers to the individual animals. The individual BLI signals of each animal are displayed for the entire study period.

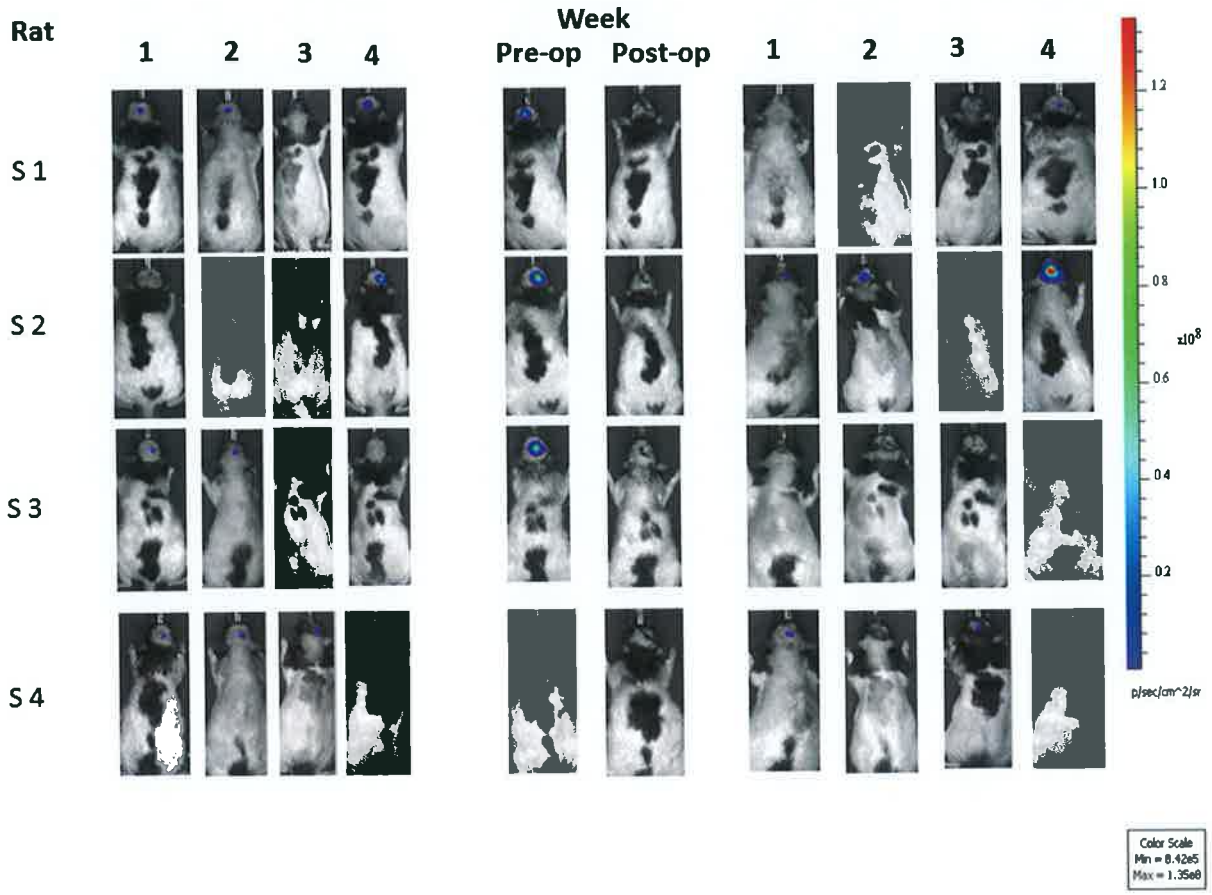

Figure 23- Standardised BLI signal from the surgical group. S1-S4 refers to the individual animals. The individual BLI signals of each animal are displayed for the entire study period. Right: pre-surgery. Middle: pre- and post-op. Left: Follow-up post-op.

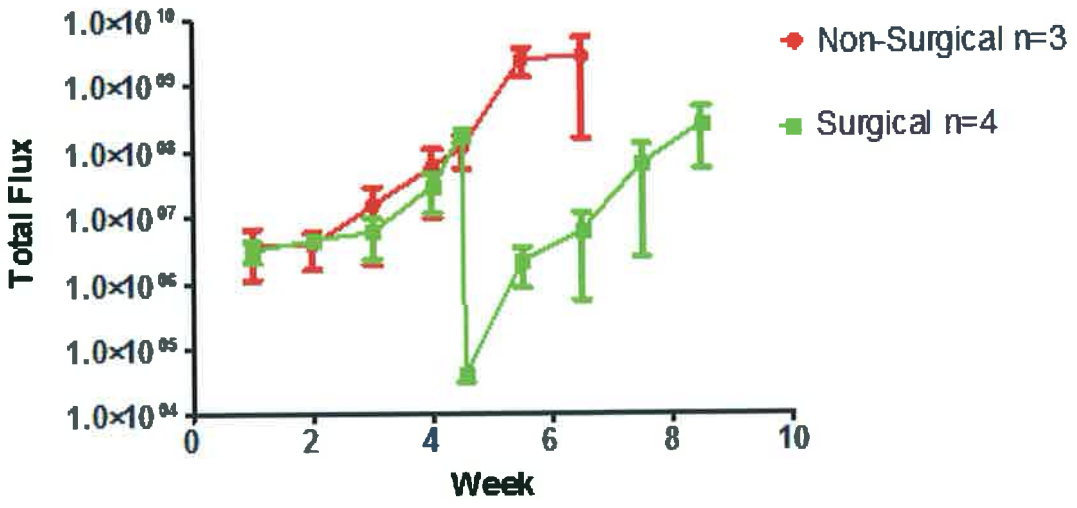

Figure 24- Mean BLI/tumour growth curves of surgical (green) and non-surgical (red) groups. Week 1 represents the first imaging point after implantation. There is a smooth exponential growth phase of

the tumours before randomisation. The sharp decline in tumour signal in the surgical (green) represents the difference between preoperative and postoperative tumour signal. Error bars represent SEM.

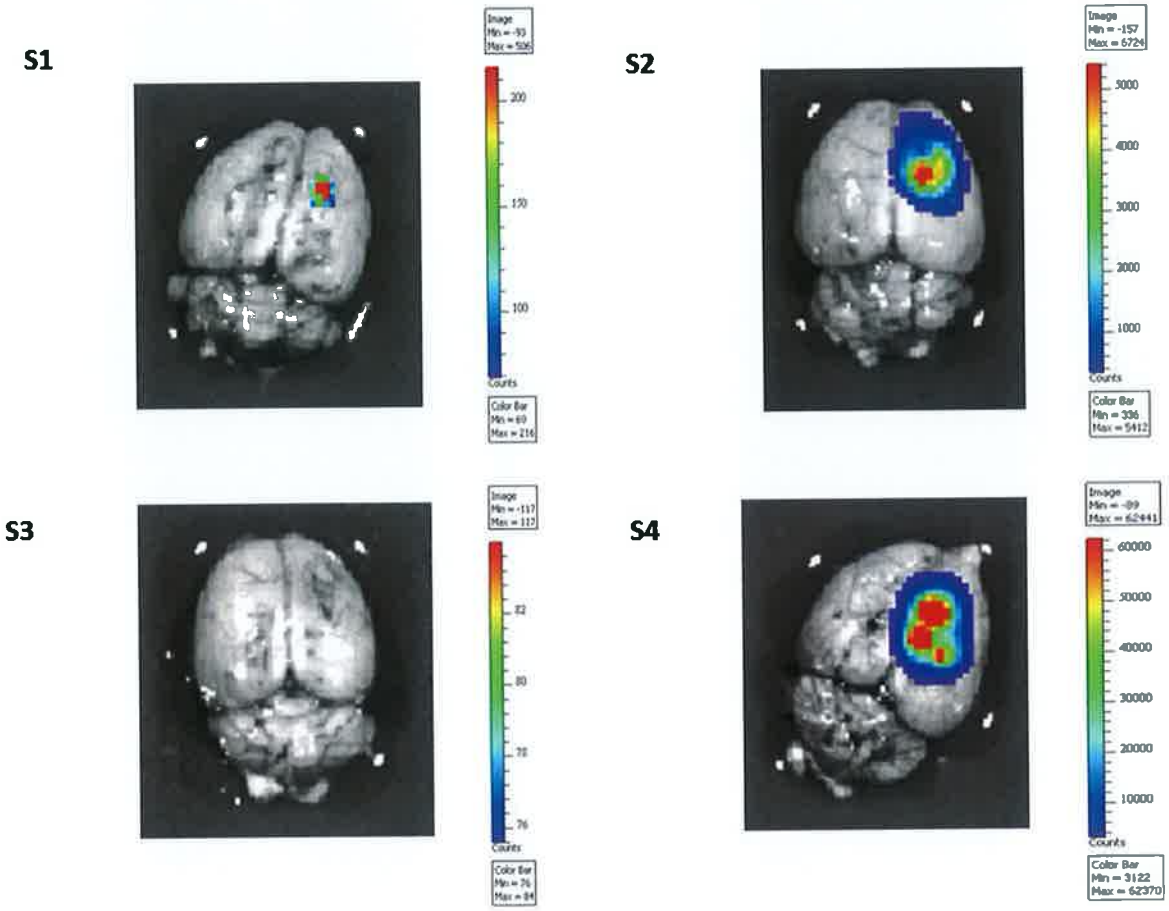

Figure 25- *Ex-vivo* BLI imaging of each of the brains from the surgical resection group demonstrating tumour recurrence in three out four animals at the end of the study period.

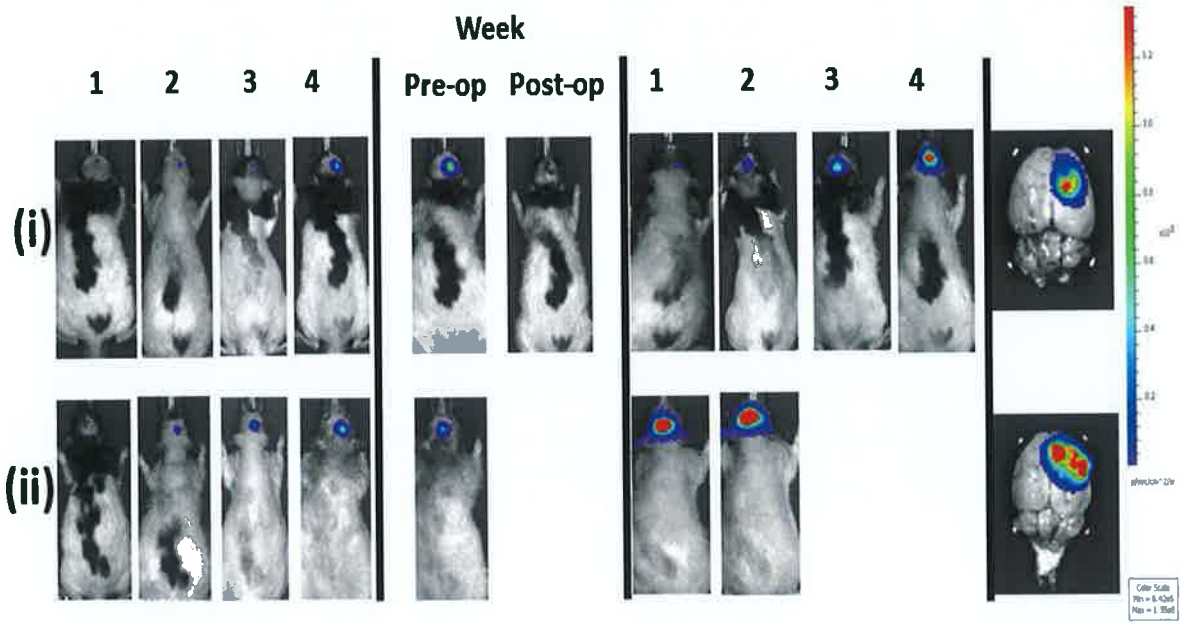

Figure 26- Representative BLI signals from (i) surgical and (ii) non-surgical groups with corresponding *ex-vivo* images are displayed for comparison. Left displays tumour growth up to randomisation. Centre (i) immediate post-surgical tumour reduction. Right (i) Post-surgical tumour recurrence which is readily imageable.

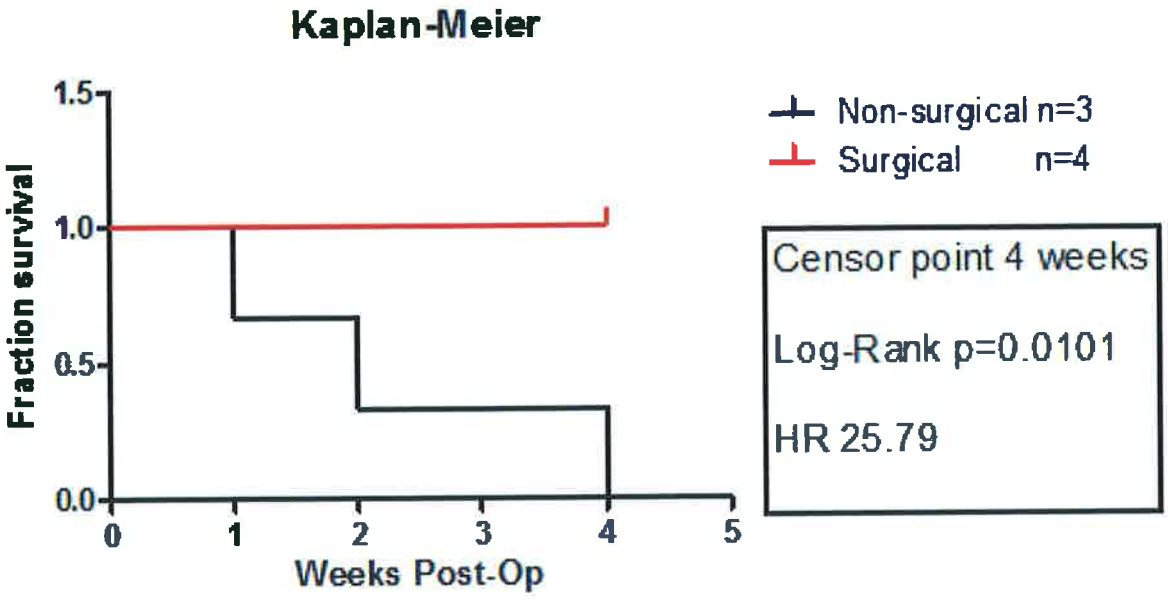

Figure 27- Kaplan-Meier survival analysis with Log-rank (Mantel-Cox) test of surgical v's non-surgical groups. All animals who underwent surgery survived to the end to the study period.

4.3.4 Histology

Post-Mortem histological analysis revealed a marked unilateral tumour causing mass effect in the superficial cortex of the non-surgical/control animals. These tumours display patchy areas of necrosis surrounded by areas of pseudopallisading. There was marked neovascularization with minimal invasion into the surrounding normal brain parenchyma (see Figure 28 and Figure 29). In the animals which underwent surgery, the resection cavity was apparent and both histological examination and *ex vivo* BLI signal confirmed tumour in this cavity. (see Figure 30)

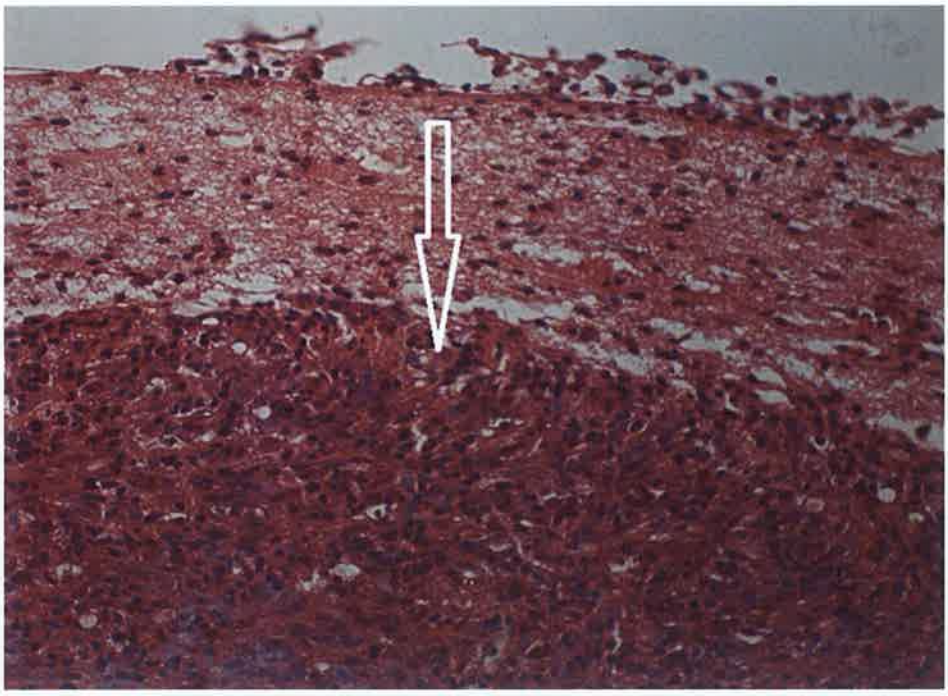

Figure 28- Low magnification of non-surgical group. A dense cellular tumour is noted in the subcortical tissue. White arrow indicates the dense cellular GBM. Magnification 10x

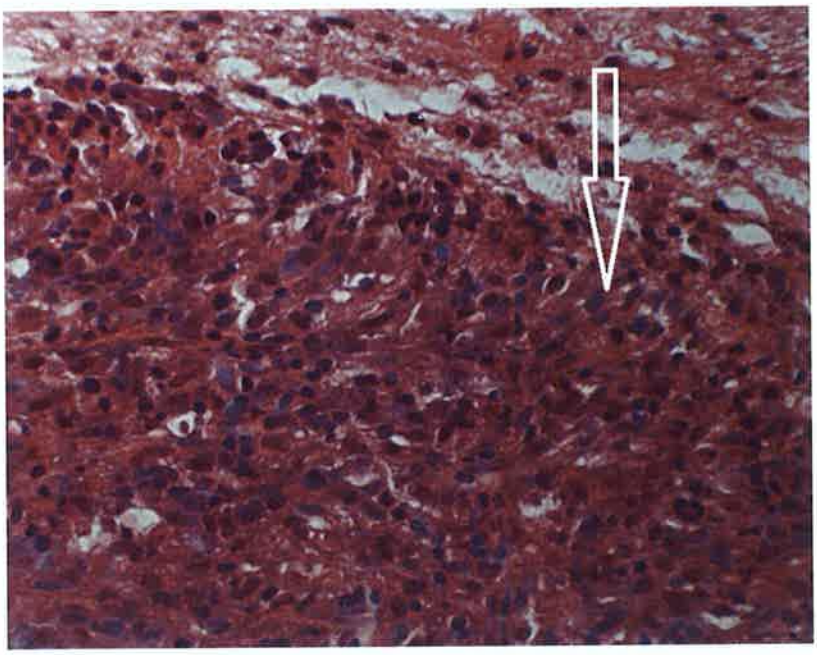

Figure 29- Higher magnification image of figure 35 at magnification 40x. White arrow indicates the dense cellular GBM with pleomorphic nuclei.

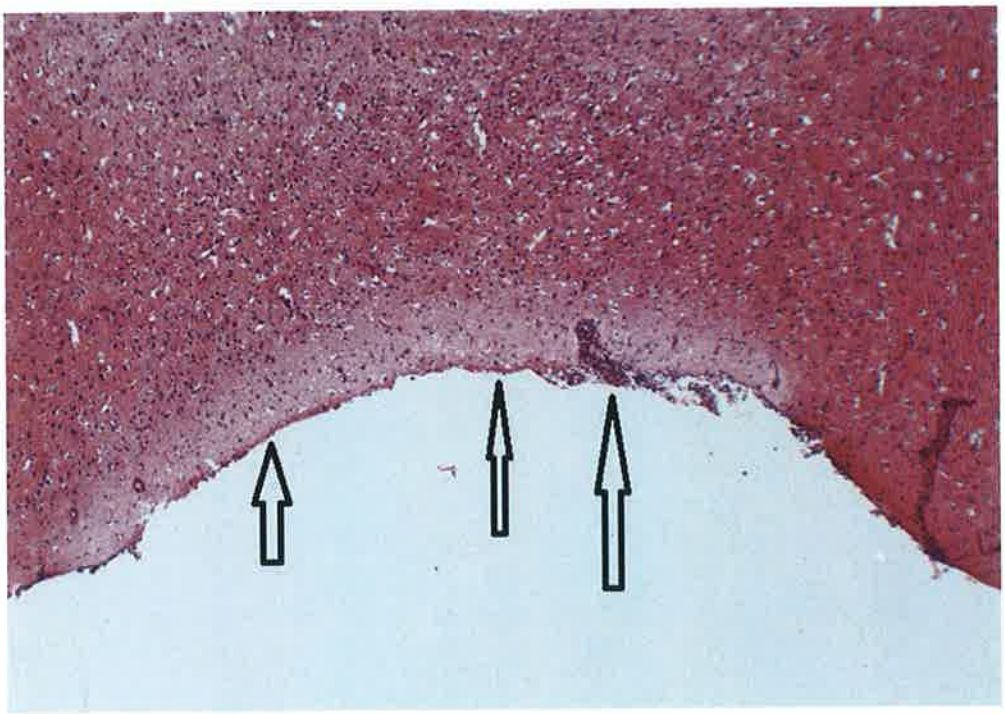

Figure 30- Low magnification image of the surgical resection cavity demonstrating residual tumour that has infiltrated the surgical resection cavity leading to tumour recurrence. This was imageable *in vivo* and confirmed *ex vivo*. Magnification 6x.

4.4 Discussion

To date a limited number of studies have utilised some form of intracranial surgical resection in pre-clinical GBM models [175-177]. All of these studies have relied on survival analysis and histology to interpret the efficacy of intracavity chemotherapeutics. None of these studies employed bioluminescence imaging combined with a modified cranial window technique as a method for serial imaging follow-up. To our knowledge, just one study has utilised a BLI/ intra-cranial window in a mouse model of GBM to investigate encapsulated stem cell migration in combination with intravital microscopy [178]. In this paper the authors report use of a "cranial window" to perform the surgical resection and deliver the encapsulated stem cells. Their "cranial window" as described in the methods sections appears to consist of craniectomy only with direct wound closure. The authors do not appear to have repaired the cranial defect. No evidence is presented that they have attempted to repair the cranial defect as described herein. Many other studies investigating interstitial intracavity and system chemotherapeutic/ targeted therapy regimens have made no attempt at resection and therefore do not reflect the clinical setting. Herein we have described a detailed step by step procedure in performing intracranial surgical resection and fashioning of a cranial window to allow BLI signalling for facile non-invasive follow-up.

In 2001 Lacroix et al published their paper in which they demonstrated a significant survival benefit associated with a 98% surgical reduction in tumour volume [17]. This established an "all-or-none" treatment paradigm in relation to surgical resection of GBM. The belief that anything less than a 98% resection did not confer any survival advantage persisted until Sanai et al, demonstrated survival benefits in subtotal resections as low as 78% [18]. In this paper they demonstrated a stepwise increase in survival advantage

in resections starting with a reduction in tumour volume of ≥78% culminating in a median survival of 16 months in the group of patients with 100% tumour resection. A basic operative strategy includes maximal resection with minimal damage to the surrounding brain. Tumour resection can be optimised with pre-operative planning using multimodality imaging, intra-operative neuronavigation, mapping and intraoperative fluorescent-guided resection and imaging. Typically the inner core is completely resected along with all or most of the enhancing neovascularised tissue surrounding the core. A variable amount of infiltrated brain is also removed, the amount of which is dependent on the eloquence of location of the tumour [179].

Hallmarks of the natural history of GBM, despite maximal standard therapy are recurrence and resistance, or poor response to re-treatment and second line/salvage therapy. It is clear that extent of tumour resection is an important determinant of survival and it has been suggested that it may also improve the efficacy of adjuvant treatment [19, 180].

Our results closely correlate with observation from clinical practice. We achieved a gross total resection rate of 75% with a 75% recurrence rate at four weeks. Clinically, depending on the Neurosurgery centre and the methods employed to maximise the surgical resection, gross total resection rates has been reported to range from 65%-94% [26, 181, 182]. We also demonstrated a survival benefit to surgery alone as noted by our Kaplan-Meier analysis with a p=0.0101 and HR 25.79, our numbers were small (n=4) and larger numbers may be required to confirm this finding. This also reflects clinically observed survival benefit as previous studies have demonstrated the patients who undergo biopsy only do worse than those who have had a surgical resection [183].

Possible mechanisms for how surgery may improve the efficacy of adjuvant treatment is by cytoreduction. Surgical reduction of the total tumour burden can reduce proportionally the amount of cytotoxic agent necessary to achieve effect. In an *in vitro* experiment

conducted by Ng et al they demonstrated that significantly higher concentrations of the alkylating agent BCNU are required to bring about tumour death for a larger tumour load [167].

GBM is a heterogeneous tumour [46] that contains a subpopulation of Glioblastoma Stem-like Cells (GSCs) which not only contribute to tumour growth but have also been implicated in resistance to both chemotherapy [166, 184] and radiotherapy [185]. The method of resistance is currently under debate in the literature as to whether it is an "intrinsic" or "extrinsic-microenvironment" phenomena [165, 186]. There are two prominent cancer stem cell niches within GBM- The perivascular niche [187, 188] and the hypoxic niche [189, 190]. Perivascular GSCs are in close association to the endothelial cells where endothelial Nitric Oxide Synthase (eNOS) has been implicated in their maintenance. The hypoxic niche maintains GSCs through up-regulation of Hypoxic-inducible factors [189] and acidic stress [190]. On radiographic preoperative planning the majority of the perivascular niche may correspond to the avidly enhancing neovascularised tissue seen on T1 post-contrast MRI. In contrast the hypoxic niche may mostly correspond to the central inner-necrotic and acidic core, adjacent to the neovascularised tumour layer; demonstrable on MRI and MRS. On a microscopic level this distinction is complicated by the fact that there can be hypoxic "watershed" areas between adjacent perivascular niches. None the less, both of these areas are the surgical targets for the operating surgeon. Thus, by removing these areas not only do we reduce tumour burden but also reduce the total number of GSCs capable of repopulating the tumour and developing resistance.

As the volume of GBM increases, so too the interstitial fluid pressure within the tumour and therefore the surrounding brain [168]. This is probably more important in intracranial tumours than extracranial tumours as intracranial tumours are located within the cranial cavity which is has fixed volume with no room for expansion, unlike the abdomen or breast. Any growth of tumour within the cranial cavity causes an exponential rise in

intracranial pressure. This can have a pharmacodynamic effect on drug uptake and clearance [169, 191, 192]. Across the normal endothelial cell Starlings forces describe the balance of outward hydrostatic and inward colloid osmotic and interstitial pressures resulting in a small net outward transudate. However, as the interstitial fluid pressure rises within the tumour, the outward flow is reversed and can result in inefficient uptake and increased clearance of the drug. High interstitial fluid pressure and flow can also promote tumour cell invasion. These forces are translated intracellularly to affect pathway changes [171, 172] with mathematical models predicting highest flow at the interface between the tumour and its surroundings [193]. Long term lowering of high interstitial fluid pressure can reduce the tumour proliferation marker Ki-67 [194].

Another biomechanical factor that influences the tumour cell migration is "durotaxis". As the tumour volume increases internal stress forces are transmitted to the surrounding extracellular matrix (ECM) causing reorganisation and stiffness [170]. Ulrich et al demonstrated an increase in cell invasion, migration and proliferation was strongly associated with the rigidity of the ECM of glioblastoma cells [195], while Tse et al demonstrated phenotypic changes in cancer cells to a more invasive phenotype when mechanical compressive forces are applied directly to the cell [173].

In summary, surgical reduction in tumour volume may improve efficacy of adjuvant therapies by cytoreduction-reducing overall tumour burden and GSCs niches- lessening the amount of cytotoxic agents required to reach the tumour across the blood-brain-barrier to achieve the desired effect and reducing possibility of acquired resistance by removing GSCs niches. Surgery, by alleviating the biomechanical compressive forces (decompression of the tumour) may improve the pharmacodynamic profile of systemic chemotherapeutic agents, and may also lessen further invasion and proliferation of residual tumour. Thus, in order for pre-clinical GBM models to better reflect these important surgical benefits, implementation of resection models are warranted.

One of the main obstacles to the development of novel system therapeutic agents is attempting to achieve therapeutic concentrations within the tumour. Oral and intravenous drugs have pharmacokinetic disadvantages such as systemic and first-pass metabolism. After this the blood-brain-barrier poses the greatest challenge. The blood-brain-barrier (BBB) is a tightly regulated barrier separating the central nervous system (CNS) from the systemic circulation, composed of endothelial and pericytes which form the vascular component and astrocytes and microglia forming the CNS component. It has been reported that only small lipophilic molecules can pass the BBB passively and that molecules lacking these properties do not [196]. Only molecules required by the CNS are permitted to cross via active transport. The BBB is composed of restrictive tight junctions between endothelial cells and highly selective active transport mechanisms [197]. Within the GBM tumour there are two zones of BBB integrity [198]. The first area is the central necrotic area which enhances following contrast administration. This area and the adjacent brain parenchyma which displays vasogenic oedema represent the area of BBB disruption allowing increased permeability to certain molecules. This is the area that is also surgically assessable and removed at the time of tumour resection. The second area involves the periphery of the tumour. This area represents where the tumour infiltrates into normal brain parenchyma. This non-enhancing area may show hyperintense signals on T2 or FLAIR MRI images and resembles vasogenic oedema. This area has the BBB intact. It is also the area that is least amenable to surgical resection as the tumour cells invade the normal white matter tracts of the surrounding area increasing the incidence of surgical morbidity and mortality. Therefore, surgical resection of the GBM removes that part of the tumour with the disrupted BBB, e.g. that part of the tumour most likely to achieve high intratumoural concentration of systemic agents. This is in contrast to pre-clinical orthotopic GBM models where the whole tumour is intact. Therefore, administration of systemic agents will have a disproportionate effect on the area of the tumour with a disrupted BBB, that area that is removed in the clinical setting, than the infiltrated brain with an intact BBB. Therefore, we are of the opinion that it is a moot point

to demonstrate efficacy in pre-clinical models where the majority of the effect will occur in the region of the tumour that would be removed in the clinical setting. Finally, as discussed above, the high interstitial fluid pressure within the GBM also creates an obstacle to achieving effective concentrations within the tumour. This can lead to higher doses of agents needed to be given systemically thereby increasing the systemic side effects-particularly myelosuppression causing leucopoenia and thrombocytopenia [199].

One method of by-passing the BBB is local delivery of the agent "behind" the BBB. There are two popular techniques. 1) At the time of maximal surgical resection to place the therapeutic agents into the resection cavity. These could be formulated into controlled release systems- nanoparticles/ biodegradable polymer matrices or cell /viral mediated delivery. The other method of local delivery is Convection-Enhanced Delivery (CED), which involves a stereotactic injection into the tumour using a positive infusion pressure.

Of the local delivery options, only one to date is licensed in the treatment of GBM. Gliadel® is the prototype for intracavity chemotherapeutics in the treatment of GBM. A poly(carboxyphenoxy-propane/sebacic acid) matrix is impregnated with bis(2-chloroethyl)-1-nitrosurea (BCNU, carmustine) . Each wafer of Gliadel® can deliver up to 7.7mg of carmustine over 21 days, the majority of which is released in the first week, diffusing to a depth of 12mm. The remaining matrix degrades over 6-8 weeks [42].

Implanting controlled release systems into the surgical cavity at the time of operation has several advantages over convection enhanced delivery- there is continuous slow release for up to weeks and this method is not plagued by technical issues such as catheter placement [200].

Preclinical development of intracavity chemotherapeutics requires an animal model that is cost effective, reproducible and available for non-invasive follow-up. The most important features are a post-surgical growth pattern that can be non-invasively monitored and a surgical resection cavity that is accessible. Moreover, the surgical

resection procedure should be facile, straight forward and require no endotracheal intubation or peri-operative antibiotics. Herein we have demonstrated such a model.

Surgical resection can confer benefits of reversing unfavourable pharmacodynamics and reducing the chemoresistance potential of the GBM, which could theoretically lead to reduced plasma concentrations of drugs required to achieve therapeutic effect thus, lowering toxic outcomes in pre-clinical studies, allowing those drugs that have shown *in vitro* benefit but *in vivo* toxicity a "second chance". One of the main failures in GBM treatment is that there is always residual tumour that has infiltrated diffusely among normal white matter tracts which is the source of recurrence. As surgery can not only alter the invasiveness of GBM cells it also removes that part of the tumour with a disrupted BBB. If pre-clinical GBM studies are to be conducted using orthotopic models then the central area with BBB disruption is the area that will show greatest efficacy. This can help explain some of the disappointing clinical trial results. All patients recruited into clinical trials of GBM will have had surgical resection. Therefore, any trial targets the residual GBM that has infiltrated the brain with an intact BBB. It is therefore imperative to include a surgical resection model in all GBM studies particularly if one is studying invasion.

4.5 Conclusion

We have established a high-throughput, cost effective, imageable surgical resection rat model of GBM. This model will account for the therapeutic benefit of surgical resection in pre-clinical models which may translate to more agents reaching clinical trials. This model will also account for the main reason of treatment failure, residual tumour protected by an intact BBB. Our model may be implemented in the future for the development of systemic and intracavity therapeutics.

Chapter 5: Conclusion

In chapter one, we gave a brief overview of how GBM is a formidable tumour. It has an abysmal survival rate even when it occurs in young patients with a good Karnofsky Performance Score who undergo maximal surgical resection and optimum chemotherapy and radiotherapy. The hallmarks of this are due to a complex network of heterogeneous and malignant cells capable of self-renewal and chemoresistance, acting as a functional and biochemical syncytium that invades deeply into normal surrounding brain precluding total excision. One of the reasons for treatment failure is that the residual GBM cells have migrated out into normal white matter tracts and are protected by a normal BBB, most impermeable drug barrier known to drug development. The vast array of genetic and epigenetic alternations leads to dysregulation in several different pathways involved in growth, proliferation and Programmed Cell Death. Each of these pathways has multiple points of crosstalk with the next and may share common receptor tyrosine kinase input which can be amplified or mutated, such as EGFR pathway.

In Chapter three we assessed the pre-clinical treatment strategy of combining the cytotoxic agent, temozolomide and the mTOR inhibitor AZD8055 which has been shown to promote autophagy and inhibit tumour growth in GBM. We first demonstrated the *in vitro* signalling effects of the mTOR inhibitor by assessing impact on the phosphorylation products upstream and downstream of mTOR in both the standard GBM cell line U87 and human GBM tumour spheroids. Both of these tissue samples have alterations in EGFR and PTEN which leads to pathological up-regulation not only of the PI3k/mTOR pathway, but also MEK/ERK and JAK/STAT pathways. By inhibiting mTORC1 and mTORC2 with variable concentrations of AZD 8055 there was a dose dependent inhibition of phosphorylation of mTOR, AKT and p70. We then proceeded to the *in vivo* assessment of the combination of temozolomide and AZD 8055 using a novel bioluminescence orthotopic murine model. In this model we used the human GBM material from patient 3. The patient's GBM tumour was transfected using viral vectors to express luciferase to facilitate high-throughput BLI imaging. This allowed longitudinal

assessment of tumour response to the treatment regimens. We found as expected a tumour growth response to TMZ as evident with the statistically significant decrease in BLI signal at two weeks when compared to control. This also translated to a survival benefit. This was in sharp contrast to AZD 8055 that displayed neither a treatment response nor improved survival.

Our *in vitro* data provisionally demonstrates that AZD8055 is a potent inhibitor of mTORC1 and mTORC2 but high concentrations of AZD8055 are required when administered with TMZ to cause a reduction in the pro-survival Bcl family protein, MCL-1. From our *in vivo* survival analysis it appears that AZD as a monotherapy conferred no survival benefit when compared to the vehicle. In the combined TMZ+AZD group the shape of the Kaplan-Meier curve closely resembled that of the TMZ only group but this did not reach significance. This may indicate a certain degree of antagonism between the two compounds. This antagonism may be explained by the observed dose-dependent downregulation of p62. As discussed previously, p62 is one of the nodal points between apoptosis and autophagy and how simultaneous induction of two interconnected Programmed Cell Death pathways can lead to antagonistic outcomes. We also reviewed the other points of crosstalk between the three principle pathways that are regulated by Receptor Tyrosine Kinases such as EGFR.

Putting the two survival results together it would provisionally appear that sub-therapeutic concentrations were being achieved within the tumour despite using an optimum dosing regimen and that at these levels antagonism can occur when combined with cytotoxic agents.

AZD 8055 has been shown to have *in vivo* efficacy in a subcutaneous mouse model of GBM [126]. In such a model the blood-brain-barrier is not considered. AZD 8055 is a small lipophilic molecule and theoretically should be capable of crossing the BBB. If AZD8055 could not penetrate an intact BBB it should still have exerted some effect on

the central tumour area which is the area with a disrupted BBB. A possible explanation as to why this did not happen could be due to the pharmacodynamic effects of intratumoural interstitial pressures. The subcutaneous model would have lower intratumoural interstitial pressures than an intracranial/orthotopic model, as an expanding tumour within a fixed volume (such as the intracranial compartment) would generate higher interstitial pressures than a subcutaneous model, where the tumour can expand. Thus, the higher interstitial pressures caused a reversal of the normal starling forces (discussed in chapter 4) leading to sub therapeutic intratumoural concentrations of AZD 8055.

In chapter four we establish a novel and versatile surgical resection model. This model is unique in that for the first time we described how to surgically remove a tumour and repair the cranial defect so as to permit longitudinal BLI imaging of the residual tumour and its recurrence. We feel it is imperative to repair the cranial defect especially in large rodent models and particularly if this model is being applied to intracavity surgically mediated delivery. If the cranial defect is not repaired, then any substance implanted into the surgical cavity is at risk of migrating out and into the dead space between the skull and overlying skin. We know from clinical experience with the use of Gliadel® wafers implanted at the time of surgery that there is a high risk of surgical wound breakdown and inadequate effect if the surgical defect is not repaired correctly. From our experience in chapter 3, and the possibility of sub-therapeutic intratumoural concentrations of AZD8055 due to high interstitial fluid pressures highlights the importance of using a surgical resection model in the area of systemic chemotherapy. In chapter four we described the therapeutic effect of GBM surgical resection by improving the pharmacodynamics profile of systemic agent, reduction in amount of agent required to cause an effect and reduction in CSCs, a likely source of chemoresistance. We also highlight how the GBM tumour can be divided into two broad zones, an inner zone with a disrupted BBB, and a peripheral zone with an intact BBB. In pre-clinical models that do not use surgical resection, it is the

inner zone that is most likely to demonstrate an effect. However, there has been little progress in translating these pre-clinical results into corresponding clinical trials. This may be due to the fact that all patients recruited into clinical trials have had surgical resection and therefore the most "responsive" zone of the tumour is removed leaving behind residual tumour with an intact BBB.

We therefore advocate widespread adoption of this model to accurately recapitulate the clinical setting which would help align pre-clinical results more closely to those observed in clinical trials and propose that this model is ideal for cost-effective imageable high-throughput modelling of the development of surgically mediated intracavity therapy.

Peer-reviewed Sections

Presentations

International Oral Presentations

British Society of Neurological Surgeons-Autumn Meeting 2012-Top Papers Session

Establishment of an imageable intracranial surgical resection animal model of Glioblastoma Multiforme

Kieron J Sweeney, Monika Jarzabek, Donncha O'Brien, Annette T. Byrne, Jochen Prehn.

National Oral Presentations

Irish Institute of Clinical Neuroscience- Registrars Prize

Establishment of an imageable intracranial surgical resection animal model of Glioblastoma Multiforme

Kieron J Sweeney, Monika Jarzabek, Donncha O'Brien, Annette T. Byrne, Jochen Prehn.

Publications

Published Abstract:

Sweeney KJ, Jarzabek M, O'Brien D, Prehn JH, Byrne A. ***Establishment of an imageable intracranial surgical resection animal model of Glioblastoma Multiforme*** [abstract]. In Proceedings of the 2012 Autumn meeting of the Society of British Neurological Surgeons; 2012 Sept 26th; Leeds,U.K. page 1, Top Paper Section, abstract no. WPM1-1; British Journal of Neurosurgery, October 2012; 26(5): pg 596.

Manuscripts Submitted:

Jarzabek, M.A, Sweeney, K. J., Evans, R.L., Jacobs, A. H., Stupp, R., O'Brien, D.F, Berger, M. S., Prehn, J. H. M., Byrne, A.T.. **Molecular Imaging in the Development of a Novel Treatment Paradigm for Glioblastoma: An Integrated Multi-Disciplinary Commentary.** Drug Discovery Today

Manuscripts in preparation:

Sweeney KJ, Jarzabek M, O'Brien D, Prehn JH, Byrne AT. **Establishment of a clinically relevant imageable intracranial surgical resection Rat model of Glioblastoma**

Sweeney KJ, Jarzabek M, O'Brien D, Bjerkvig R, Prehn JH, Byrne AT

Investigation of the effect of combining Temozolomide with the mTOR inhibitor AZD8055, *in vitro* and using an orthotopic patient derived animal model

References

1. Chan, W.Y., S. Kohsaka, and P. Rezaie, *The origin and cell lineage of microglia—New concepts.* Brain Research Reviews, 2007. **53**(2): p. 344-354.
2. David N. Louis, H.O., Otmar D. Wiestler, Webster K. Cavenee., ed. *The WHO Classification of Tumours of the Central Nervous System*. 4th ed. WHO Classification of Tumours of the Central Nervous System, ed. E.S.J. Fred T. Bosman, Sunil R. Lakhani,Hiroko Ohgaki,. 2007, IARC: Lyon. 309.
3. Ohgaki, H. and P. Kleihues, *Epidemiology and etiology of gliomas.* Acta Neuropathol, 2005. **109**(1): p. 93-108.
4. Cocco, P., M. Dosemeci, and E.F. Heineman, *Brain cancer and occupational exposure to lead.* J Occup Environ Med, 1998. **40**(11): p. 937-42.
5. van Wijngaarden, E. and M. Dosemeci, *Brain cancer mortality and potential occupational exposure to lead: findings from the National Longitudinal Mortality Study, 1979-1989.* Int J Cancer, 2006. **119**(5): p. 1136-44.
6. Cordier, S., et al., *Parental exposure to polycyclic aromatic hydrocarbons and the risk of childhood brain tumors: The SEARCH International Childhood Brain Tumor Study.* Am J Epidemiol, 2004. **159**(12): p. 1109-16.
7. Norman, M.A., et al., *Prenatal exposure to tobacco smoke and childhood brain tumors: results from the United States West Coast childhood brain tumor study.* Cancer Epidemiol Biomarkers Prev, 1996. **5**(2): p. 127-33.
8. Chen, H., et al., *Diet and risk of adult glioma in eastern Nebraska, United States.* Cancer Causes Control, 2002. **13**(7): p. 647-55.
9. Little, M.P., et al., *Mobile phone use and glioma risk: comparison of epidemiological study results with incidence trends in the United States.* BMJ, 2012. **344**: p. e1147.
10. Davis, D.L., et al., *Swedish review strengthens grounds for concluding that radiation from cellular and cordless phones is a probable human carcinogen.* Pathophysiology, 2013. **20**(2): p. 123-9.
11. Pandey, J.P., *Genetic and Viral Etiology of Glioblastoma--a Unifying Hypothesis.* Cancer Epidemiology Biomarkers & Prevention, 2011. **20**(6): p. 1061-1063.
12. Dziurzynski, K., et al., *Consensus on the role of human cytomegalovirus in glioblastoma.* Neuro Oncol, 2012. **14**(3): p. 246-55.
13. Cowppli-Bony, A., et al., *Brain tumors and hormonal factors: review of the epidemiological literature.* Cancer Causes & Control, 2011. **22**(5): p. 697-714.
14. Walter, A.W., et al., *Secondary brain tumors in children treated for acute lymphoblastic leukemia at St Jude Children's Research Hospital.* J Clin Oncol, 1998. **16**(12): p. 3761-7.
15. Ron, E., et al., *Tumors of the brain and nervous system after radiotherapy in childhood.* N Engl J Med, 1988. **319**(16): p. 1033-9.
16. Osborn, A.G., K.L. Salzman, and A.J. Barkovick, *Diagnostic Imaging: Brain*. Second ed. 2009: Amirsys.
17. Lacroix, M., et al., *A multivariate analysis of 416 patients with glioblastoma multiforme: prognosis, extent of resection, and survival.* J Neurosurg, 2001. **95**(2): p. 190-8.
18. Sanai, N., et al., *An extent of resection threshold for newly diagnosed glioblastomas.* Journal of Neurosurgery, 2011. **115**(1): p. 3-8.
19. Stummer, W., M.J. Bent, and M. Westphal, *Cytoreductive surgery of glioblastoma as the key to successful adjuvant therapies: new arguments in an old discussion.* Acta Neurochirurgica, 2011. **153**(6): p. 1211-1218.
20. Kuhnt, D., et al., *Correlation of the extent of tumor volume resection and patient survival in surgery of glioblastoma multiforme with high-field intraoperative MRI guidance.* Neuro-Oncology, 2011. **13**(12): p. 1339-1348.

21. Nabavi, A., et al., *Five-Aminolevulinic Acid for Fluorescence-Guided Resection of Recurrent Malignant Gliomas.* Neurosurgery, 2009. **65**(6): p. 1070-1077.
22. Valdes, P.A., et al., *d-aminolevulinic acid-induced protoporphyrin IX concentration correlates with histopathologic markers of malignancy in human gliomas: the need for quantitative fluorescence-guided resection to identify regions of increasing malignancy.* Neuro-Oncology, 2011. **13**(8): p. 846-856.
23. Valdes, P., et al., *Quantitative fluorescence in intracranial tumor: implications for ALA-induced PpIX as an.* J Neurosurg, 2011. **115**(1): p. 11-17.
24. Roberts, D.W., et al., *Coregistered fluorescence-enhanced tumor resection of malignant glioma: relationships between δ-aminolevulinic acid induced protoporphyrin IX fluorescence, magnetic resonance imaging enhancement, and neuropathological parameters.* J Neurosurg, 2011. **114**(3): p. 595-603.
25. Stockhammer, F., et al., *Association of F18-fluoro-ethyl-tyrosin uptake and 5-aminolevulinic acid-induced fluorescence in gliomas.* Acta Neurochirurgica, 2009. **151**(11): p. 1377-1383.
26. Stummer, W., et al., *Fluorescence-guided surgery with 5-aminolevulinic acid for resection of malignant glioma: a randomised controlled multicentre phase III trial.* The Lancet Oncology, 2006. **7**(5): p. 392-401.
27. Matthias Preusser, M., 1 Sandrine de Ribaupierre, MD,2 Adelheid Wo¨ hrer, MD,3 and M. Sara C. Erridge, 4 Monika Hegi, PhD,5 Michael Weller, MD,6 and Roger Stupp, MD, *Current Concepts and Management of glioblastoma.* Annals of Neurology, 2011. **70**: p. 9-21.
28. Roger Stupp, M.D., Warren P. Mason, M.D., Martin J. van den Bent, M.D.,, et al., *Radiotherapy plus Concomitant and Adjuvant Temozolomide for Glioblastoma.* N Engl J Med, 2005. **352**(10): p. 987-96.
29. Stupp, R., et al., *Effects of radiotherapy with concomitant and adjuvant temozolomide versus radiotherapy alone on survival in glioblastoma in a randomised phase III study: 5-year analysis of the EORTC-NCIC trial.* The Lancet Oncology, 2009. **10**: p. 459-466.
30. Günther, W., et al., *Temozolomide induces apoptosis and senescence in glioma cells cultured as multicellular spheroids.* British Journal of Cancer, 2003. **88**(3): p. 463-469.
31. Hirose, Y., M.S. Berger, and R.O. Pieper, *p53 effects both the duration of G2/M arrest and the fate of temozolomide-treated human glioblastoma cells.* Cancer Res, 2001. **61**(5): p. 1957-63.
32. Hermisson, M., et al., *O6-methylguanine DNA methyltransferase and p53 status predict temozolomide sensitivity in human malignant glioma cells.* J Neurochem, 2006. **96**(3): p. 766-76.
33. Roos, W.P., et al., *Apoptosis in malignant glioma cells triggered by the temozolomide-induced DNA lesion O6-methylguanine.* Oncogene, 2007. **26**(2): p. 186-197.
34. Wick, W., et al., *Prevention of irradiation-induced glioma cell invasion by temozolomide involves caspase 3 activity and cleavage of focal adhesion kinase.* Cancer Res, 2002. **62**(6): p. 1915-9.
35. Kurzen, H., et al., *Inhibition of angiogenesis by non-toxic doses of temozolomide.* Anticancer Drugs, 2003. **14**(7): p. 515-22.
36. Kim, J.T., et al., *Metronomic treatment of temozolomide inhibits tumor cell growth through reduction of angiogenesis and augmentation of apoptosis in orthotopic models of gliomas.* Oncol Rep, 2006. **16**(1): p. 33-9.
37. Jung, *Changes of the O6-methylguanine-DNA methyltransferase promoter methylation and MGMT protein expression after adjuvant treatment in glioblastoma.* Oncology Reports, 2010. **23**(5).
38. Andreana L. Rivera†, C.E.P., Mark R. Gilbert, Howard Colman, and E.P.S. Clarissa De La Cruz, B. Nebiyou Bekele, and Kenneth D. Aldape, *MGMT promoter methylation is*

predictive of response to radiotherapy and prognostic in absence of adjuvant alkylating chemotherapy for glioblastoma. Neuro Oncol, 2010. **12**(2): p. 116-121.
39. Hegi, M.E., et al., *MGMT gene silencing and benefit from temozolomide in glioblastoma.* N Engl J Med, 2005. **352**(10): p. 997-1003.
40. Niyazi, M., et al., *Therapeutic options for recurrent malignant glioma.* Radiotherapy and Oncology, 2011. **98**(1): p. 1-14.
41. Dixit, S., et al., *The sequential use of carmustine wafers (Gliadel®) and post-operative radiotherapy with concomitant temozolomide followed by adjuvant temozolomide: a clinical review.* British Journal of Neurosurgery, 2011. **25**(4): p. 459-469.
42. Bota, D.A., et al., *Interstitial chemotherapy with biodegradable BCNU (Gliadel®) wafers in the treatment of malignant gliomas.* Therapeutics and Clinical Risk Management, 2007. **3**(5): p. 707-715.
43. Nduom, E.K., C.G. Hadjipanayis, and E.G. Van Meir, *Glioblastoma cancer stem-like cells: implications for pathogenesis and treatment.* Cancer J, 2012. **18**(1): p. 100-6.
44. Charles, N.A., et al., *The brain tumor microenvironment.* Glia, 2012. **60**(3): p. 502-514.
45. Lyons, J.G., et al., *Clonal diversity in carcinomas: its implications for tumour progression and the contribution made to it by epithelial-mesenchymal transitions.* Clin Exp Metastasis, 2008. **25**(6): p. 665-77.
46. Bonavia, R., et al., *Heterogeneity Maintenance in Glioblastoma: A Social Network.* Cancer Research, 2011. **71**(12): p. 4055-4060.
47. He, H., M.W. Li, and C.S. Niu, *The pathological characteristics of glioma stem cell niches.* Journal of Clinical Neuroscience, 2012. **19**(1): p. 121-127.
48. Schichor, C., et al., *Mesenchymal stem cells and glioma cells form a structural as well as a functional syncytium in vitro.* Experimental Neurology, 2012. **234**(1): p. 208-219.
49. Karsy, M., et al., *Established and emerging variants of glioblastoma multiforme: review of morphological and molecular features.* Folia Neuropathol, 2012. **50**(4): p. 301-21.
50. Tran, B. and M.A. Rosenthal, *Survival comparison between glioblastoma multiforme and other incurable cancers.* J Clin Neurosci, 2010. **17**(4): p. 417-21.
51. Darefsky, A.S., J.T. King, and R. Dubrow, *Adult glioblastoma multiforme survival in the temozolomide era: A population-based analysis of surveillance, epidemiology, and end results registries.* Cancer, 2011: p. n/a-n/a.
52. Chargari, C., et al., *Treatment of elderly patients with glioblastoma: from clinical evidence to molecular highlights.* Cancer Treat Rev, 2012. **38**(8): p. 988-95.
53. *Comprehensive genomic characterization defines human glioblastoma genes and core pathways.* Nature, 2008. **455**(7216): p. 1061-8.
54. Mao, H., et al., *Deregulated Signaling Pathways in Glioblastoma Multiforme: Molecular Mechanisms and Therapeutic Targets.* Cancer Investigation, 2012. **30**(1): p. 48-56.
55. Masui, K., T.F. Cloughesy, and P.S. Mischel, *Molecular pathology in adult high-grade gliomas: from molecular diagnostics to target therapies.* Neuropathology and Applied Neurobiology, 2012. **38**(3): p. 271-291.
56. Nobusawa, S., et al., *IDH1 mutations as molecular signature and predictive factor of secondary glioblastomas.* Clin Cancer Res, 2009. **15**(19): p. 6002-7.
57. Verhaak, R.G.W., et al., *Integrated Genomic Analysis Identifies Clinically Relevant Subtypes of Glioblastoma Characterized by Abnormalities in PDGFRA, IDH1, EGFR, and NF1.* Cancer Cell, 2010. **17**(1): p. 98-110.
58. Woehrer, A., et al., *Clinical neuropathology practice guide 1-2013: Molecular subtyping of glioblastoma: ready for clinical use?* Clin Neuropathol, 2013. **32**(1): p. 5-8.
59. Berdasco, M. and M. Esteller, *Aberrant epigenetic landscape in cancer: how cellular identity goes awry.* Dev Cell, 2010. **19**(5): p. 698-711.
60. Kreth, S., N. Thon, and F.W. Kreth, *Epigenetics in human gliomas.* Cancer Lett, 2012.
61. Nagarajan, R.P. and J.F. Costello, *Epigenetic mechanisms in glioblastoma multiforme.* Seminars in Cancer Biology, 2009. **19**(3): p. 188-197.

62. Margueron, R. and D. Reinberg, *Chromatin structure and the inheritance of epigenetic information.* Nat Rev Genet, 2010. **11**(4): p. 285-96.
63. Etcheverry, A., et al., *DNA methylation in glioblastoma: impact on gene expression and clinical outcome.* BMC Genomics, 2010. **11**(1): p. 701.
64. Kim, Y.S., et al., *MGMT Gene Promoter Methylation as a Potent Prognostic Factor in Glioblastoma Treated with Temozolomide-Based Chemoradiotherapy: A Single-Institution Study.* Int J Radiat Oncol Biol Phys, 2012.
65. Rivera, A.L., et al., *MGMT promoter methylation is predictive of response to radiotherapy and prognostic in the absence of adjuvant alkylating chemotherapy for glioblastoma.* Neuro-Oncology, 2009. **12**(2): p. 116-121.
66. Pang, J.C., et al., *Oncogenic role of microRNAs in brain tumors.* Acta Neuropathol, 2009. **117**(6): p. 599-611.
67. Zhang, B., et al., *microRNAs as oncogenes and tumor suppressors.* Dev Biol, 2007. **302**(1): p. 1-12.
68. Lynam-Lennon, N., S.G. Maher, and J.V. Reynolds, *The roles of microRNA in cancer and apoptosis.* Biol Rev Camb Philos Soc, 2009. **84**(1): p. 55-71.
69. Mendrysa, S.M., S. Ghassemifar, and R. Malek, *p53 in the CNS: Perspectives on Development, Stem Cells, and Cancer.* Genes & Cancer, 2011. **2**(4): p. 431-442.
70. Vigneron, A., E. Gamelin, and O. Coqueret, *The EGFR-STAT3 oncogenic pathway up-regulates the Eme1 endonuclease to reduce DNA damage after topoisomerase I inhibition.* Cancer Res, 2008. **68**(3): p. 815-25.
71. Wu, J., et al., *EGFR-STAT3 signaling promotes formation of malignant peripheral nerve sheath tumors.* Oncogene, 2013.
72. Inda, M.M., et al., *Tumor heterogeneity is an active process maintained by a mutant EGFR-induced cytokine circuit in glioblastoma.* Genes Dev, 2010. **24**(16): p. 1731-45.
73. Tchirkov, A., et al., *Interleukin-6 gene amplification and shortened survival in glioblastoma patients.* Br J Cancer, 2007. **96**(3): p. 474-6.
74. Mukherjee, B., et al., *EGFRvIII and DNA Double-Strand Break Repair: A Molecular Mechanism for Radioresistance in Glioblastoma.* Cancer Research, 2009. **69**(10): p. 4252-4259.
75. Tanaka, K., et al., *Oncogenic EGFR Signaling Activates an mTORC2-NF- B Pathway That Promotes Chemotherapy Resistance.* Cancer Discovery, 2011. **1**(6): p. 524-538.
76. Ye, F., Q. Gao, and M.-J. Cai, *Therapeutic targeting of EGFR in malignant glioma.* Expert Opin. Ther. Targets, 2010. **14**(3): p. 303-316.
77. Jung, C.H., et al., *mTOR regulation of autophagy.* FEBS Letters, 2010. **584**(7): p. 1287-1295.
78. Zoncu, R., A. Efeyan, and D.M. Sabatini, *mTOR: from growth signal integration to cancer, diabetes and ageing.* Nat Rev Mol Cell Biol, 2011. **12**(1): p. 21-35.
79. Magnuson, B., B. Ekim, and Diane C. Fingar, *Regulation and function of ribosomal protein S6 kinase (S6K) within mTOR signalling networks.* Biochemical Journal, 2012. **441**(1): p. 1-21.
80. Zhou, H. and S. Huang, *Role of mTOR signaling in tumor cell motility, invasion and metastasis.* Curr Protein Pept Sci, 2011. **12**(1): p. 30-42.
81. Gao, N., et al., *G1 cell cycle progression and the expression of G1 cyclins are regulated by PI3K/AKT/mTOR/p70S6K1 signaling in human ovarian cancer cells.* Am J Physiol Cell Physiol, 2004. **287**(2): p. C281-91.
82. Maiese, K., et al., *mTOR: on target for novel therapeutic strategies in the nervous system.* Trends Mol Med, 2012.
83. Beauchamp, E.M. and L.C. Platanias, *The evolution of the TOR pathway and its role in cancer.* Oncogene, 2012.
84. Jhanwar-Uniyal, M., et al., *Deconstructing mTOR complexes in regulation of Glioblastoma Multiforme and its stem cells.* Adv Biol Regul, 2012.

85. Koul, D., *PTEN signaling pathways in glioblastoma.* Cancer Biol Ther, 2008. **7**(9): p. 1321-5.
86. Lino, M.M. and A. Merlo, *PI3Kinase signaling in glioblastoma.* Journal of Neuro-Oncology, 2010. **103**(3): p. 417-427.
87. Zhao, Y. and Y. Sun, *Targeting the mTOR-DEPTOR pathway by CRL E3 ubiquitin ligases: therapeutic application.* Neoplasia, 2012. **14**(5): p. 360-7.
88. Ouyang, L., et al., *Programmed cell death pathways in cancer: a review of apoptosis, autophagy and programmed necrosis.* Cell Prolif, 2012. **45**(6): p. 487-98.
89. Chaabane, W., et al., *Autophagy, Apoptosis, Mitoptosis and Necrosis: Interdependence Between Those Pathways and Effects on Cancer.* Archivum Immunologiae et Therapiae Experimentalis, 2012.
90. Elmore, S., *Apoptosis: a review of programmed cell death.* Toxicol Pathol, 2007. **35**(4): p. 495-516.
91. Norberg, E., S. Orrenius, and B. Zhivotovsky, *Mitochondrial regulation of cell death: processing of apoptosis-inducing factor (AIF).* Biochem Biophys Res Commun, 2010. **396**(1): p. 95-100.
92. Sevrioukova, I.F., *Apoptosis-inducing factor: structure, function, and redox regulation.* Antioxid Redox Signal, 2011. **14**(12): p. 2545-79.
93. Wong, R.S., *Apoptosis in cancer: from pathogenesis to treatment.* J Exp Clin Cancer Res, 2011. **30**: p. 87.
94. Surova, O. and B. Zhivotovsky, *Various modes of cell death induced by DNA damage.* Oncogene, 2012.
95. Lieberman, J. and Z. Fan, *Nuclear war: the granzyme A-bomb.* Curr Opin Immunol, 2003. **15**(5): p. 553-9.
96. Mizushima, N. and M. Komatsu, *Autophagy: renovation of cells and tissues.* Cell, 2011. **147**(4): p. 728-41.
97. Morselli, E., et al., *Anti- and pro-tumor functions of autophagy.* Biochim Biophys Acta, 2009. **1793**(9): p. 1524-32.
98. Wang, S.-y., et al., *Core signaling pathways of survival/death in autophagy-related cancer networks.* The International Journal of Biochemistry & Cell Biology, 2011. **43**(9): p. 1263-1266.
99. Han, J., C.Q. Zhong, and D.W. Zhang, *Programmed necrosis: backup to and competitor with apoptosis in the immune system.* Nat Immunol, 2011. **12**(12): p. 1143-9.
100. Papatriantafyllou, M., *Cell death: Programmed necrosis: putting the pieces together.* Nat Rev Mol Cell Biol, 2012. **13**(3): p. 135.
101. Galluzzi, L. and G. Kroemer, *Necroptosis: a specialized pathway of programmed necrosis.* Cell, 2008. **135**(7): p. 1161-3.
102. Appenzeller-Herzog, C. and M.N. Hall, *Bidirectional crosstalk between endoplasmic reticulum stress and mTOR signaling.* Trends Cell Biol, 2012. **22**(5): p. 274-82.
103. Moll, U.M., N. Marchenko, and X.K. Zhang, *p53 and Nur77/TR3 - transcription factors that directly target mitochondria for cell death induction.* Oncogene, 2006. **25**(34): p. 4725-43.
104. Chipuk, J.E., et al., *PUMA couples the nuclear and cytoplasmic proapoptotic function of p53.* Science, 2005. **309**(5741): p. 1732-5.
105. Tasdemir, E., et al., *Regulation of autophagy by cytoplasmic p53.* Nat Cell Biol, 2008. **10**(6): p. 676-87.
106. Morselli, E., et al., *Mutant p53 protein localized in the cytoplasm inhibits autophagy.* Cell Cycle, 2008. **7**(19): p. 3056-61.
107. Pei, D., Y. Zhang, and J. Zheng, *Regulation of p53: a collaboration between Mdm2 and Mdmx.* Oncotarget, 2012. **3**(3): p. 228-35.
108. Maiuri, M.C., et al., *Control of autophagy by oncogenes and tumor suppressor genes.* Cell Death Differ, 2009. **16**(1): p. 87-93.

109. Starr, C.M., et al., *Primary sequence and heterologous expression of nuclear pore glycoprotein p62.* J Cell Biol, 1990. **110**(6): p. 1861-71.
110. Komatsu, M., S. Kageyama, and Y. Ichimura, *p62/SQSTM1/A170: physiology and pathology.* Pharmacol Res, 2012. **66**(6): p. 457-62.
111. Duran, A., et al., *p62 is a key regulator of nutrient sensing in the mTORC1 pathway.* Mol Cell, 2011. **44**(1): p. 134-46.
112. Itakura, E. and N. Mizushima, *p62 Targeting to the autophagosome formation site requires self-oligomerization but not LC3 binding.* J Cell Biol, 2011. **192**(1): p. 17-27.
113. Jin, Z., et al., *Cullin3-based polyubiquitination and p62-dependent aggregation of caspase-8 mediate extrinsic apoptosis signaling.* Cell, 2009. **137**(4): p. 721-35.
114. Sehgal, S.N., H. Baker, and C. Vezina, *Rapamycin (AY-22,989), a new antifungal antibiotic. II. Fermentation, isolation and characterization.* J Antibiot (Tokyo), 1975. **28**(10): p. 727-32.
115. Heitman, J., N.R. Movva, and M.N. Hall, *Targets for cell cycle arrest by the immunosuppressant rapamycin in yeast.* Science, 1991. **253**(5022): p. 905-9.
116. Brown, E.J., et al., *A mammalian protein targeted by G1-arresting rapamycin-receptor complex.* Nature, 1994. **369**(6483): p. 756-8.
117. Tsang, C.K., et al., *Targeting mammalian target of rapamycin (mTOR) for health and diseases.* Drug Discovery Today, 2007. **12**(3-4): p. 112-124.
118. Proud, Christopher G., *mTOR Signalling in Health and Disease.* Biochemical Society Transactions, 2011. **39**(2): p. 431-436.
119. Eshleman, J.S., et al., *Inhibition of the mammalian target of rapamycin sensitizes U87 xenografts to fractionated radiation therapy.* Cancer Res, 2002. **62**(24): p. 7291-7.
120. Arcella, A., et al., *Rapamycin inhibits the growth of glioblastoma.* Brain res, 2012.
121. Geoerger, B., et al., *Antitumor activity of the rapamycin analog CCI-779 in human primitive neuroectodermal tumor/medulloblastoma models as single agent and in combination chemotherapy.* Cancer Res, 2001. **61**(4): p. 1527-32.
122. Chang, S.M., et al., *Phase II study of CCI-779 in patients with recurrent glioblastoma multiforme.* Invest New Drugs, 2005. **23**(4): p. 357-61.
123. Galanis, E., et al., *Phase II trial of temsirolimus (CCI-779) in recurrent glioblastoma multiforme: a North Central Cancer Treatment Group Study.* J Clin Oncol, 2005. **23**(23): p. 5294-304.
124. Zheng, X.F., et al., *TOR kinase domains are required for two distinct functions, only one of which is inhibited by rapamycin.* Cell, 1995. **82**(1): p. 121-30.
125. Mukherjee, B., et al., *The dual PI3K/mTOR inhibitor NVP-BEZ235 is a potent inhibitor of ATM- and DNA-PKCs-mediated DNA damage responses.* Neoplasia, 2012. **14**(1): p. 34-43.
126. Chresta, C.M., et al., *AZD8055 Is a Potent, Selective, and Orally Bioavailable ATP-Competitive Mammalian Target of Rapamycin Kinase Inhibitor with In vitro and In vivo Antitumor Activity.* Cancer Research, 2010. **70**(1): p. 288-298.
127. Liu, T.J., et al., *NVP-BEZ235, a novel dual phosphatidylinositol 3-kinase/mammalian target of rapamycin inhibitor, elicits multifaceted antitumor activities in human gliomas.* Molecular Cancer Therapeutics, 2009. **8**(8): p. 2204-2210.
128. de Vries, N.A., J.H. Beijnen, and O. van Tellingen, *High-grade glioma mouse models and their applicability for preclinical testing.* Cancer Treatment Reviews, 2009. **35**(8): p. 714-723.
129. Hambardzumyan, D., et al., *Genetic modeling of gliomas in mice: New tools to tackle old problems.* Glia, 2011. **59**(8): p. 1155-1168.
130. Heyer, J., et al., *Non-germline genetically engineered mouse models for translational cancer research.* Nature Reviews Cancer, 2010. **10**(7): p. 470-480.
131. Halpern, W., et al., *Stems to GEMs: Impact of Stem Cell Technology on Engineered Animal Models.* Veterinary Pathology, 2011. **48**(5): p. 1041-1043.

132. Schmid, R.S., M. Vitucci, and C.R. Miller, *Genetically engineered mouse models of diffuse gliomas.* Brain Research Bulletin, 2011.
133. Keyaerts, M., V. Caveliers, and T. Lahoutte, *Bioluminescence imaging: looking beyond the light.* Trends Mol Med, 2012. **18**(3): p. 164-72.
134. Jarzabek, M., et al., *In vivo bioluminescence imaging validation of a human biopsy-derived orthotopic mouse model of Glioblastoma Multiforme.* Molecular Imaging, 2012. **in press**.
135. Rolf Bjerkvig, P.D., Audun Tønnesen, M.D., Ole Didrik Laerum, M.D., and Erik-Olof Backlund, M.D, *Multicellular tumor spheroids from human gliomas maintained in organ culture.* JNS, 1990. **72**(3).
136. Keunen, O., et al., *Anti-VEGF treatment reduces blood supply and increases tumor cell invasion in glioblastoma.* Proceedings of the National Academy of Sciences, 2011. **108**(9): p. 3749-3754.
137. Naumann, S.C., et al., *Temozolomide- and fotemustine-induced apoptosis in human malignant melanoma cells: response related to MGMT, MMR, DSBs, and p53.* British Journal of Cancer, 2009. **100**(2): p. 322-333.
138. Short, S.C., et al., *Rad51 inhibition is an effective means of targeting DNA repair in glioma models and CD133+ tumor-derived cells.* Neuro-Oncology, 2011. **13**(5): p. 487-499.
139. Giubellino, A., et al., *Combined Inhibition of mTORC1 and mTORC2 Signaling Pathways Is a Promising Therapeutic Option in Inhibiting Pheochromocytoma Tumor Growth: In Vitro and In Vivo Studies in Female Athymic Nude Mice.* Endocrinology, 2013. **154**(2): p. 646-655.
140. Garcia-Martinez, J.M., et al., *Effect of PI3K- and mTOR-specific inhibitors on spontaneous B-cell follicular lymphomas in PTEN/LKB1-deficient mice.* Br J Cancer, 2011. **104**(7): p. 1116-25.
141. Willems, L., et al., *The dual mTORC1 and mTORC2 inhibitor AZD8055 has anti-tumor activity in acute myeloid leukemia.* Leukemia, 2012. **26**(6): p. 1195-202.
142. Hammond, L.A., et al., *A randomized phase I and pharmacological trial of sequences of 1,3-bis(2-chloroethyl)-1-nitrosourea and temozolomide in patients with advanced solid neoplasms.* Clin Cancer Res, 2004. **10**(5): p. 1645-56.
143. Schmidt, E.V., et al., *Growth controls connect: interactions between c-myc and the tuberous sclerosis complex-mTOR pathway.* Cell Cycle, 2009. **8**(9): p. 1344-51.
144. Vadysirisack, D.D., et al., *Feedback Control of p53 Translation by REDD1 and mTORC1 Limits the p53-Dependent DNA Damage Response.* Molecular and Cellular Biology, 2011. **31**(21): p. 4356-4365.
145. Sunayama, J., et al., *Crosstalk Between the PI3K/mTOR and MEK/ERK Pathways Involved in the Maintenance of Self-Renewal and Tumorigenicity of Glioblastoma Stem-Like Cells.* Stem Cells, 2010. **28**(11): p. 1930-1939.
146. Ma, L., et al., *Phosphorylation and functional inactivation of TSC2 by Erk implications for tuberous sclerosis and cancer pathogenesis.* Cell, 2005. **121**(2): p. 179-93.
147. Clark, M.J., et al., *U87MG decoded: the genomic sequence of a cytogenetically aberrant human cancer cell line.* PLoS Genet, 2010. **6**(1): p. e1000832.
148. Rodrik-Outmezguine, V.S., et al., *mTOR Kinase Inhibition Causes Feedback-Dependent Biphasic Regulation of AKT Signaling.* Cancer Discovery, 2011. **1**(3): p. 248-259.
149. Chandarlapaty, S., et al., *AKT inhibition relieves feedback suppression of receptor tyrosine kinase expression and activity.* Cancer Cell, 2011. **19**(1): p. 58-71.
150. Xing, W.J., et al., *Effects of EGFR and PTEN gene expressions on the inhibition of U87MG glioblastoma cell proliferation induced by protein kinase inhibitors.* Clin Exp Pharmacol Physiol, 2012.
151. Mut, M., et al., *Both mitogen-activated protein kinase (MAPK)/extracellular-signal-regulated kinases (ERK) 1/2 and phosphatidylinositide-3-OH kinase (PI3K)/Akt pathways*

regulate activation of E-twenty-six (ETS)-like transcription factor 1 (Elk-1) in U138 glioblastoma cells. Int J Biochem Cell Biol, 2012. **44**(2): p. 302-10.
152. Ma, L., et al., *Identification of S664 TSC2 phosphorylation as a marker for extracellular signal-regulated kinase mediated mTOR activation in tuberous sclerosis and human cancer.* Cancer Res, 2007. **67**(15): p. 7106-12.
153. Guardiola-Diaz, H.M., A. Ishii, and R. Bansal, *Erk1/2 MAPK and mTOR signaling sequentially regulates progression through distinct stages of oligodendrocyte differentiation.* Glia, 2012. **60**(3): p. 476-486.
154. Turke, A.B., et al., *MEK inhibition leads to PI3K/AKT activation by relieving a negative feedback on ERBB receptors.* Cancer Res, 2012. **72**(13): p. 3228-37.
155. Li, Z., et al., *Leptin Induces Cyclin D1 Expression and Proliferation of Human Nucleus Pulposus Cells via JAK/STAT, PI3K/Akt and MEK/ERK Pathways.* PLoS ONE, 2012. **7**(12): p. e53176.
156. Dalby, K.N., et al., *Targeting the prodeath and prosurvival functions of autophagy as novel therapeutic strategies in cancer.* Autophagy, 2010. **6**(3): p. 322-9.
157. Mathew, R., et al., *Autophagy Suppresses Tumorigenesis through Elimination of p62.* Cell, 2009. **137**(6): p. 1062-1075.
158. Natsumeda, M., et al., *Induction of autophagy in temozolomide treated malignant gliomas.* Neuropathology, 2011. **31**(5): p. 486-493.
159. Papait, R., et al., *Temozolomide and carmustine cause large-scale heterochromatin reorganization in glioma cells.* Biochemical and Biophysical Research Communications, 2009. **379**(2): p. 434-439.
160. Moscat, J. and M.T. Diaz-Meco, *p62: a versatile multitasker takes on cancer.* Trends Biochem Sci, 2012. **37**(6): p. 230-6.
161. Moscat, J. and M.T. Diaz-Meco, *p62 at the Crossroads of Autophagy, Apoptosis, and Cancer.* Cell, 2009. **137**(6): p. 1001-1004.
162. Huang, S., et al., *Inhibition of mTOR kinase by AZD8055 can antagonize chemotherapy-induced cell death through autophagy induction and down-regulation of p62/sequestosome 1.* J Biol Chem, 2011. **286**(46): p. 40002-12.
163. Han, W., et al., *EGFR tyrosine kinase inhibitors activate autophagy as a cytoprotective response in human lung cancer cells.* PLoS ONE, 2011. **6**(6): p. e18691.
164. Pistollato, F., et al., *Intratumoral Hypoxic Gradient Drives Stem Cells Distribution and MGMT Expression in Glioblastoma.* Stem Cells, 2010: p. N/A-N/A.
165. Mannino, M. and A.J. Chalmers, *Radioresistance of glioma stem cells: Intrinsic characteristic or property of the 'microenvironment-stem cell unit'?* Molecular Oncology, 2011. **5**(4): p. 374-386.
166. Shi, L., *MicroRNA-125b-2 confers human glioblastoma stem cells resistance to temozolomide through the mitochondrial pathway of apoptosis.* International Journal of Oncology, 2011.
167. Ng, W.H., G.Q. Wan, and H.P. Too, *Higher glioblastoma tumour burden reduces efficacy of chemotherapeutic agents: in vitro evidence.* Journal of Clinical Neuroscience, 2007. **14**(3): p. 261-266.
168. Boucher, Y., et al., *Interstitial fluid pressure in intracranial tumours in patients and in rodents.* Br J Cancer, 1997. **75**(6): p. 829-36.
169. Heldin, C.-H., et al., *High interstitial fluid pressure — an obstacle in cancer therapy.* Nature Reviews Cancer, 2004. **4**(10): p. 806-813.
170. Shieh, A.C., *Biomechanical Forces Shape the Tumor Microenvironment.* Annals of Biomedical Engineering, 2011. **39**(5): p. 1379-1389.
171. Shieh, A.C., et al., *Tumor Cell Invasion Is Promoted by Interstitial Flow-Induced Matrix Priming by Stromal Fibroblasts.* Cancer Research, 2011. **71**(3): p. 790-800.
172. Shieh, A.C. and M.A. Swartz, *Regulation of tumor invasion by interstitial fluid flow.* Physical Biology, 2011. **8**(1): p. 015012.

173. Tse, J.M., et al., *Mechanical compression drives cancer cells toward invasive phenotype.* Proc Natl Acad Sci U S A, 2012. **109**(3): p. 911-6.
174. Jarzabek, M.A., et al., *Molecular Imaging in the Development of a Novel Treatment Paradigm for Glioblastoma: An Integrated Multi-Disciplinary Commentary.* Drug Discovery Today, 2013. **in press**.
175. Zhang, X., et al., *Combination of surgical resection and photodynamic therapy of 9L gliosarcoma in the nude rat.* Photochem Photobiol, 2006. **82**(6): p. 1704-11.
176. Emerich, D.F., et al., *Injectable chemotherapeutic microspheres and glioma I: enhanced survival following implantation into the cavity wall of debulked tumors.* Pharm Res, 2000. **17**(7): p. 767-75.
177. Akbar, U., et al., *Delivery of temozolomide to the tumor bed via biodegradable gel matrices in a novel model of intracranial glioma with resection.* Journal of Neuro-Oncology, 2009. **94**(2): p. 203-212.
178. Kauer, T.M., et al., *Encapsulated therapeutic stem cells implanted in the tumor resection cavity induce cell death in gliomas.* Nature Neuroscience, 2011. **15**(2): p. 197-204.
179. Moliterno, J.A., T.R. Patel, and J.M. Piepmeier, *Neurosurgical approach.* Cancer J, 2012. **18**(1): p. 20-5.
180. Stummer, W., et al., *Prospective cohort study of radiotherapy with concomitant and adjuvant temozolomide chemotherapy for glioblastoma patients with no or minimal residual enhancing tumor load after surgery.* Journal of Neuro-Oncology, 2012. **108**(1): p. 89-97.
181. Lenaburg, H.J., K.E. Inkabi, and T.W. Vitaz, *The use of intraoperative MRI for the treatment of glioblastoma multiforme.* Technol Cancer Res Treat, 2009. **8**(2): p. 159-62.
182. Kubben, P.L., et al., *Intraoperative MRI-guided resection of glioblastoma multiforme: a systematic review.* Lancet Oncol, 2011. **12**(11): p. 1062-70.
183. Patwardhan, R.V., et al., *Survival trends in elderly patients with glioblastoma multiforme: resective surgery, radiation, and chemotherapy.* Surg Neurol, 2004. **62**(3): p. 207-13; discussion 214-5.
184. Sato, A., et al., *MEK-ERK Signaling Dictates DNA-Repair Gene MGMT Expression and Temozolomide Resistance of Stem-Like Glioblastoma Cells Via the MDM2-P53 Axis.* Stem Cells, 2011: p. N/A-N/A.
185. Jamal, M., et al., *The brain microenvironment preferentially enhances the radioresistance of CD133(+) glioblastoma stem-like cells.* Neoplasia, 2012. **14**(2): p. 150-8.
186. Beier, D., J.B. Schulz, and C.P. Beier, *Chemoresistance of glioblastoma cancer stem cells - much more complex than expected.* Molecular Cancer, 2011. **10**(1): p. 128.
187. Calabrese, C., et al., *A Perivascular Niche for Brain Tumor Stem Cells.* Cancer Cell, 2007. **11**(1): p. 69-82.
188. Hjelmeland, A.B., et al., *Twisted tango: brain tumor neurovascular interactions.* Nature Neuroscience, 2011. **14**(11): p. 1375-1381.
189. Heddleston, J.M., et al., *The hypoxic microenvironment maintains glioblastoma stem cells and promotes reprogramming towards a cancer stem cell phenotype.* Cell Cycle, 2009. **8**(20): p. 3274-84.
190. Hjelmeland, A.B., et al., *Acidic stress promotes a glioma stem cell phenotype.* Cell Death and Differentiation, 2010. **18**(5): p. 829-840.
191. Navalitloha, Y., et al., *Therapeutic implications of tumor interstitial fluid pressure in subcutaneous RG-2 tumors.* Neuro Oncol, 2006. **8**(3): p. 227-33.
192. Baxter, L.T. and R.K. Jain, *Transport of fluid and macromolecules in tumors. I. Role of interstitial pressure and convection.* Microvasc Res, 1989. **37**(1): p. 77-104.

193. Wu, J., et al., *Study of tumor blood perfusion and its variation due to vascular normalization by anti-angiogenic therapy based on 3D angiogenic microvasculature.* Journal of Biomechanics, 2009. **42**(6): p. 712-721.
194. Hofmann, M., et al., *Long-term lowering of tumour interstitial fluid pressure reduces Ki-67 expression.* J Biomech, 2007. **40**(10): p. 2324-9.
195. Ulrich, T.A., E.M. de Juan Pardo, and S. Kumar, *The Mechanical Rigidity of the Extracellular Matrix Regulates the Structure, Motility, and Proliferation of Glioma Cells.* Cancer Research, 2009. **69**(10): p. 4167-4174.
196. Pardridge, W.M., *CNS drug design based on principles of blood-brain barrier transport.* J Neurochem, 1998. **70**(5): p. 1781-92.
197. de Boer, A.G. and P.J. Gaillard, *Strategies to improve drug delivery across the blood-brain barrier.* Clin Pharmacokinet, 2007. **46**(7): p. 553-76.
198. Wolburg, H., et al., *The disturbed blood-brain barrier in human glioblastoma.* Mol Aspects Med, 2012. **33**(5-6): p. 579-89.
199. Clarke, J.L., et al., *Randomized Phase II Trial of Chemoradiotherapy Followed by Either Dose-Dense or Metronomic Temozolomide for Newly Diagnosed Glioblastoma.* Journal of Clinical Oncology, 2009. **27**(23): p. 3861-3867.
200. Sampson, J.H., et al., *Poor drug distribution as a possible explanation for the results of the PRECISE trial.* J Neurosurg, 2010. **113**(2): p. 301-9.